Bio-morphodynamics of the Choked Passage seagrass meadow on Calvert Island, British Columbia, Canada.

By

Keegan Mae Paterson

BSc, University of Victoria, 2020

A Thesis Submitted in Partial Fulfillment of

the Requirements for the Degree of

Master of Science

in the Department of Geography

Bio-morphodynamics of the Choked Passage seagrass meadow on Calvert Island, British Columbia, Canada.

By

Keegan Mae Paterson

BSc, University of Victoria, 2020

Supervisory Committee:

Dr. Eva Kwoll, Supervisor

Department of Geography, University of Victoria.

Dr. Margot Hessing-Lewis, Outside Member

Nearshore Ecology, Hakai Institute

Abstract

Seagrasses are ecosystem engineers, forming extensive meadows that provide critical habitat and modulate local morphodynamics. Their canopies induce drag on flow to attenuate mean flow and reduce near-bed flow velocities, which can shield the bed from erosion and sediment suspension. Alternatively, seagrass loss can enhance erosion and sediment suspension, which can be initiated through short-lived extreme events, or chronic long-term disturbances. Physical process and disturbances can govern the evolution of seagrass meadow ecosystems. In two separate chapters, this research examined 1) the influence of climate variability and storms on seagrass loss and erosion at a high spatial resolution, and 2) how flow attenuation by seagrass varies across tidal cycles and at different locations in the Choked Passage meadow, on the Central Coast of British Columbia. We used high resolution multibeam echosounder (MBES) bathymetry and backscatter data from 2018 to 2021, drone mapped seagrass delineations from 2014 to 2021, and wind and wave data from 2014 to 2021. Flow data (i.e. velocity magnitude, velocity direction, and acoustic backscatter) above the seagrass canopy was collected with an Acoustic Doppler Current Profiler (ADCP) along transects and moored to the seafloor over a tidal cycle. Sediment samples were collected from the bed to estimate critical shear stress and verify sediment classes from an acoustic backscatter analysis. From 2018 to 2021, the meadow experienced significant erosion (net surface lowering of -18,768 m^3) and loss of seagrass (10% reduction), which we attribute to the preceding winter storm activity driven by moderate La Niña conditions. The spatial patterns of erosion and seagrass loss was non-uniform across the meadow. Coupled erosion and seagrass loss resulted in the generation and/or expansion of blowouts. We observed a trend of a reduction in seagrass coverage following winters with a high number of storm events and/or high recorded storm intensity from 2014 to 2021. We believe the Choked Passage seagrass meadow undergoes cyclic behaviour with reduction in seagrass coverage during energetic ENSO years, followed by a recovery period during weak years. The ADCP was used to detect the seagrass canopy height, measure flow, and estimate shear stress. Overall, flow is fastest in the northern section of the main meadow, particularly in the north-west corner where the meadow is patchy. Moreover, flow appears to accelerate through the meadow interior, which suggests that topographic steering and the strength of incoming currents exceeds the ability of seagrass to dampen flow velocity. During the transition from peak flood to ebb, flow velocity remained heightened for longer above the southern meadow and lagged the other

sections. Shear stress results indicate that sediment can be transported as bedload and in suspension under peak flow velocities at some of the sites examined within the meadow. Shear stress is largest in the meadow center and lower towards the southern margin of the main meadow. Based on our results, when sediment transport is initiated under peak tidal and/or extreme conditions, sediment is likely primarily transported as bedload, creating the observed sand wave and blowout bedforms. This research demonstrated linkages between extreme storms (during ENSO years), seabed morphology, and seagrass coverage, and examined the variability in the interaction between flow, seagrass, and sediment transport. Geomorphic processes and disturbances have an important influence on ecosystem structure and function over time, therefore, it is important to understand how these processes operate and are modified by external drivers. The results of this study have significant implications on seagrass conservation, restoration, and the evolution of coastal landscapes.

Table of Contents

List of Figures

Chapter 1.0

Chapter 2.0

Chapter 3.0

Appendix

List of Tables

Chapter 2.0

Chapter 3.0

Appendix

Acknowledgments

First, I would like to acknowledge the Wuikinuxv and Heiltsuk peoples, whose territory Choked Passage resides in, and express my sincerest gratitude for allowing me and many others to research and learn within their lands. Thank you to the Hakai Institute as a whole, for providing me with the incredible opportunity to spend a month on Calvert Island. It was an experience I will never forget. A special thank you to Nick Viner, Rob White, and Derek Heathfield, for accompanying me in the field, providing their expertise and lots of laughs.

Thank you to my supervisor, Dr. Eva Kwoll, for her incredible guidance, support, and enthusiasm for research. Thanks to the rest of the past and present GECOS lab members, Amanda Wild, Katie Hughes, Darcy Harrison, Felipe Gomez, Narges Raee, Jordan Prior, Wyatt Maddox, and Bryn Forrest, for your support and companionship over the years. Finally, thank you to my friends and family, especially my partner Jordan Johnson, for helping me get through it all.

1.0 Introduction

1.10 Seagrass

Seagrasses are marine flowering plants that are ubiquitous to temperate and tropical coastlines (Short *et al.*, 2007). These marine plants form extensive meadows that provide critical habitat, food, and modulate local hydrodynamic, sediment transport, and biogeochemical processes (Duarte and Chiscano, 1999; McRoy and Helfferich, 1977). There are three major families of seagrasses: Hydrocharitaceae, Cymodoceaceae, and Zosteraceae, with approximately 60 total species in the world (Les *et al*., 1997; Orth *et al.,* 2006). *Zostera marina* is one of the most widely distributed species of seagrass in the Northern Hemisphere (Larkum *et al.,* 2006). In temperate regions, maximum biomass occurs during the summer, followed by a winter period of senescence (Olesen and Sand-Jensen, 1994). Seagrasses colonize on soft substrates of mud and sand and are limited to depths above 6m. Their distribution is primarily controlled by light availability, sediment type, and wave exposure (Duarte, 1991). Seagrasses prefer areas relatively protected from wave-exposure (Koch *et al.,* 2009). However, their distribution is highly variable at a given site, as they are modified by variability in physical forces (Frederiksen *et al.*, 2004). To withstand the hydrodynamic conditions of coastal areas, seagrasses establish strong rhizomes embedded into the seafloor to withstand the hydrodynamic forces of the nearshore environment. This extensive network of roots and rhizomes is important in binding sediments (Duarte and Chiscano, 1999). Their widespread distribution and ability to modify their environment to create favorable conditions contributes to their high ecological significance (Waycott *et al.,* 2009).

Seagrass meadows are highly productive nearshore ecosystems that serve as critical habitat for a diversity of species (Orth *et al.,* 2006). Seagrasses are an important food source for many species of herbivorous marine mammals, sea turtles, and fishes, and foraging habitat for many species (Espadero *et. al.,* 2020; Ganter, 2000; Orth *et al.*, 2006). Individual seagrass blades are colonized by epiphytes (e.g. macroalgae, phytoplankton, and bacteria) that exploit the light and nutrient availability within patches of seagrass, which subsequently support micro-grazing organisms, such as gastropods, zooplankton, polychaete worms, and other invertebrate groups (Orth and Van Montfrans, 1984). Not only do seagrass meadows provide abundant food resources, but their structural complexity serves as shelter to avoid predators and harsh

environmental conditions (Boström and Mattila, 1999), making it ideal juvenile nursery habitat (Heck Jr., Hays, and Orth, 2003).

1.20 Seagrass Hydrodynamics

Hydrodynamics is defined as the movement of fluids, and includes flow velocity, acceleration, and the forces acting on and generated by fluids. Hydrodynamics contribute to coastal landscape change, ecosystem processes, and exert a significant influence on all aspects of marine environments (Koch et al., 2006). In settings with un-vegetated bottoms and unidirectional flow, velocity profiles follow the logarithmic law of the wall (Kundu et al., 2015). The law of the wall recognizes three distinct flow zones (Figure 1 A): a thin viscous sub-layer, a logarithmic layer, and a turbulent outer layer, or Ekman layer, where the magnitude of turbulent flow depends on boundary roughness elements and the thickness of the viscous sub-layer (Le Roux, 2004).

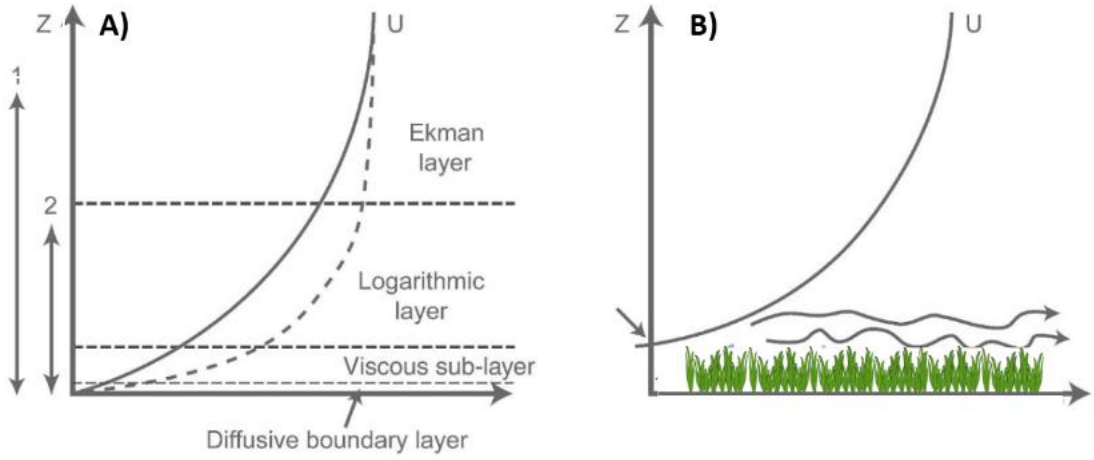

Figure 8 - A) Velocity profile of a smooth boundary with weak currents (solid line) and strong currents (dashed line) showing three zones: viscous sub-layer, logarithmic layer, and Ekman layer (i.e. turbulent outer layer). B) Velocity profile of a rough boundary layer over a seagrass canopy, where the logarithmic profile begins above the height of the roughness elements. Figure modified from Koch et al., 2006.

Velocity profiles are measured through the Law of the Wall with the following formula (Spalding, 1961):

$$u(z) = \frac{u_*}{k} \ln \frac{z}{z_o} \quad \text{(Eq.1)}$$

In equation 1, $u(z)$ is the mean velocity at height z above the bed, u_* is shear velocity, k is the Von Kármán constant, and z_o is the roughness length. Fitting the logarithmic relationship between velocity and roughness to measured velocity profiles can be used to estimate bed-shear stress, drag (*i.e.* fluid resistance), and eddy viscosity (Lefebvre et al., 2010; Rippeth et al., 2002). The shape of the logarithmic profile is modified by acceleration and deceleration, such as those caused by tides, variations in upstream roughness, bedforms, stratification, current meter array errors, and waves (Dyer & New, 1986). In aquatic environments, submerged vegetation modifies the flow, altering the velocity profile (Figure 1 B; Koch et al., 2006). Flow through submerged vegetation shows generally the same three layers as in unvegetated bottoms, but with a thicker diffusive boundary layer due to the canopy roughness, and an inflection point of maximum shear at the canopy water interface and base of the logarithmic layer (Lacy & Wyllie-Echeverria, 2011; Lefebvre et al., 2010; Nepf, 2012).

Vegetation density is one of the most important parameters influencing hydrodynamics and sediment transport within patches of submerged aquatic vegetation (S. Lawson et al., 2012). Many studies have identified a threshold in vegetation density that promotes either erosion or deposition (S. Lawson et al., 2012; Yager & Schmeeckle, 2013). These thresholds are referred to as the dense and sparse canopy limits (Belcher et al., 2003; Nepf, 2012). In sparse canopies, stem-scale turbulence is generated throughout the meadow and acts on the bed to suspend sediment (Figure 2 a; Nepf, 2012). As well, horizontal flow may be diverted around individual stems, creating stem-wakes and local scour (Nepf, 1999). At densities between the sparse and dense canopy limits, canopy-scale turbulence, or Kelvin-Helmotz vortices (Figure 2 b; Ghisalberti & Nepf, 2002; Nepf, 2012), creates a region of strong shear directly above the canopy. Canopy-scale turbulence may penetrate the meadow and act on the bed to suspend sediment depending on the canopy height and magnitude of turbulent energy. Above the dense canopy limit, canopy-scale turbulence often lacks sufficient energy to penetrate through the canopy (Figure 2 c; Nepf, 2012). Moreover, at high densities much of the flow may be diverted vertically above the canopy (S. Lawson et al., 2012), or laterally around the patch (Larsen & Harvey, 2011). The most turbulence and sediment suspension is produced at densities between

the sparse and dense canopy limits (S. Lawson et al., 2012; Moore, 2004). In this manner, dense vegetation shields the bed from turbulence and bed-shear stresses (Nepf, 2012).

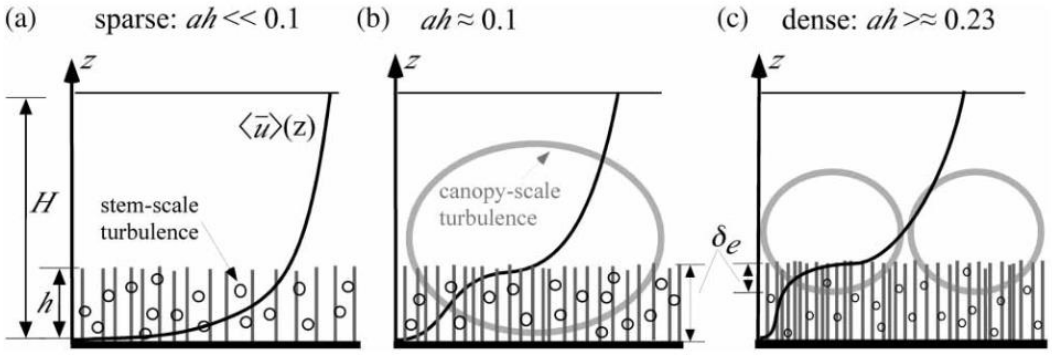

Figure 9 - Mean velocity profiles of flow through submerged seagrass at the sparse and dense canopy limits. Here, *H* is water depth, *h* is canopy height. (a) Rough boundary-layer profile of a sparse canopy, where $ah < 0.1$. (b) Canopy-scale turbulence generated at densities between the sparse and dense limit, where $ah \geq 0.1$. (c) Flow profile through a dense canopy ($ah > 0.23$), where the bed is shielded from canopy-scale turbulence (Figure from Nepf, 2012).

1.20 Coastal & Seagrass Morphodynamics

Coastal landscapes are driven by physical forces and geomorphic processes, which generate a dynamic environment with diverse habitats and landforms, at many different spatial scales (Nepf, 2012; van der Heide et al., 2007). Morphodynamics refers to feedbacks between hydrodynamic processes, sediment transport, and bed morphology (Wright and Thorne, 1977). This interactive process of coastal morphodynamics is shown in Figure 3, where external forces drive hydrodynamics, influencing sediment transport and bathymetry through erosion and deposition. The creation of bedforms and bathymetric changes then in turn modifies the local hydrodynamics to feedback into this process. Biogenic habitats (e.g. seagrass meadows and kelp forests) also fit into this feedback, by modifying and being modified by hydrodynamics and sediment transport (Vacchi et al., 2017).

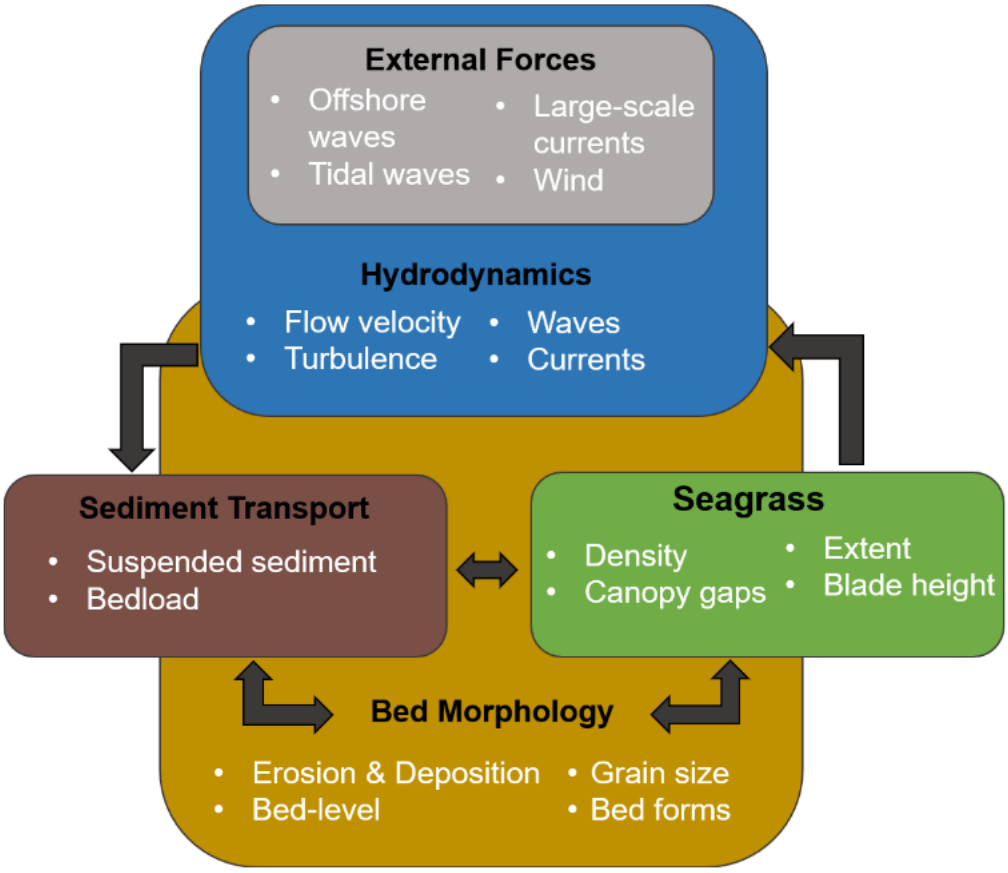

Figure 10 - Framework of coastal morphodynamic models, modified from Ribas et al., 2015 to include the influence of seagrass.

Sediment transport is controlled by hydrodynamics, but influenced by the presence of bedforms, bathymetry, and vegetation that interfere with flow (Belcher et al., 2003). Vegetation controls sediment transport and spatio-temporal patterns of erosion and deposition by altering the velocity, shear stress, and turbulence of the flow (Follett & Nepf, 2012; Yager & Schmeeckle, 2013; Zong & Nepf, 2011). Broadly speaking, aquatic vegetation tends to trap sediment and increase deposition locally by generating drag and reducing flow velocities and bed-shear stress below the critical thresholds for sediment transport (Vargas-Luna et al., 2015, p.; Yager & Schmeeckle, 2013). Moreover, vegetative-drag breaks up the laminar flow field, creating unstable fluid-vortices and turbulence. The production of turbulence reduces the mean velocity of the flow field but can act on the bed to create shear stresses under certain conditions (Nepf, 2012). If the bed-stresses exceed the critical shear stress threshold, then sediment will become entrained and transported (Durán et al., 2012).

Given that seagrass heavily influences morphodynamics (Vacchi et al., 2017), they are important to incorporate into sediment transport and coastal landscape change models (Zhu et al., 2021). Within seagrass, bed morphology (e.g. bed-level, slope, sediment type) vary as a function of sediment supply and hydrodynamic forces (Bos et al., 2007; van Katwijk et al., 2010), and are influenced by seagrass characteristics (e.g. meadow extent, canopy height, blade density; Lacy & Wyllie-Echeverria, 2011). This dynamic interaction between seagrass, flow, and sediment, creates complex patterns of sediment transport, bed morphology, and meadow configuration (Frederiksen et al., 2004; Nepf, 2012; Zhu et al., 2021), which vary across seasonal and tidal cycles (Hansen & Reidenbach, 2012; Hasegawa et al., 2008).

Like other types of aquatic vegetation, seagrasses attenuate wave and current energy within their canopy, resulting in a reduction of near-bed mean velocities and wave-orbital velocities (Hansen & Reidenbach, 2012). In general, flow reductions may be proportional to the canopy height relative to water depth (Ward et al., 1984); however, flexible blades can bend downwards under high flow velocities, which can temporarily reduce canopy height and drag. Seagrass characteristics (e.g. blade height and density) are heterogenous across space, therefore, its effect on flow and sediment transport is highly variable (Allaoui et al., 2016; Carr et al., 2016). Both deposition and resuspension can operate concurrently within a meadow, but the relative magnitude of each process depends on meadow characteristics (Nepf, 1999; van Katwijk et al., 2010), flow velocity, and sediment grain size (de Boer, 2007). Much of the knowledge related to the morphodynamics of seagrass meadows has been generated from flume studies and applied to numerical models. However, several field studies provide important information relevant to the morphodynamics of seagrass meadows.

A field study by Lacy and Wyllie-Echeverria (2011), stationed an acoustic doppler velocimeter (ADV) and pulse-coherent acoustic doppler current profiler (PCADCP) examined flow and turbulence through *Z. marina* canopies of different densities in Puget Sound. They observed increased canopy drag in higher density canopies, resulting in a greater flow attenuation. In sparse *Z. marina* canopies, each blade acted as an individual roughness element to increase drag and turbulence (Lacy & Wyllie-Echeverria, 2011). In agreement with many flume studies (Hasegawa et al., 2008; Luhar et al., 2008), this study demonstrated that the mean flow fields and shear stress varies with vegetation density, canopy height, and current speed. In

addition, they observed strong turbulent mixing and large-scale velocity fluctuations at the canopy-water interface, through intermittent sweeps (i.e. downward mixing of high momentum fluid) and ejections (i.e. upward mixing of low momentum fluid), which transport fluid between the canopy and the overlying water. Sweep events can cause blades to bend, while ejections lift (Hansen & Reidenbach, 2012) blades upright (Lacy & Wyllie-Echeverria, 2011).

Another field study by Hansen and Reidenbach (2012), deployed an ADV, to measure the attenuation of wave and tidal flows, turbulence, and shear stress under different *Z. marina* canopy densities in the Virginia Coast Reserve (VCR). They observed large reductions in near-bottom velocities (70-90% reduction), wave height (45-70%), and wave orbital velocities within the canopy (20% reduction), which increased with canopy density. Velocity attenuation reduced Reynolds stress by 60%. Both turbulent kinetic energy (TKE) and shear stress were reduced within the canopy relative to flow above the canopy, but TKE remained higher within the canopy than shear stress, likely due to stem generated TKE. Flow velocity and suspended sediment concentration (SSC) decreased with distance from the meadow edge into the interior, thus retaining fine sediments (Hansen & Reidenbach, 2012). Moreover, seagrass canopies were most effective at attenuating high frequency wave energy (Hansen & Reidenbach, 2012), which agrees with the results of Bradley and Houser (2009). Ultimately, seagrasses serve as a low-pass filter on high frequency waves, but attenuation decreases with wave height (Bradley & Houser, 2009; Hansen & Reidenbach, 2012). Given that seagrass density is greatest during the summer (Olesen & Sand-Jensen, 1994), flow and wave attenuation is maximized during peak summer biomass.

Using similar methods, Hansen and Reidenbach (2013), found the reduction in flow velocities to be much greater in summer (60%) than in winter (40%), which is the period of meadow senescence, low biomass, and increased storm frequency. Similar to velocity, SSC was lower in the seagrass sites during peak summer biomass, whereas SSC was enhanced during the winter under minimum seagrass density. Furthermore, SSC was almost 2x greater in unvegetated sites than those in seagrass during peak summer biomass. As in Lacy and Wyllie-Echeverria (2011), this study observed short-lived turbulent sweeps and ejections, which mixes the fluid across the shear-layer in the canopy-water interface and is the dominant turbulent motion within the meadow in all seasons (Hansen & Reidenbach, 2013). Moreover, Hansen and Reidenbach (2017), showed further evidence that turbulence production at the shear layer may extend into

within the canopy in sparse densities, but is significantly reduced in dense canopies. Turbulent ejections were the dominant form of momentum transfer within low density patches, whereas sweeps were dominant in high density patches (Hansen & Reidenbach, 2017). This agrees with the findings of Finnigan (2000) and suggests that sweeps enhance fluid exchange between the canopy and the overlying water over a short time (Finnigan, 2000; Hansen & Reidenbach, 2017). Turbulence is reduced within the canopy, however, the efficiency of momentum transfer is increased, due to sweeps and ejection events (Hansen & Reidenbach, 2013). Additionally, Hansen and Reidenbach (2017) found that turbulence produced by wave oscillatory motion was significantly greater than from currents. However, there was a significant reduction in vertical mixing efficiency and stresses under wave-driven flows (Hansen & Reidenbach, 2017). Ultimately, these patterns of flow attenuation and momentum transfer within meadows modify local sediment transport and bed morphology.

By reducing water currents, seagrasses enhance deposition and reduce resuspension, which drives sedimentation patterns within meadows (Terrados & Duarte, 2000). Generally, meadows tend to accumulate fine grained sediments, such as sand, mud, and silt (de Boer, 2007; van Katwijk et al., 2010). A key study by Bos *et al.* (2007) transplanted *Z. marina* seedlings on unvegetated sediment in the Wadden Sea and observed a net deposition of 5-7 mm of fine silt and sands (Bos et al., 2007). Expanding on these results, Van Katwijk *et al.* (2010) observed that in dense seagrass beds with reduced flow velocities, there is an increase in fine silt and organic material. Alternatively, sparse beds showed an increase in larger grained sand content, with a smaller reduction in flow velocity (van Katwijk et al., 2010). Other studies have also found that changes in sediment composition depend on flow velocity, seagrass density, and underlying sediment type (Oreska et al., 2017; Widdows et al., 2008). Based on Hjulstrom's curve, larger grains require higher velocities to transport, whereas transportation of fine grains can be initiated at relatively lower flow velocities (Hjulstrom, 1939). However, clays and silt can form cohesive bonds and require higher velocities to initiate transportation, which may alter this general pattern of resuspension within beds with higher clay and silt content (de Boer, 2007). Both velocity and seagrass density can vary seasonally and across a tidal cycle, which modifies these sedimentation patterns (Herman et al., 2001; Lacy & Wyllie-Echeverria, 2011) and generates spatially and temporally variable patterns of sediment transport and the subsequent bed morphology (Jankowska et al., 2014).

Within a seagrass meadow, edges are the most dynamic location, while the interior is typically stable (Carr et al., 2016; Chen et al., 2007; Gruber & Kemp, 2010). Flow may be concentrated along edges and interact with the bed and seagrass blades to generate shear stress, turbulence, and scouring along the margins (Chen et al., 2007; Fonseca et al., 2007; Zhu et al., 2021). As flow travels through the meadow edge, suspended sediment can be trapped by individual blades and flow velocities reduced to levels below the threshold to transport suspended sediment (Carr et al., 2016), which can increase local bed-levels (Zhu et al., 2021). This creates a region of increased deposition immediately downstream of the meadow edge (Beudin et al., 2017; Zong & Nepf, 2011), until most suspended sediment is removed from the water column (van der Heide et al., 2007; Zhu et al., 2021). Sections of the interior and edges with lower densities and canopy gaps may experience increased scouring and resuspension (Colomer et al., 2017; Hansen & Reidenbach, 2012). In areas of high-moderate plant densities, such as interiors, sediments are stabilized by the reduction in turbulence and shear stresses below thresholds required to transport sediment (Lacy & Wyllie-Echeverria, 2011; Zhu et al., 2021), even in moderately exposed environments (Bos et al., 2007). These conclusions are generally useful to understand the patterns of flow and sediment transport throughout a meadow. However, have been generalized from the combination of flume studies, relatively small-scale field studies, and modelling efforts.

At the meadow-scale, feedbacks between patches, gaps, and hydrodynamics govern the evolution of the meadow through the transport of sediment and mechanical disturbance (Larsen & Harvey, 2011; Uhrin & Turner, 2018), which vary across the growing season (Hansen & Reidenbach, 2013; Hasegawa et al., 2008), and through natural and anthropogenic disturbances (Short & Wyllie-Echeverria, 1996; Walter et al., 2020). As biomass, density, and extent increases, sediment accumulates and increases bed-level across the growing season (Bos et al., 2007). A recent study by Zhu *et al.* (2021), used the coupled Delft3D-FLOW and SWAN models to predict sediment and flow dynamics at different seasons in the VCR. At peak densities (400-500 shoots m^{-2}), the model predicted that flow velocity and SSC were reduced by 60% and 85%, respectively. As well, flow was concentrated along the meadow edges causing scour. Alternatively, with low seagrass densities (50-100 shoots m^{-2}) flow velocities and SSC were considerably higher, and erosion was enhanced in the interior (Zhu et al., 2021). Although this model produced reasonable simulations, it relies on uniform seagrass characteristics averaged

across the entire meadow and has a grid size of 70 m. Therefore, this model cannot resolve heterogenous seagrass patterns (e.g density changes, canopy gaps), which influences the production of turbulence, bed-shear stress, and sediment transport (Carr et al., 2016; Ganthy et al., 2013), and oversimplifies the predicted morphodynamics.

The dynamic interplay between seagrass, hydrodynamics and sediment transport yields heterogenous patterns of bed-level changes and suspended sediment concentrations due to fine-scale variability in turbulence, shear stress, scouring, and deposition (Bos et al., 2007; Carr et al., 2016; Ganthy et al., 2013). Both flume and field research have yielded somewhat contradictory results related to the morphodynamics within seagrass and similar types of flexible vegetation (Bouma et al., 2007; Heide et al., 2010; Widdows et al., 2008). The tendency for seagrass to stabilize sediments and enhance deposition or generate erosion and resuspension is not yet fully understood (Tinoco et al., 2020), possibly due to simplification of complex spatio-temporal patterns. Therefore, further field studies under different physical settings with varying seagrass characteristics will help resolve the local drivers of seagrass morphodynamics.

1.30 Seagrass Patch Dynamics

Seascape ecology, an application of landscape ecology in marine environments, examines the spatio-temporal pattern dynamics and heterogeneity of habitats. Seascape structure can be represented with the 'patch-matrix' model, where patches of a particular habitat (e.g. seagrass) are embedded within a matrix of a different habitat (e.g. sand; Bell, 1999). Spatial pattern metrics characterize the configuration and composition of landscapes at three levels of spatial hierarchy: patch, habitat class, and seascape (Pittman, 2017; Turner & Gardner, 2015; Wedding et al., 2011).

Seagrass landscapes can range from contiguous seagrass cover to complex fragmentated seagrass patches, driven in part by depth, sediment type, and exposure to physical disturbances (Bell, 1999; Duarte et al., 2006). Seagrasses typically colonize fine sandy substrates and depths less than 6 m, as they require sufficient light conditions for photosynthesis (Duarte, 1991; Frederiksen et al., 2004). Canopy gaps can originate from disturbances through the removal or mortality of vegetation, or changes in local topography and soil/sediment quality that are not suitable for seagrass growth (Bell, 1999). Areas exposed to greater wave and current energy

often have a lower patch size, aerial coverage, and number of patches, as these disturbances prevent growth and enhance seagrass losses (See Figure 4; Uhrin & Turner, 2018). Moreover, seagrass patches can migrate across the nearshore in response to disturbances and sediment transport processes (Fonseca et al., 2007). The configuration of patches and gaps influences habitat quality, ecosystem function, and sediment transport processes (Boström et al., 2011, 2014; Carr et al., 2016).

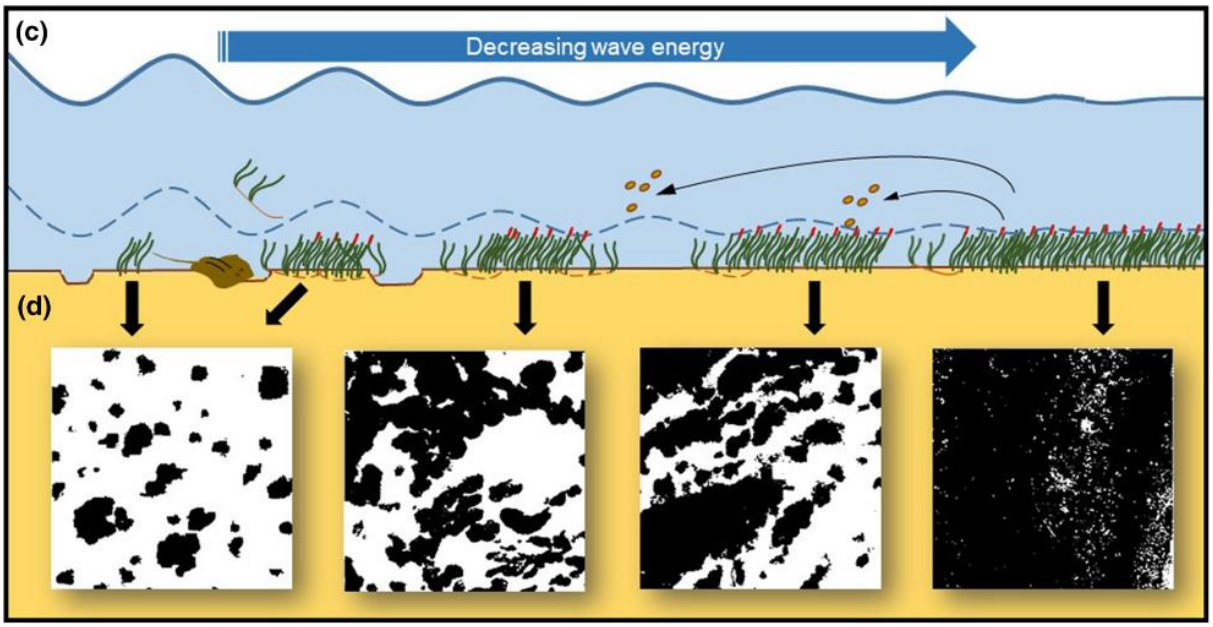

Figure 11 -Schematic diagram of the effect of wave exposure on seagrass spatial pattern. Figure from Uhrin & Turner 2018.

Increasing canopy gaps, or patchiness, is associated with fragmentation. Habitat fragmentation is the process where a contiguous patch is broken up into smaller more isolated patches and can be related to natural and/or anthropogenic disturbances (Fahrig, 2003; Folkard, 2019). Fragmented meadows have increased amount of edge, which results in a reduction of seagrass shoot density (Yarnall et al., 2022). Because dense seagrass patches modify flow, heavily fragmented seagrass canopies are dampened in their ability to reduce flow and sediment resuspension (Folkard, 2005, 2019; Nepf, 2012). A 2017 study by Pace et al., examined the patch dynamics of a *Posidonia oceanica* meadow in relation to a gradient of wave and energy exposure. They concluded that increased near-bed shear forces lead to increased meadow patchiness (i.e. fragmentation) and configuration. Moreover, they found that both patch size and shape complexity were primarily driven by wave climate (Pace et al., 2017). Seagrass patchiness

and complexity can be modified through exposure to continuous tidal currents and average wave conditions, or through disturbances of differing magnitude, frequency, and duration.

Physical disturbances are one of the main drivers of seagrass spatial pattern (Uhrin & Turner, 2018). Here, a disturbance is defined as an event that disrupts the structure of an ecosystem, community, or population, and modifies resource availability or the physical environment (Turner, 2010). There are three main categories of disturbances that influence seagrass spatial pattern: Pulse, Press, and Ramps (Figure 5). Pulse disturbance are low frequency high magnitude events, such as an extreme storm or cyclone. A press disturbance occurs rapidly and maintains constant level, such as persistent pollution. A ramp disturbance is the gradual increase in biophysical conditions that slowly disturbs the seagrass landscape over time, for example ocean acidification (Pittman, 2017). Short-lived disturbances operate in tandem with other physical drivers (e.g. wave exposure and tidal currents) to control seagrass spatial pattern over time. Increase in patchiness and canopy gaps reflects the spatially variable hydrodynamics, disturbances, and recovery of seagrass. The balance between recovery and losses depends on the life history traits and reproductive strategies of the seagrass species and the frequency and magnitude of disturbance (Duarte et al., 2006).

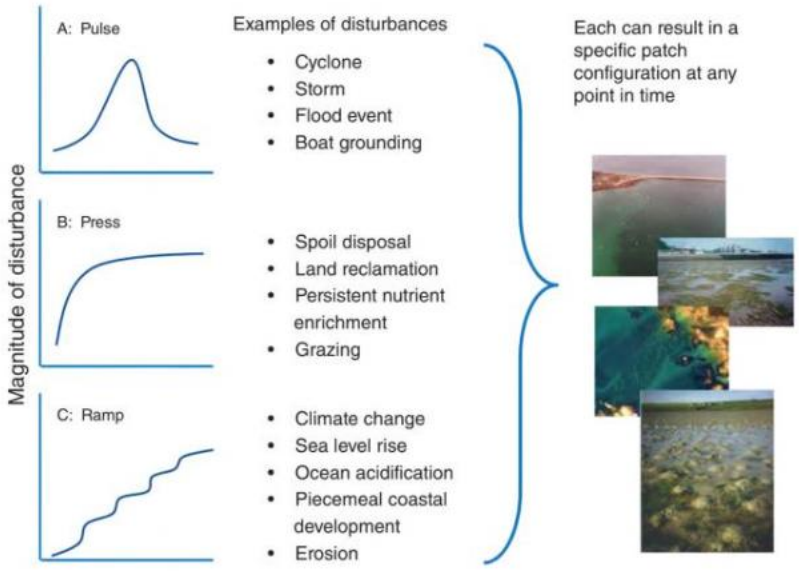

Figure 12 - Three main disturbance categories that influence seagrass spatial pattern and patch dynamics. From Pittman 2017.

1.40 Seagrass Threats and Restoration

A recent meta-analysis on global seagrass communities are in decline by 1%-2% each year (Dunic et al., 2021). Seagrass declines are the result of multiple anthropogenic stressors amplified by natural processes (Orth et al., 2006). Seagrass meadows are almost exclusively monospecific, which makes them vulnerable to disease outbreaks. In the 1930s, approximately 90% of *Z. marina* meadows were lost in the North Atlantic Ocean, primarily due to seagrass wasting disease (Waycott et al., 2009). Seagrass wasting disease, caused by slime mould Labyrinthula sp. resulted in the most significant global loss in seagrass coverage to date (Larkum et al., 2006). Most human populations live near our coastlines, which has resulted in extreme anthropogenic pressures. In particular, the armouring of shorelines with breakwaters, rock-walls, and groins, has altered the sediment dynamics and inhibited the natural migration of meadows (Orth et al., 2006). Under predicted climate change scenarios, armoured shorelines will likely prevent the landward migration of seagrasses with rising sea-levels, referred to as 'coastal squeeze' (Mills et al., 2016). Deteriorating water quality due to excessive nutrient and sediment run-off from industries (e.g. agriculture and logging) and urban development within watersheds can have deleterious effects on seagrasses (Waycott et al., 2009). Fisheries directly and indirectly impact seagrasses by physically disturbing meadows with bottom-trawlers, boat-propellors, mooring, and trophic cascades by predator removal that increase seagrass herbivory (Colomer et al., 2017; Hughes et al., 2013). Another major stressor facing seagrass is accelerating global climate change, which may amplify seagrass declines through the cumulative effects of all stressors. Increasing sea-surface temperature, storm frequency, extreme climatic events, and shifts in large-scale oceanic process, have been attributed to losses in seagrasses, and are expected to become even more prevalent in the future (Orth et al., 2006). The widespread degradation of seagrass meadows has led to a considerable effort to restore these valuable habitats (van Katwijk et al., 2016).

A European study observed a reversal in the declining trends for seagrass meadows in certain locations (de los Santos et al., 2019). This provides evidence that with proper management action, restoration, and conservation efforts, we may be able to prevent further loss of seagrass meadows and even restore those previously lost. However, different seagrass species vary in their recovery trajectories, reflecting their different growth rates and tolerances to

environmental conditions (de los Santos et al., 2019). *Z. marina* is the most widespread species of seagrass in the Northern Hemisphere, and as a generalist, may be more easily restored than more specialized seagrasses (Short et al., 2007). The invasion of non-native seagrasses (e.g. *Zostera japonica*) may hinder seagrasses recovery by outcompeting and displacing native seagrasses (Williams, 2007). To conserve global seagrass biodiversity and ecosystem function, it is important to understand the different physical and environmental requirements, as well as life history traits, of seagrass species, and how they may influence seagrass restoration.

In order to combat widespread seagrass losses, significant measures have been implemented to recover seagrass beds through improving water quality and planting. Although restoration efforts have lead to full or partial recovery of seagrass meadows (Orth et al., 2012), many restoration attempts have failed (Tanner & Parham, 2010). A global analysis estimated a success rate of only 37% for seagrass restoration efforts (van Katwijk et al., 2016). The reason for these restoration failures is believed to be partially explained by inadequate site selection due to physical setting, regime shifts (i.e. non-linear change in the stable state of a system after reaching a threshold; Stallins & Corenblit, 2018), or altered feedback loops (Nyström et al., 2012). A recent study by Moksnes, Eriander, Infantes, and Holmer (2018) examined the factors inhibiting natural seagrass recovery in areas that experienced severe losses. Although drastic improvements to regional water quality were made, there was no natural seagrass recovery. This study concluded that recovery was inhibited due to a regime shift in these areas where local morphodynamic processes now acted as a positive feedback loop preventing seagrass growth. Following the loss of the meadow, the system shifted to a new regime state lacking the negative feedback mechanisms that enhances seagrass colonization and growth (Moksnes et al., 2018). The failure of restoration projects highlights the need for more comprehensive research on the key processes and feedbacks related to seagrass morphodynamics, which will have important implications for restoring lost and degraded seagrass meadows.

Feedback loops often dictate the non-linear response of seagrass ecosystems to changes in environmental conditions (Nyström et al., 2012). Negative feedback loops (i.e. self-dampening) help to maintain system stability by mitigating effects of changes in environmental conditions and system states (Walker et al., 2006). Seagrasses are photosynthetic organisms, therefore, their distribution is dependent on light availability (Duarte, 1991). The seagrass-sediment-light

feedback has been identified as a major driver in the trajectory of seagrass ecosystems. When seagrass meadows attenuate flow velocity, there is a reduction near-bed turbulence and shear stresses, which promotes sediment deposition and retention (Hansen & Reidenbach, 2012). Water turbidity is reduced as sediment is captured from the water column, which improves light penetration and enhances seagrass growth (Lawson et al., 2007). As patches of seagrass continues to grow and expand, they further enhance the conditions suitable for seagrass meadow ecosystems (Lacy & Wyllie-Echeverria, 2011). Once the state variables (i.e. density, extent, and biomass) have reached specific threshold values, the system will maintain its stable state, and buffer environmental disturbances below a certain magnitude (Moksnes et al., 2018).

This feedback loop is dependent on seagrass density and biomass, where destabilizing effects may occur below a biomass and density threshold when flow velocities are high. This causes a shift to a positive feedback loop (i.e. self-amplifying), which inhibits seagrass growth and colonization (Lawson et al., 2012). The positive feedback loop follows the same mechanism as the negative seagrass-sediment-light feedback, but in the reverse direction. When the state variables decrease to below a critical threshold value, the ability of seagrass to prevent resuspension is compromised. As more sediment is resuspended, turbidity increases, and light penetration into the seagrass canopy decreases. Given that seagrasses require sufficient light conditions for photosynthesis, this inhibits growth and can accelerate meadow loss (Moksnes et al., 2018; van der Heide et al., 2007). Once a meadow is lost, the system becomes dominated by unvegetated sand and drifting algae, which leads to further sediment resuspension and erosion (Moksnes et al., 2018). This process whereby a stable state transitions into an altered stable state following a large-magnitude disturbance is referred to as a regime shift (Nyström et al., 2012). Regime shifts and altered feedback loops have important implications for conservation management and restoration projects of seagrass meadows (van der Heide et al., 2007).

1.50 Thesis Structure and Research Questions

Most field studies on sediment and seagrass dynamics have occurred in relatively low-energy estuarine systems, therefore, our current understanding of these biophysical processes may not be relevant to all seagrass systems. Off the Central Coast of British Columbia, Canada, the *Z. marina* seagrass meadow within Choked Passage is exposed to significant current and wave energy (Prentice et al., 2019) and is relatively free from human disturbance. Therefore, this

site presents a unique opportunity to study the natural biophysical processes operating in an undeveloped and hydrodynamically exposed environment. The objective of this research is to examine the morphodynamics (i.e interaction between flow, sediment transport, and bed morphology) of the Choked Passage seagrass meadow.

This thesis is organized into two research chapters with different, but related research questions:

- Chapter 2.0: How do storm events influence seagrass and bed level? and are bed-level changes linked to changes in seagrass coverage?
- Chapter 3.0: How does tidal flow behave within and outside of the meadow? and do tidal currents drive sediment transport in Choked Passage?

1.60 Bibliography

Allaoui, N. E., Serra, T., Colomer, J., Soler, M., Casamitjana, X., & Oldham, C. (2016). Interactions between Fragmented Seagrass Canopies and the Local Hydrodynamics. *PLOS ONE*, *11*(5), e0156264. https://doi.org/10.1371/journal.pone.0156264

Anthony Stallins, J., & Corenblit, D. (2018). Interdependence of geomorphic and ecologic resilience properties in a geographic context. *Geomorphology*, *305*, 76–93. https://doi.org/10.1016/j.geomorph.2017.09.012

Belcher, S. E., Jerram, N., & Hunt, J. C. R. (2003). Adjustment of a turbulent boundary layer to a canopy of roughness elements. *Journal of Fluid Mechanics*, *488*, 369–398. https://doi.org/10.1017/S0022112003005019

Bell, S. S. (1999). Gap Dynamics in a Seagrass Landscape. *Ecosystems*, *2*(6), 493–504. https://doi.org/10.1007/s100219900097

Beudin, A., Kalra, T. S., Ganju, N. K., & Warner, J. C. (2017). Development of a coupled wave-flow-vegetation interaction model. *Computers & Geosciences*, *100*, 76–86. https://doi.org/10.1016/j.cageo.2016.12.010

Bos, A. R., Bouma, T. J., de Kort, G. L. J., & van Katwijk, M. M. (2007). Ecosystem engineering by annual intertidal seagrass beds: Sediment accretion and modification. *Estuarine, Coastal and Shelf Science*, *74*(1–2), 344–348. https://doi.org/10.1016/j.ecss.2007.04.006

Boström, C., Baden, S., Bockelmann, A.-C., Dromph, K., Fredriksen, S., Gustafsson, C., Krause-Jensen, D., Möller, T., Nielsen, S. L., Olesen, B., Olsen, J., Pihl, L., & Rinde, E. (2014). Distribution, structure and function of Nordic eelgrass (Zostera marina) ecosystems: Implications for coastal management and conservation. *Aquatic Conservation: Marine and Freshwater Ecosystems*, *24*(3), 410–434. https://doi.org/10.1002/aqc.2424

Boström, C., Pittman, S., Simenstad, C., & Kneib, R. (2011). Seascape ecology of coastal biogenic habitats: Advances, gaps, and challenges. *Marine Ecology Progress Series*, *427*, 191–217. https://doi.org/10.3354/meps09051

Bouma, T. J., van Duren, L. A., Temmerman, S., Claverie, T., Blanco-Garcia, A., Ysebaert, T., & Herman, P. M. J. (2007). Spatial flow and sedimentation patterns within patches of epibenthic structures: Combining field, flume and modelling experiments. *Continental Shelf Research*, *27*(8), 1020–1045. https://doi.org/10.1016/j.csr.2005.12.019

Bradley, K., & Houser, C. (2009). Relative velocity of seagrass blades: Implications for wave attenuation in low-energy environments. *Journal of Geophysical Research: Earth Surface*, *114*(F1). https://doi.org/10.1029/2007JF000951

Carr, J. A., D'Odorico, P., McGlathery, K. J., & Wiberg, P. L. (2016). Spatially explicit feedbacks between seagrass meadow structure, sediment and light: Habitat suitability for seagrass growth. *Advances in Water Resources*, *93*, 315–325. https://doi.org/10.1016/j.advwatres.2015.09.001

Chen, S.-N., Sanford, L. P., Koch, E. W., Shi, F., & North, E. W. (2007). A nearshore model to investigate the effects of seagrass bed geometry on wave attenuation and suspended sediment transport. *Estuaries and Coasts*, *30*(2), 296–310. https://doi.org/10.1007/BF02700172

Colomer, J., Soler, M., Serra, T., Casamitjana, X., & Oldham, C. (2017). Impact of anthropogenically created canopy gaps on wave attenuation in a Posidonia oceanica seagrass meadow. *Marine Ecology Progress Series*, *569*, 103–116. https://doi.org/10.3354/meps12090

de Boer, W. F. (2007). Seagrass–sediment interactions, positive feedbacks and critical thresholds for occurrence: A review. *Hydrobiologia*, *591*(1), 5–24. https://doi.org/10.1007/s10750-007-0780-9

de los Santos, C. B., Krause-Jensen, D., Alcoverro, T., Marbà, N., Duarte, C. M., van Katwijk, M. M., Pérez, M., Romero, J., Sánchez-Lizaso, J. L., Roca, G., Jankowska, E., Pérez-Lloréns, J. L., Fournier, J., Montefalcone, M., Pergent, G., Ruiz, J. M., Cabaço, S., Cook, K., Wilkes, R. J., … Santos, R. (2019). Recent trend reversal for declining European seagrass meadows. *Nature Communications*, *10*(1), 3356. https://doi.org/10.1038/s41467-019-11340-4

Duarte, C. M. (1991). Seagrass depth limits. *Aquatic Botany*, *40*(4), 363–377. https://doi.org/10.1016/0304-3770(91)90081-F

Duarte, C. M., Fourqurean, J. W., Krause-Jensen, D., & Olesen, B. (2006). Dynamics of Seagrass Stability and Change. In A. W. D. LARKUM, R. J. ORTH, & C. M. DUARTE (Eds.), *SEAGRASSES: BIOLOGY, ECOLOGYAND CONSERVATION* (pp. 271–294). Springer Netherlands. https://doi.org/10.1007/978-1-4020-2983-7_11

Dunic, J. C., Brown, C. J., Connolly, R. M., Turschwell, M. P., & Côté, I. M. (2021). Long-term declines and recovery of meadow area across the world's seagrass bioregions. *Global Change Biology*, *27*(17), 4096-4109.

Durán, O., Andreotti, B., & Claudin, P. (2012). Numerical simulation of turbulent sediment transport, from bed load to saltation. *Physics of Fluids*, *24*(10), 103306. https://doi.org/10.1063/1.4757662

Dyer, K. R., & New, A. L. (1986). INTERMITTENCY IN ESTUARINE MIXING. In D. A. Wolfe (Ed.), *Estuarine Variability* (pp. 321–339). Academic Press. https://doi.org/10.1016/B978-0-12-761890-6.50025-3

Fahrig, L. (2003). Effects of Habitat Fragmentation on Biodiversity. *Annual Review of Ecology, Evolution, and Systematics*, *34*(1), 487–515. https://doi.org/10.1146/annurev.ecolsys.34.011802.132419

Finnigan, J. (n.d.). Turbulence in plant canopies. *Ann. Rev. Fluid Mech*, 519–571.

Folkard, A. M. (2005). Hydrodynamics of model Posidonia oceanica patches in shallow water. *Limnology and Oceanography*, *50*(5), 1592–1600. https://doi.org/10.4319/lo.2005.50.5.1592

Folkard, A. M. (2019). Biophysical Interactions in Fragmented Marine Canopies: Fundamental Processes, Consequences, and Upscaling. *Frontiers in Marine Science*, *6*. https://doi.org/10.3389/fmars.2019.00279

Follett, E. M., & Nepf, H. M. (2012). Sediment patterns near a model patch of reedy emergent vegetation. *Geomorphology*, *179*, 141–151.https://doi.org/10.1016/j.geomorph.2012.08.006

Fonseca, M. S., Koehl, M. A. R., & Kopp, B. S. (2007). Biomechanical factors contributing to self-organization in seagrass landscapes. *Journal of Experimental Marine Biology and Ecology*, *340*(2), 227–246. https://doi.org/10.1016/j.jembe.2006.09.015

Frederiksen, M., Krause-Jensen, D., Holmer, M., & Laursen, J. S. (2004). Spatial and temporal variation in eelgrass (Zostera marina) landscapes: Influence of physical setting. *Aquatic Botany*, *78*(2), 147–165. https://doi.org/10.1016/j.aquabot.2003.10.003

Ganthy, F., Sottolichio, A., & Verney, R. (2013). Seasonal modification of tidal flat sediment dynamics by seagrass meadows of Zostera noltii (Bassin d'Arcachon, France). *Journal of Marine Systems*, *109–110*, S233–S240. https://doi.org/10.1016/j.jmarsys.2011.11.027

Ghisalberti, M., & Nepf, H. M. (2002). Mixing layers and coherent structures in vegetated aquatic flows. *Journal of Geophysical Research: Oceans*, *107*(C2), 3-1-3–11. https://doi.org/10.1029/2001JC000871

Gruber, R. K., & Kemp, W. M. (2010). Feedback effects in a coastal canopy-forming submersed plant bed. *Limnology and Oceanography*, *55*(6), 2285–2298. https://doi.org/10.4319/lo.2010.55.6.2285

Hansen, J. C. R., & Reidenbach, M. A. (2013). Seasonal Growth and Senescence of a Zostera marina Seagrass Meadow Alters Wave-Dominated Flow and Sediment Suspension Within a Coastal Bay. *Estuaries and Coasts*, *36*(6), 1099–1114. https://doi.org/10.1007/s12237-013-9620-5

Hansen, J. C. R., & Reidenbach, M. A. (2017). Turbulent mixing and fluid transport within Florida Bay seagrass meadows. *Advances in Water Resources*, *108*, 205–215. https://doi.org/10.1016/j.advwatres.2017.08.001

Hansen, J., & Reidenbach, M. (2012). Wave and tidally driven flows in eelgrass beds and their effect on sediment suspension. *Marine Ecology Progress Series*, *448*, 271–287. https://doi.org/10.3354/meps09225

Hasegawa, N., Hori, M., & Mukai, H. (2008). Seasonal changes in eelgrass functions: Current velocity reduction, prevention of sediment resuspension, and control of sediment–water column nutrient flux in relation to eelgrass dynamics. *Hydrobiologia*, *596*(1), 387–399. https://doi.org/10.1007/s10750-007-9111-4

Heide, T. van der, Bouma, T. J., Nes, E. H. van, Koppel, J. van de, Scheffer, M., Roelofs, J. G. M., Katwijk, M. M. van, & Smolders, A. J. P. (2010). Spatial self-organized patterning in seagrasses along a depth gradient of an intertidal ecosystem. *Ecology*, *91*(2), 362–369. https://doi.org/10.1890/08-1567.1

Herman, P. M. J., Middelburg, J. J., & Heip, C. H. R. (2001). Benthic community structure and sediment processes on an intertidal flat: Results from the ECOFLAT project. *Continental Shelf Research*, *21*(18), 2055–2071. https://doi.org/10.1016/S0278-4343(01)00042-5

Hjulstrom, F. (1939). *Transportation of Detritus by Moving Water: Part 1. Transportation*. *142*, 5–31.

Hughes, B. B., Eby, R., Dyke, E. V., Tinker, M. T., Marks, C. I., Johnson, K. S., & Wasson, K. (2013). Recovery of a top predator mediates negative eutrophic effects on seagrass. *Proceedings of the National Academy of Sciences*, *110*(38), 15313–15318. https://doi.org/10.1073/pnas.1302805110

Jankowska, E., Włodarska-Kowalczuk, M., Kotwicki, L., Balazy, P., & Kuliński, K. (2014). Seasonality in vegetation biometrics and its effects on sediment characteristics and meiofauna in Baltic seagrass meadows. *Estuarine, Coastal and Shelf Science*, *139*, 159–170. https://doi.org/10.1016/j.ecss.2014.01.003

Koch, E. W., Ackerman, J. D., Verduin, J., & Keulen, M. van. (2006). Fluid Dynamics in Seagrass Ecology—From Molecules to Ecosystems. In A. W. D. LARKUM, R. J. ORTH, & C. M. DUARTE (Eds.), *SEAGRASSES: BIOLOGY, ECOLOGYAND CONSERVATION* (pp. 193–225). Springer Netherlands. https://doi.org/10.1007/978-1-4020-2983-7_8

Kundu, P. K., Cohen, I. M., & Dowling, D. R. (2015). *Fluid Mechanics*. Academic Press.

Lacy, J. R., & Wyllie-Echeverria, S. (2011). The influence of current speed and vegetation density on flow structure in two macrotidal eelgrass canopies: A field study of eelgrass hydrodynamics. *Limnology and Oceanography: Fluids and Environments*, *1*(1), 38–55. https://doi.org/10.1215/21573698-1152489

Larkum, A. W., Orth, R. J., & Duarte, C. M. (2006). Seagrasses: biology, ecology and conservation. *Phycologia*, *45*(5), 5.

Larsen, L. G., & Harvey, J. W. (2011). Modeling of hydroecological feedbacks predicts distinct classes of landscape pattern, process, and restoration potential in shallow aquatic ecosystems. *Geomorphology*, *126*(3–4), 279–296. https://doi.org/10.1016/j.geomorph.2010.03.015

Lawson, S. E., Wiberg, P. L., McGlathery, K. J., & Fugate, D. C. (2007). Wind-driven sediment suspension controls light availability in a shallow coastal lagoon. *Estuaries and Coasts*, *30*(1), 102–112. https://doi.org/10.1007/BF02782971

Lawson, S., McGlathery, K., & Wiberg, P. (2012). Enhancement of sediment suspension and nutrient flux by benthic macrophytes at low biomass. *Marine Ecology Progress Series*, *448*, 259–270. https://doi.org/10.3354/meps09579

Le Roux, J. P. (2004). An integrated law of the wall for hydrodynamically transitional flow over plane beds. *Sedimentary Geology*, *163*(3–4), 311–321. https://doi.org/10.1016/j.sedgeo.2003.07.005

Lefebvre, A., Ernstsen, V. B., & Winter, C. (2013). Estimation of roughness lengths and flow separation over compound bedforms in a natural-tidal inlet. *Continental Shelf Research*, *61–62*, 98–111. https://doi.org/10.1016/j.csr.2013.04.030

Lefebvre, A., Paarlberg, A. J., Ernstsen, V. B., & Winter, C. (2014). Flow separation and roughness lengths over large bedforms in a tidal environment: A numerical investigation. *Continental Shelf Research*, *91*, 57–69. https://doi.org/10.1016/j.csr.2014.09.001

Lefebvre, A., Thompson, C. E. L., & Amos, C. L. (2010). Influence of Zostera marina canopies on unidirectional flow, hydraulic roughness and sediment movement. *Continental Shelf Research*, *30*(16), 1783–1794. https://doi.org/10.1016/j.csr.2010.08.006

Luhar, M., Rominger, J., & Nepf, H. (2008). Interaction between flow, transport and vegetation spatial structure. *Environmental Fluid Mechanics*, *8*(5–6), 423–439. https://doi.org/10.1007/s10652-008-9080-9

Mills, M., Leon, J. X., Saunders, M. I., Bell, J., Liu, Y., O'Mara, J., Lovelock, C. E., Mumby, P. J., Phinn, S., Possingham, H. P., Tulloch, V. J. D., Mutafoglu, K., Morrison, T., Callaghan, D. P., Baldock, T., Klein, C. J., & Hoegh-Guldberg, O. (2016). Reconciling Development and Conservation under Coastal Squeeze from Rising Sea Level. *Conservation Letters*, *9*(5), 361–368. https://doi.org/10.1111/conl.12213

Moksnes, P.-O., Eriander, L., Infantes, E., & Holmer, M. (2018). Local Regime Shifts Prevent Natural Recovery and Restoration of Lost Eelgrass Beds Along the Swedish West Coast. *Estuaries and Coasts*, *41*(6), 1712–1731. https://doi.org/10.1007/s12237-018-0382-y

Moore, K. A. (2004). Influence of Seagrasses on Water Quality in Shallow Regions of the Lower Chesapeake Bay. *Journal of Coastal Research*, *10045*, 162–178. https://doi.org/10.2112/SI45-162.1

Nepf, H. M. (1999). Drag, turbulence, and diffusion in flow through emergent vegetation. *Water Resources Research*, *35*(2), 479–489. https://doi.org/10.1029/1998WR90006

Nepf, H. M. (2012). Hydrodynamics of vegetated channels. *Journal of Hydraulic Research*, *50*(3), 262–279. https://doi.org/10.1080/00221686.2012.696559

Nyström, M., Norström, A. V., Blenckner, T., de la Torre-Castro, M., Eklöf, J. S., Folke, C., Österblom, H., Steneck, R. S., Thyresson, M., & Troell, M. (2012). Confronting Feedbacks of Degraded Marine Ecosystems. *Ecosystems*, *15*(5), 695–710. https://doi.org/10.1007/s10021-012-9530-

Olesen, B., & Sand-Jensen, K. (1994). Biomass-density patterns in the temperate seagrass Zostera marina. *Mar. Ecol. Prog. Ser.*, 9.

Oreska, M. P. J., McGlathery, K. J., & Porter, J. H. (2017). Seagrass blue carbon spatial patterns at the meadow-scale. *PLOS ONE*, *12*(4), e0176630. https://doi.org/10.1371/journal.pone.0176630

Orth, R. J., Carruthers, T. J. B., Dennison, W. C., Duarte, C. M., Fourqurean, J. W., Heck, K. L., Hughes, A. R., Kendrick, G. A., Kenworthy, W. J., Olyarnik, S., Short, F. T., Waycott, M., & Williams, S. L. (2006). A Global Crisis for Seagrass Ecosystems. *BioScience*, *56*(12), 987. https://doi.org/10.1641/0006-3568(2006)56[987:AGCFSE]2.0.CO;2

Orth, R. J., Moore, K. A., Marion, S. R., Wilcox, D. J., & Parrish, D. B. (2012). Seed addition facilitates eelgrass recovery in a coastal bay system. *Marine Ecology Progress Series*, *448*, 177–195. https://doi.org/10.3354/meps09522

Pace, M., Borg, J. A., Galdies, C., & Malhotra, A. (2017). Influence of wave climate on architecture and landscape characteristics of Posidonia oceanica meadows. *Marine Ecology*, *38*(1), e12387. https://doi.org/10.1111/maec.12387

Perlin, A., Moum, J. N., Klymak, J. M., Levine, M. D., Boyd, T., & Kosro, P. M. (2005). A modified law-of-the-wall applied to oceanic bottom boundary layers. *Journal of Geophysical Research: Oceans*, *110*(C10). https://doi.org/10.1029/2004JC002310

Pittman, S. J. (2017). *Seascape Ecology*. John Wiley & Sons.

Ribas, F., Falqués, A., de Swart, H. E., Dodd, N., Garnier, R., & Calvete, D. (2015). Understanding coastal morphodynamic patterns from depth-averaged sediment concentration. *Reviews of Geophysics*, *53*(2), 362–410. https://doi.org/10.1002/2014RG000457

Rippeth, T. P., Williams, E., & Simpson, J. H. (2002). Reynolds Stress and Turbulent Energy Production in a Tidal Channel. *Journal of Physical Oceanography*, *32*(4), 1242–1251. https://doi.org/10.1175/1520-0485(2002)032<1242:RSATEP>2.0.CO;2

Short, F., Carruthers, T., Dennison, W., & Waycott, M. (2007). Global seagrass distribution and diversity: A bioregional model. *Journal of Experimental Marine Biology and Ecology*, *350*(1–2), 3–20. https://doi.org/10.1016/j.jembe.2007.06.012

Short, F. T., & Wyllie-Echeverria, S. (1996). Natural and human-induced disturbance of seagrasses. *Environmental Conservation*, *23*(1), 17–27. https://doi.org/10.1017/S0376892900038212

Spalding, D. B. (1961). A single formula for the law of the wall. *Journal of Applied Mechanics*, *28*(3), 455-458.

Tanner, C. E., & Parham, T. (2010). Growing Zostera marina (eelgrass) from Seeds in Land-Based Culture Systems for Use in Restoration Projects. *Restoration Ecology*, *18*(4), 527–537. https://doi.org/10.1111/j.1526-100X.2010.00693.x

Terrados, J., & Duarte, C. M. (2000). Experimental evidence of reduced particle resuspension within a seagrass (Posidonia oceanica L.) meadow. *Journal of Experimental Marine Biology and Ecology*, *243*(1), 45–53. https://doi.org/10.1016/S0022-0981(99)00110-0

Tinoco, R. O., Juan, J. E. S., & Mullarney, J. C. (2020). Simplification bias: Lessons from laboratory and field experiments on flow through aquatic vegetation. *Earth Surface Processes and Landforms*, *45*(1), 121–143. https://doi.org/10.1002/esp.4743

Turner, M. G. (2010). Disturbance and landscape dynamics in a changing world. *Ecology*, *91*(10), 2833–2849. https://doi.org/10.1890/10-0097.1

Turner, M. G., & Gardner, R. H. (2015). *Landscape Ecology in Theory and Practice*. Springer New York. https://doi.org/10.1007/978-1-4939-2794-4

Uhrin, A. V., & Turner, M. G. (2018). Physical drivers of seagrass spatial configuration: The role of thresholds. *Landscape Ecology*, *33*(12), 2253–2272. https://doi.org/10.1007/s10980-018-0739-4

Vacchi, M., Falco, G. D., Simeone, S., Montefalcone, M., Morri, C., Ferrari, M., & Bianchi, C. N. (2017). Biogeomorphology of the Mediterranean Posidonia oceanica seagrass meadows. *Earth Surface Processes and Landforms*, *42*(1), 42–54. https://doi.org/10.1002/esp.3932

van der Heide, T., van Nes, E. H., Geerling, G. W., Smolders, A. J. P., Bouma, T. J., & van Katwijk, M. M. (2007). Positive Feedbacks in Seagrass Ecosystems: Implications for Success in Conservation and Restoration. *Ecosystems*, *10*(8), 1311–1322. https://doi.org/10.1007/s10021-007-9099-7

van Katwijk, M. M., Bos, A. R., Hermus, D. C. R., & Suykerbuyk, W. (2010). Sediment modification by seagrass beds: Muddification and sandification induced by plant cover and environmental conditions. *Estuarine, Coastal and Shelf Science*, *89*(2), 175–181. https://doi.org/10.1016/j.ecss.2010.06.008

van Katwijk, M. M., Thorhaug, A., Marbà, N., Orth, R. J., Duarte, C. M., Kendrick, G. A., Althuizen, I. H. J., Balestri, E., Bernard, G., Cambridge, M. L., Cunha, A., Durance, C., Giesen, W., Han, Q., Hosokawa, S., Kiswara, W., Komatsu, T., Lardicci, C., Lee, K.-S., … Verduin, J. J. (2016). Global analysis of seagrass restoration: The importance of large-scale planting. *Journal of Applied Ecology*, *53*(2), 567–578. https://doi.org/10.1111/1365-2664.1256

Vargas-Luna, A., Crosato, A., & Uijttewaal, W. S. J. (2015). Effects of vegetation on flow and sediment transport: Comparative analyses and validation of predicting models. *Earth Surface Processes and Landforms*, *40*(2), 157–176. https://doi.org/10.1002/esp.363

Walker, D. I., Kendrick, G. A., & McComb, A. J. (2006). Decline and Recovery of Seagrass Ecosystems—The Dynamics of Change. In A. W. D. LARKUM, R. J. ORTH, & C. M.

DUARTE (Eds.), *SEAGRASSES: BIOLOGY, ECOLOGYAND CONSERVATION* (pp. 551–565). Springer Netherlands. https://doi.org/10.1007/978-1-4020-2983-7_23

Walter, R. K., O'Leary, J. K., Vitousek, S., Taherkhani, M., Geraghty, C., & Kitajima, A. (2020). Large-scale erosion driven by intertidal eelgrass loss in an estuarine environment. *Estuarine, Coastal and Shelf Science*, *243*, 106910. https://doi.org/10.1016/j.ecss.2020.106910

Ward, L. G., Michael Kemp, W., & Boynton, W. R. (1984). The influence of waves and seagrass communities on suspended particulates in an estuarine embayment. *Marine Geology*, *59*(1), 85–103. https://doi.org/10.1016/0025-3227(84)90089-6

Waycott, M., Duarte, C. M., Carruthers, T. J. B., Orth, R. J., Dennison, W. C., Olyarnik, S., Calladine, A., Fourqurean, J. W., Heck, K. L., Hughes, A. R., Kendrick, G. A., Kenworthy, W. J., Short, F. T., & Williams, S. L. (2009). Accelerating loss of seagrasses across the globe threatens coastal ecosystems. *Proceedings of the National Academy of Sciences*, *106*(30), 12377–12381. https://doi.org/10.1073/pnas.0905620106

Wedding, L., Lepczyk, C., Pittman, S., Friedlander, A., & Jorgensen, S. (2011). Quantifying seascape structure: Extending terrestrial spatial pattern metrics to the marine realm. *Marine Ecology Progress Series*, *427*, 219–232. https://doi.org/10.3354/meps09119

Widdows, J., Pope, N., Brinsley, M., Asmus, H., & Asmus, R. (2008). Effects of seagrass beds (Zostera noltii and Z. marina) on near-bed hydrodynamics and sediment resuspension. *Marine Ecology Progress Series*, *358*, 125–136. https://doi.org/10.3354/meps07338

Williams, S. L. (2007). Introduced species in seagrass ecosystems: Status and concerns. *Journal of Experimental Marine Biology and Ecology*, *350*(1–2), 89–110. https://doi.org/10.1016/j.jembe.2007.05.032

Wright, L. D., & Thom, B. G. (1977). Coastal depositional landforms: a morphodynamic approach. *Progress in Physical Geography*, *1*(3), 412-459.

Yager, E. M., & Schmeeckle, M. W. (2013). The influence of vegetation on turbulence and bed load transport. *Journal of Geophysical Research: Earth Surface*, *118*(3), 1585–1601. https://doi.org/10.1002/jgrf.20085

Yarnall, A. H., Byers, J. E., Yeager, L. A., & Fodrie, F. J. (2022). Comparing edge and fragmentation effects within seagrass communities: A meta-analysis. *Ecology*, *103*(3), e3603. https://doi.org/10.1002/ecy.3603

Zhu, Q., Wiberg, P. L., & Reidenbach, M. A. (2021). Quantifying Seasonal Seagrass Effects on Flow and Sediment Dynamics in a Back-Barrier Bay. *Journal of Geophysical Research: Oceans*, *126*(2), e2020JC016547. https://doi.org/10.1029/2020JC016547

Zong, L., & Nepf, H. (2011). Spatial distribution of deposition within a patch of vegetation: DEPOSITION PATTERN WITHIN A PATCH. *Water Resources Research*, *47*(3). https://doi.org/10.1029/2010WR009516

2.0 Bio-geomorphic response of an exposed seagrass meadow to storm events

2.10 Abstract

Seagrasses serve as ecosystem engineers by providing critical habitat and reducing near bed flow velocities to shield the bed from erosion and sediment suspension. Seagrass loss can enhance erosion and sediment suspension, which can be initiated through short-lived extreme events, or chronic long-term disturbances. Natural and anthropogenic disturbances can govern the evolution of seagrass meadows. This study examined how climate variability and storms influence seagrass and bed morphology in the Choked Passage seagrass meadow off the Central Coast of British Columbia. We used high resolution multibeam echosounder (MBES) bathymetry and backscatter data from 2018 and 2021, drone mapped seagrass delineations from 2014 to 2021, and wind and wave data from 2014 to 2021. From 2018 to 2021, the meadow experienced significant erosion and loss of seagrass, which we attribute to the preceding winter storm activity driven by moderate La Niña conditions. Coupled erosion and seagrass loss resulted in the generation or expansion of blowouts. The spatial patterns of erosion and seagrass loss was non-uniform across the meadow and at times decoupled. In locations where seagrass loss was decoupled from bed level changes, we observed increased fragmentation without blowout formation. We observed a reduction in seagrass coverage following winters with a high number of storm events and/or high recorded storm intensity from 2014 to 2021. We believe the Choked Passage seagrass meadow undergoes cyclic behaviour with reduction in seagrass coverage during energetic ENSO years, followed by a recovery period during weak years, which is likely coupled to sediment erosion and deposition in certain areas of the meadow. Geomorphic processes and disturbances have an important influence on ecosystem structure and function over time, therefore, it is important to understand how these processes operate and are modified by external drivers. Climate variability is predicted to increase, while seagrasses continue to decline worldwide, and effort should be made to understand how seagrass will respond to the changing climate.

2.20 Introduction

Globally, there has been a rapid decline in seagrasses due to a myriad of anthropogenic stressors (Waycott et al., 2009), such as deteriorating water quality, coastal development, and climate change (Orth et al., 2006). Seagrasses are marine flowering plants that are widely

distributed across temperate and tropical coastlines (Short et al., 2007). Seagrasses are ecosystem engineers (Bos et al., 2007), forming extensive meadows that provide critical habitat, modulate local hydrodynamics, sediment transport, and biogeochemical processes (Duarte & Chiscano, 1999). Their canopies induce drag on flow to attenuate flow and reduce near-bed flow velocities (Hansen & Reidenbach, 2012; Koch et al., 2006). This process shields the seabed from shear stress, erosion, and sediment suspension. Alternatively, loss or changes to seagrass habitat can enhance erosion and sediment suspension, which can be initiated through short-lived extreme events, or chronic long-term disturbances (Boström et al., 2017; Cabaço et al., 2008).

Natural and anthropogenic disturbances can govern the evolution of seagrass meadows (Short & Wyllie-Echeverria, 1996; Walter, 2020). Large disturbances can cause seagrass mortality and/or blade uprooting, which destabilizes the sediment to cause erosion (Robbins & Bell, 2000). For example, a recent study observed a regime shift to an erosional environment following severe collapse of *Z. marina* due to cumulative effects of dredging, siltation, and shifting climate in the Morro Bay estuary, CA, USA (Walter, 2020). Another study documented a 50% loss in *Posidonia oceanica*, coupled with significant sediment erosion and burial after an extreme storm event in the NW Mediterranean (Oprandi et al., 2020). Under certain conditions, wave exposure and storm activity can be linked to gap formation and habitat fragmentation within seagrass meadows (Bell, 1999; Frederiksen et al., 2004; Pace et al., 2017; Stevens & Lacy, 2012).

The frequency and intensity of natural disturbances are controlled by weather patterns, climate change, and El Niño–Southern Oscillation (ENSO). Strong ENSO events (*i.e.* El Niño and La Niña) can cause severe storms and lead to coastal erosion on the Pacific Coast of North America (Barnard et al., 2015, 2017). The increase in wave energy and storm severity associated with these events can reduce seagrass coverage, increase fragmentation and canopy gaps, and erode sediment (Duarte, 2002; Oprandi et al., 2020; Short & Wyllie-Echeverria, 1996). Given their high ecological value, it is important to understand the physical processes that drive the distribution and health of seagrass meadows, particularly under a changing climate (Orth et al., 2006).

Seagrass meadows are a mosaic of seagrass patches, embedded with patches of unvegetated sediment, where biotic and abiotic factors control their spatial pattern (Frederiksen

et al., 2004). Remote sensing techniques, such as drones and multibeam acoustic echosounders (MBES or multibeam) are well-suited to examine the complex patterns and biophysical changes (e.g. sediment and seagrass coverage) within a seagrass meadow (Gumusay et al., 2019). Multibeams can be used to map seabed bathymetry and substrate types (Brown et al., 2019), while drones can produce high resolution seagrass delineations (Nahirnick et al., 2019). These methods together can help identify the relationship between seagrass and bed morphology. Moreover, by pairing these data sources with climatological data, we can determine how storms and climate variability influences the spatial pattern of seagrass and bed morphology.

Most field studies on sediment and seagrass dynamics have occurred in relatively low-energy estuarine systems (Carr et al., 2016; Hansen & Reidenbach, 2013; Hansen & Reidenbach, 2012; Nardin et al., 2018). Therefore, our current understanding of these biophysical processes may not be relevant to all seagrass systems. Off the Central Coast of British Columbia, Canada, the *Zostera marina* seagrass meadow within Choked Passage is exposed to significant current and wave energy (Prentice et al., 2019) and is relatively free from human disturbance. Therefore, this site presents a unique opportunity to study to natural biophysical processes operating in an undeveloped and hydrodynamically exposed environment. The objective of this study is to examine the relationship between the seagrass meadow and bed morphology over time and whether changes to seagrass and sediment are linked to storm activity and climate variability. Specifically, we will answer the following questions: 1) How do storm events influence seagrass and bed level? and 2) are bed-level changes linked to changes in seagrass coverage? To answer these questions, we analyzed high resolution bathymetry data from 2018 and 2021, seagrass delineations from 2014 to 2021, and wind and wave observations from 2014 to 2021. The results from this research will provide important insight into the geomorphology of seagrass meadows and generate novel information on the dynamics of a large meadow in a high-energy environment.

2.21 Study Area

Choked Passage is located on Calvert Island, approximately 60 km north of Vancouver Island, British Columbia (Figure 1). The Choked Passage seagrass meadow is situated on a shallow shoal in water depths of -2.0 m to -11.0 m. The meadow is one of the largest in the region with near-contiguous area of 367,300 m^2 (Olson *et al.,* 2018), an average blade density of

81 m^2, and blade length of 1.65 m (Monteith et al., 2021). This meadow is situated between Calvert Island (334 km^2) to the east and exposed islets to the west. Kelp forests of *Nereocystis luetkeana* form around the rocky reefs, and large patches of unvegetated sand are located along the shoreline of Calvert Island (Olson et al., 2019). The bottom substrate is predominately coarse to fine sand with a high shell content. This area is highly dynamic, with minimal freshwater input, in a macro-tidal setting with high-current tidal exchanges (Prentice et al., 2019; Hakai, 2021).

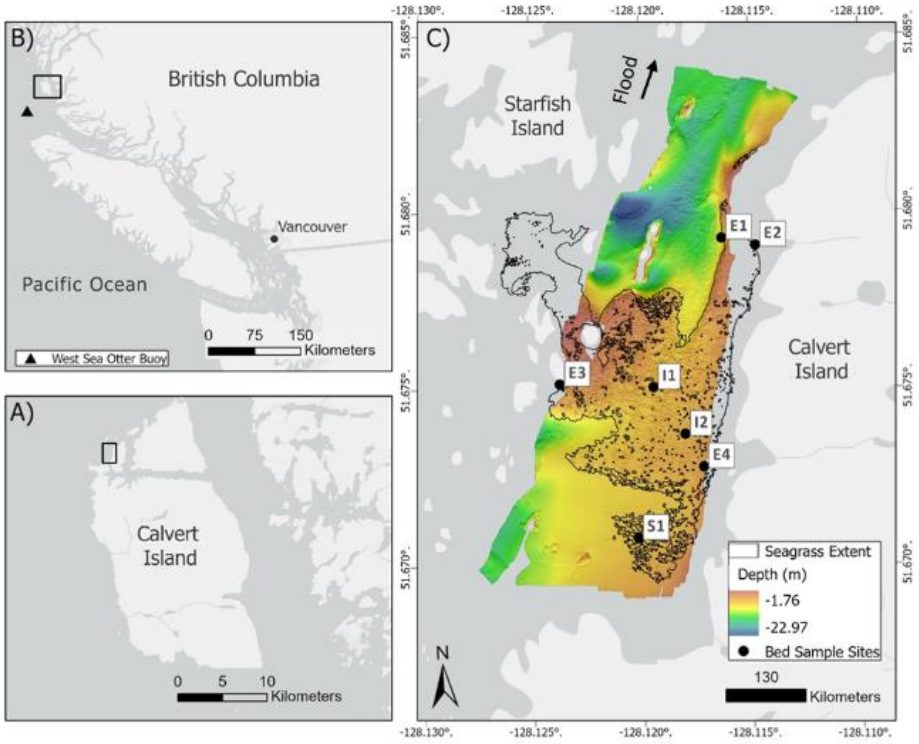

Figure 1 - (A) Map of Choked Passage on the northwest of Calvert Island, British Columbia, Canada (B), showing (C) 2021 bathymetry and seagrass extent, seabed sample site locations, and direction of flood flow. Seagrass data was provided by the Hakai Institute and data from the West Sea Otter Buoy (#46204) was acquired from the Department of Fisheries and Oceans (DFO).

2.30 Methods

2.31 Storm and Weather Analysis

Hourly wave and wind observation data was acquired from the Department of Fisheries and Oceans (DFO) West Sea Otter station (#46204; Figure 1 A). First, the data was subset from 2012-2022 to determine a 10-year monthly baseline of significant wave height (m), wind speed

(m/s), and wind direction (°). A 14-day moving average was calculated from the raw significant wave height data from 2014 to 2021 to match our observation period. Next, the wave data was subset to include only observations during the months of January, February, March, October, November, and December of each year, as significant storms occur during these winter months. The number of hourly measurements per winter month greater than 3 times the standard deviation of that month from the 10-year baseline were extracted from 2014 to 2021. It is assumed that these events represent true significant wave events with the ability to perform geomorphic work. The Oceanic Niño Index values (i.e. ENSO strength indicator based on sea surface temperature) for each year from 2014 to 2022 were obtained from the National Oceanic Atmospheric Administration (NOAA) National Weather Service Climate Prediction Center (NOAA, 2022).

2.32 Seagrass Spatial Analysis

The Hakai Institute has performed unmanned aerial vehicle (UAV) surveys to acquire ortho-mosaic images of Choked Passage and map the seagrass extent each summer since 2014. The seagrass area was calculated for each shapefile from 2014 to 2021. To determine the changes in seagrass extent for the years with MBES surveys, each shapefile was converted to a Boolean raster, where 1 = seagrass presence and 0 = no seagrass. Simple raster math was performed between the 2018 and 2021 seagrass Boolean raster's to calculate whether each cell experienced seagrass loss, gain, or no change.

To examine seagrass structure, spatial pattern metrics were calculated for 2021 using FRAGSTATS. First, the meadow was segmented into zones for analysis. Next, we calculated the Shape Index and Perimeter-Area Fractal Dimension for 2021. Shape Index is the ratio between the patch perimeter and a hypothetical minimum patch perimeter to describe patch complexity. The Perimeter-Area Fractal Dimension describes the patch complexity independent of scale (McGarigal et al., 2012).

2.33 MBES Data Collection & Processing

Multibeam echo-sounders (MBES) emit short length acoustic pings that transmit acoustic energy to the seafloor in a fan-shaped swath (Parnum & Gavrilov, 2011). The ping is scattered off the bed and returns to the receiver array, while the length of time delay and the angle of returning ping are used to calculate bathymetric and morphological parameters of the bed

(Lamarche & Lurton, 2018). In July and August of 2018, the Hakai Institute surveyed Choked Passage using a Teledyne Seabat Reson T50-R MBES mounted to the hull of a 23 ft aluminum research vessel (Hakai Blue). On May 6-8th and August 4-5th 2021, Choked Passage was surveyed again using a Norbit iWBMS Turnkey MBES mounted to the Hakai Blue. Data was collected at 400-550 kHz with an FM beam form, dynamic ping rate, and auto pulse width. An AML Minos X sensor was deployed at the beginning and end of each survey day to measure sound velocity profiles of the water column.

To examine geomorphic changes within the meadow, seagrass was removed from the bathymetry surfaces. Otherwise, natural changes in the seagrass meadow would be interpreted as bed-level changes. Each point cloud was imported into Cloud Compare, and a Cloth Simulation Filter (CSF) was performed to extract ground points (Zhang et al., 2016). The filtered point cloud was exported as a raster at 1 m resolution and loaded into ArcGIS. A shapefile of the 2018 and 2021 meadow extent was used as a mask to clip the meadow from the raster. The clipped raster was aggregated into a 2 m resolution with each cell containing the minimum value of each input cell, to ensure the cell value was that of the seabed and not vegetation. Next, the 2 m raster of the meadow was merged with a 2 m raster of Choked Passage without a CSF filter. Figure 3 shows the depth profile of the bathymetry with seagrass (A) and after the seagrass was removed (B). The combination of CSF and aggregation sufficiently removed the seagrass from the seabed (Figure 3 C & E). Finally, the .tiff raster files were loaded into Cloud Compare and co-registered in the z-direction to each surface.

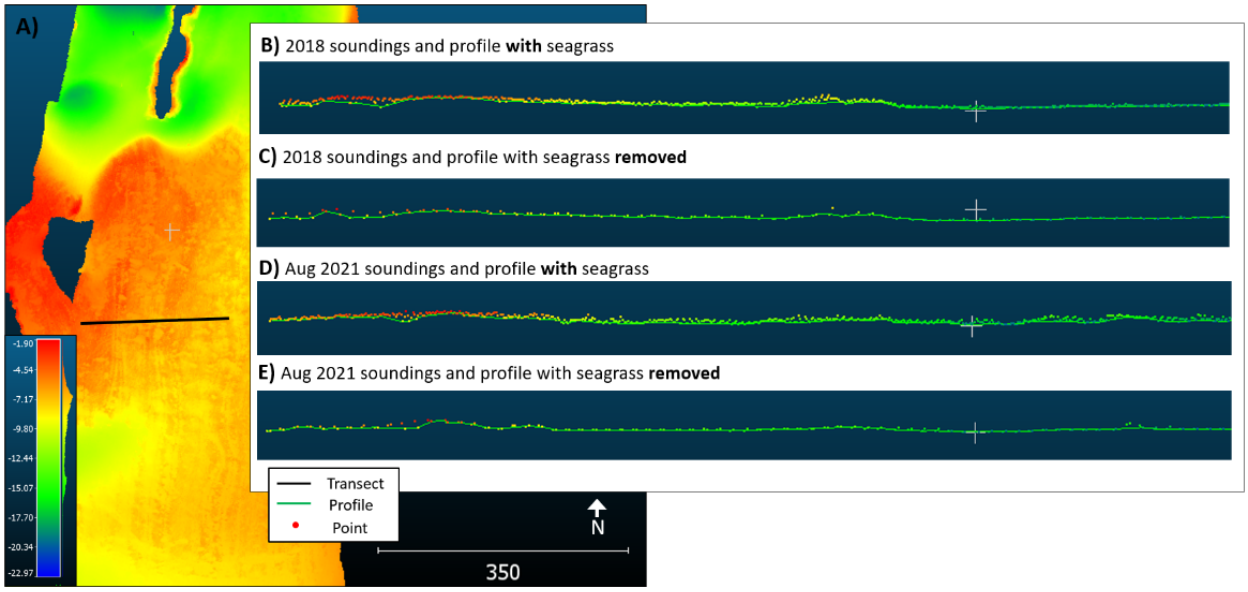

Figure 2 – Confirmation of seagrass removal from MBES bathymetry necessary for surface differencing. A) Point cloud of August 2021 MBES bathymetry (m) and transect line in Cloud Compare, B) July/August 2018 MBES soundings and profile with seagrass soundings and C) without seagrass soundings, D) August 2021 MBEs soundings and profile with seagrass soundings and E) without seagrass soundings.

2.34 Change Detection - M3C2

The Multiscale Model to Model Cloud Comparison (M3C2) plugin was used in Cloud Compare to quantify bed-level changes from each surface (Lague et al., 2013). The M3C2 algorithm works exclusively on the point cloud (i.e. not gridded surfaces) to calculate the local distance between two clouds, and uses the roughness and registration error to estimate the 95% confidence interval of each points distance estimate (Lague et al., 2013). The registration errors for the co-registered surfaces were 0.093 m, 0.051 m, and 0.093 m. Only distances in the Z-orientation were calculated, to determine the vertical change of each point between each cloud. Finally, the calculated M3C2 distances and significant changes (95% confidence interval) were exported as a 2 m raster.

2.35 Substrate Classification

The backscatter data and cleaned bathymetry files were processed using QPS FMGT software to create backscatter mosaics for the three time periods to be classified. The mosaics, a low pass filtered bathymetry, a hillshade of the bathymetry and a seagrass polygon, all at 1 m resolution were loaded into ArcGIS to perform an unsupervised classification of backscatter following the

methods of Bosma (2019). Using the isocluster tool, a classification of the mosaic was performed based on similar areas. Three classes were identified based on the resulting maps, and prior knowledge of the seafloor. Rock features were identified via two methods: the Arc-Chord Ratio (ACR) rugosity was calculated and areas with steep slopes identified by thresholding ACR. Next a bathymetric position index (BPI) was determined to find areas which are sufficiently different from the surrounding neighbourhood. A sensitivity analysis was performed to derive the best inner and outer radius for calculations in this method. Finally, cells were identified as rock when both the BPI and ACR marked them as outliers from the overall topography. A fourth class was created for all cells containing rock. Lastly, using the seagrass polygon, all cells that were covered by the seagrass polygon, were added to a fifth class, representing seagrass. These steps were performed for all backscatter mosaics from July/August 2018 to May 2021 and August 2021. However, the results were inconsistent with the changes that were detected in the multibeam topography and differed from the other two surfaces. The material that was designated as fine sand around the southern meadow in July/August 2018 and May 2021, was classified as cobble/boulder in August 2021 with little change in bed surface elevation. We suspect some of these errors are related to different water column properties that are not adequately accounted for when creating the mosaic. For this reason, we refrain from showing the August 2021 and discuss pre- and post-storm change using July/August 2018 and May 2021, only.

2.36 Grain Size Analysis

Seven sediment samples were collected by divers from the seabed in Choked Passage in August 2021 (Figure 1 C). Samples were immediately frozen and transported to the lab for grain size analysis. The frozen samples were thawed at room temperature for 24 hrs, and then oven dried at 110°C for 24 hrs. Fragments of organic material (e.g. macro-algae, invertebrates) were removed from the sample prior to drying. The dry samples were burned at 500°C for 1 hr to combust any other organics within the sample. Due to the high shell-content of Choked Passage sediments, clumps and aggregations were broken up by hand, rather than a mortar and pestle to prevent damaging the shells and altering their size. Approximately 500 g of each sample were collected for sieve grain size analysis. The finest grain sediments within the receiving pan were collected for hydrometer analysis of fine sands, silts, and clays (ASTM, 2017; Hossain et al., 2021; Kalra & Manard, 1991).

2.40 Results

2.41 Climate Variability and Seagrass Coverage

The dominant wind direction was South-East from 2014 to 2021 and 2018 to 2021 (Figure 4 A & B) with maximum wind velocities reaching up to 25 m/s. A secondary wind direction was from the North-West, which was enhanced during the 2018 to 2021 period, with wind velocities reaching up to 15 m/s. According to NOAA's Oceanic Niño Index (ONI), the winter of 2015/2016 was a very strong El Niño event, while 2020/2021 and 2021/2022 were both moderate La Niña events (Figure 4 C). All other years were weak ENSO years. Hourly significant wave height (m) observations and a 14-day average are shown in Figure 4 D. The average significant wave height was 2.73 m +/- 0.60 cm during this time period. The winter of 2015 and 2016 had the highest number of hours with increased wave heights (i.e. significant hourly wave height observations greater than 3x the monthly standard deviation) (N > 1500, on average 12h/day), and 2014 had the fewest events (Figure 4 E). The largest significant wave height (0.4 m) was recorded in the winter of 2020 (Figure 4 F).

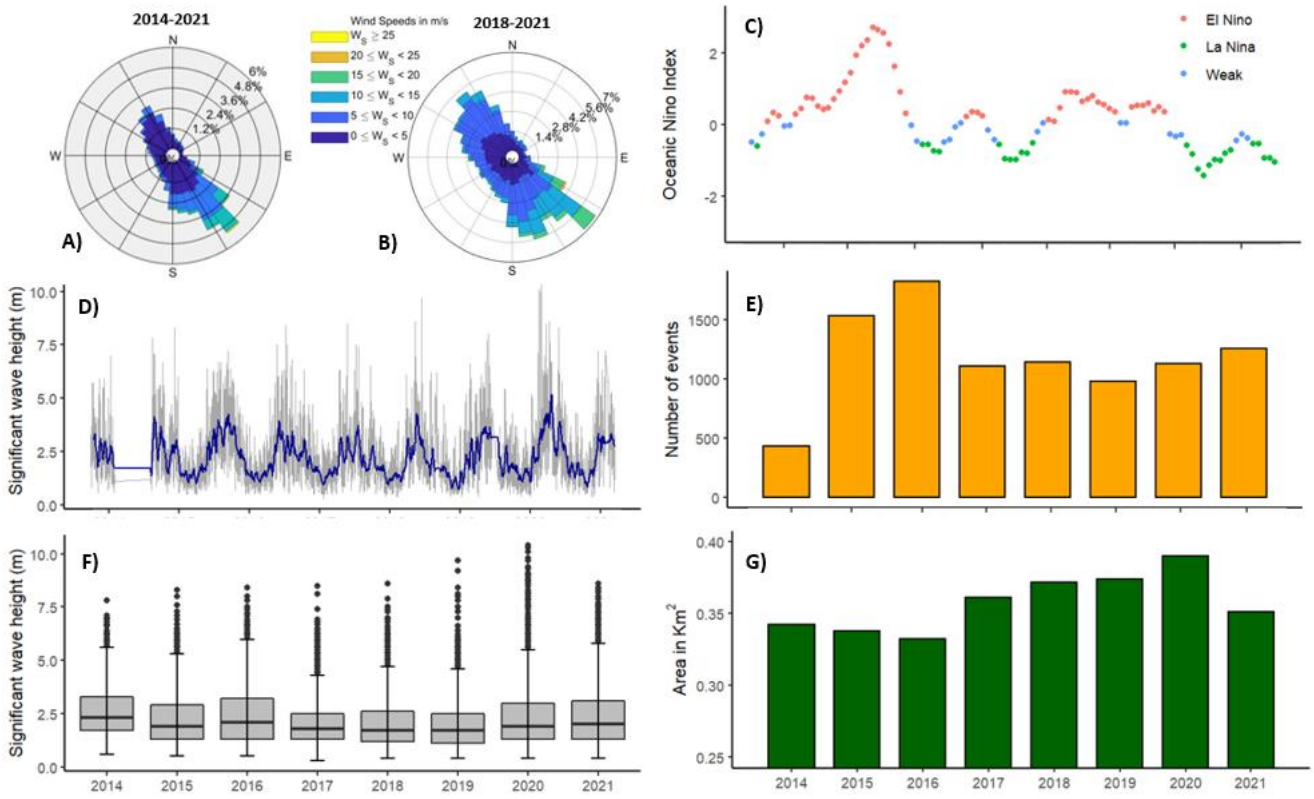

Figure 3 - Wind rose for West Sea Otter station (#46204) from A) 2014 to 2021 and B) 2018 to 2021 showing the distribution of wind speed (w_s, m/s) and direction (°) during both time periods. C) Oceanic Nino Index from 2014- 2021. D) Time series of significant wave height (m) hourly observations (gray line) and a 14-day moving average from West Sea Otter station (#46204). E) The number of winter wave height events greater than or equal to three times the monthly standard deviation for each year from 2014 to 2021. F) Boxplot of hourly significant winter wave height observations per year showing median (black horizontal line, range between 25 and 75 percentile values (grey box) and outliers (dots). G) Choked Passage seagrass meadow area (km^2) from 2014 to 2021, note the y-scale from 0.25 – 0.40 km^2 to emphasize change in area.

The spatial extent of the Choked Pass seagrass meadow varies each year (Figure 4 G), the greatest total coverage occurred in 2020 with 0.39 km^2. There was a slight decrease in area from 2014-2016, followed by an increase from 0.33 km^2 in 2016 to a maximum of 0.39 km^2 in 2020, and a sudden 10% reduction in area in 2021. Figure 5 A shows the change in seagrass coverage from 2018 to 2021, our two observation windows. The southern portion of the meadow experienced the most significant changes and lost a total 12,486 m^2 of seagrass. The rest of the meadow lost a total of 7,601 m^2, most of which occurred in the interior of the North-East and North-West portion of the meadow. The southern portion lost a disproportionate amount of seagrass coverage from 2018 to 2021. Gain in seagrass coverage occurred along the meadow edges, particularly in the South of the main meadow, in the center of the main meadow, and along the corridor connecting the main and southern meadow.

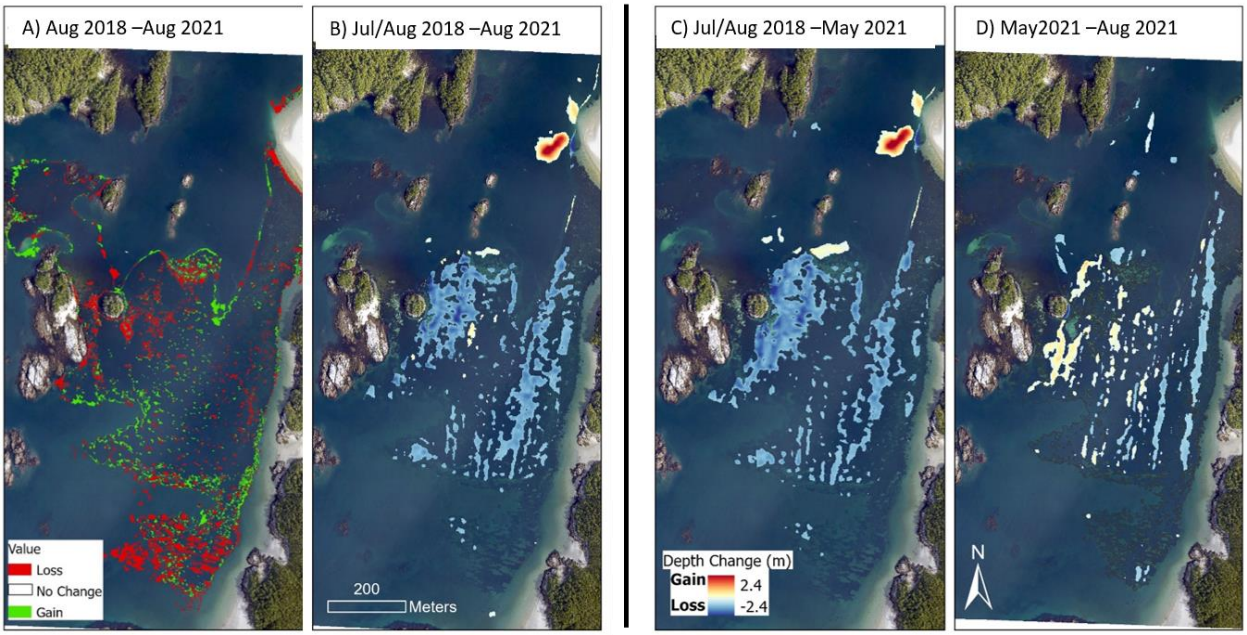

Figure 4 - Change in seagrass cover (A) and significant surface difference (m) at a 95% confidence interval (B) in Choked Passage from Jul/ Aug 2018 - Aug 2021, (C) significant surface difference (m) from Jul/Aug 2018 - May 2021, and (D) May 2021 – Aug 2021. Imagery collected in August 2021 by the Hakai Institute.

2.42 Surface Difference

Within Choked Passage, there were considerable bed-level changes between the survey periods (Figure 5 B-C). The significant surface differences from July/August 2018 – May 2021, May-August 2021, and July/August 2018-August 2021 are presented in Table 1. Overall, Choked Passage experienced erosion and net surface lowering of -18,768 m^3 from Jul/August 2018 to August 2021. Deposition occurred mainly outside the meadow, with a large depositional feature located in the northern part near a sand spit (Figure 6B). We presume that this was formed from a barge beached on the sandspit for the nearby fishing lodge. An erosional feature can be observed on the aerial imagery and is believed to be the source of the material (Figure 6 B). Therefore, we will not include this feature in our discussion and interpretation of natural bed level changes in Choked Passage. Most of the erosion in the meadow (-29,391 m^3) occurred between Jul/August 2018 and May 2021 (Figure 6C), predominately in the North-West and North-East portion of the main meadow, while the center remained stable within the detection limits. Deposition occurred on the slope leading into the meadow in the North-West. From May 2021 to Aug 2021, sediment was deposited in the North-West region and the center of the main meadow, while erosion occurred in the North-East and on the slope leading into the meadow in the North-West (Figure 6D). The volume of material deposited offset the ongoing erosion and a net surface raising occurred (2,630 m^3, Table 1). The southern meadow experienced very little change during both observation periods.

Table 1 – Summary statistics of significant surface differences (m) and volumetric changes (m^3) at 95% confidence intervals between each MBES survey.

Time Period	Mean (m)	SD (m)	Total volume of erosion (m^3)	Total volume of deposition (m^3)	Net surface volume change (m^3)
Jul/Aug 2018 – May 2021	-0.28	0.44	-29,391	+ 6,804	-22,587
May – Aug 2021	0.05	0.28	-5,067	+ 7,697	+ 2,630
Jul/Aug 2018 – Aug 2021	-0.26	0.43	- 25,281	+ 6,513	-18,768

2.43 Seabed Grain Size and Backscatter Characteristics

All seabed sediment samples were predominately sand (Table 2) with differing amounts of shell material. The finest material occurred in the southern meadow (S1) and near the sandspit

in the north (E1), with respective median grain size diameters of 0.13 mm and 0.16 mm. All other samples were slightly coarser, with median grain size diameters between 0.2 mm and 0.25 mm in the main meadow. A significant amount of shell fragments were present in the majority of sediment samples, ranging from whole shells in largest clast size to very fine fragments in the smallest clast size. The southern meadow (S1) and sandspit (E1) samples both contained the least amount of shell fragments. All other sites contained large quantities of shell fragments. The main meadow interior site I1 and western edge (E3) sites all contained the highest proportion of shell fragments.

Table 2 - Grain Size distribution values of seabed sediment samples in Choked Passage collected in August 2021.

Site	D10 (mm)	D30 (mm)	D50 (mm)	D60 (mm)	D90 (mm)
E1	0.084	0.11	**0.16**	0.2	0.33
E2	0.1	0.18	**0.25**	0.3	0.51
E3	0.084	0.125	**0.21**	0.28	0.55
E4	0.09	0.14	**0.22**	0.28	0.50
I1	0.09	0.16	**0.24**	0.3	0.42
I2	0.86	0.12	**0.2**	0.24	0.41
S1	0.09	0.16	**0.13**	0.3	0.4

Three sedimentary classes, one bedrock, and one seagrass class were identified within the Choked Passage seabed from the multibeam backscatter surface for July/August 2018 and May of 2021 (Figure 6). Only these two backscatter surfaces were classified into sediment groups, due to a significant error with the August 2021 backscatter. Two of these classes occurred in the vicinity of our bed sediment samples (Figure 1), which are referred to as Sand (yellow) and Sand/Mixed Shell Hash (blue). Sand was the dominant class within Choked Passage and occupied the greatest area around the meadow and in the southern unvegetated region. The final class, Gravel/Cobble (lavender) is located predominately outside of the meadow in the deeper areas and was identified based on information from the Hakai Institute. Bedrock was identified around rocky outcrops and islands. The major differences between July/August 2018 and May 2021 was the appearance of the large depositional feature made up of sand adjacent to the northern sandspit, some small patches of sand in the deeper northern section outside of the

meadow, and increased gravel/cobble in the southern meadow and the surrounding area (Figure 6 B).

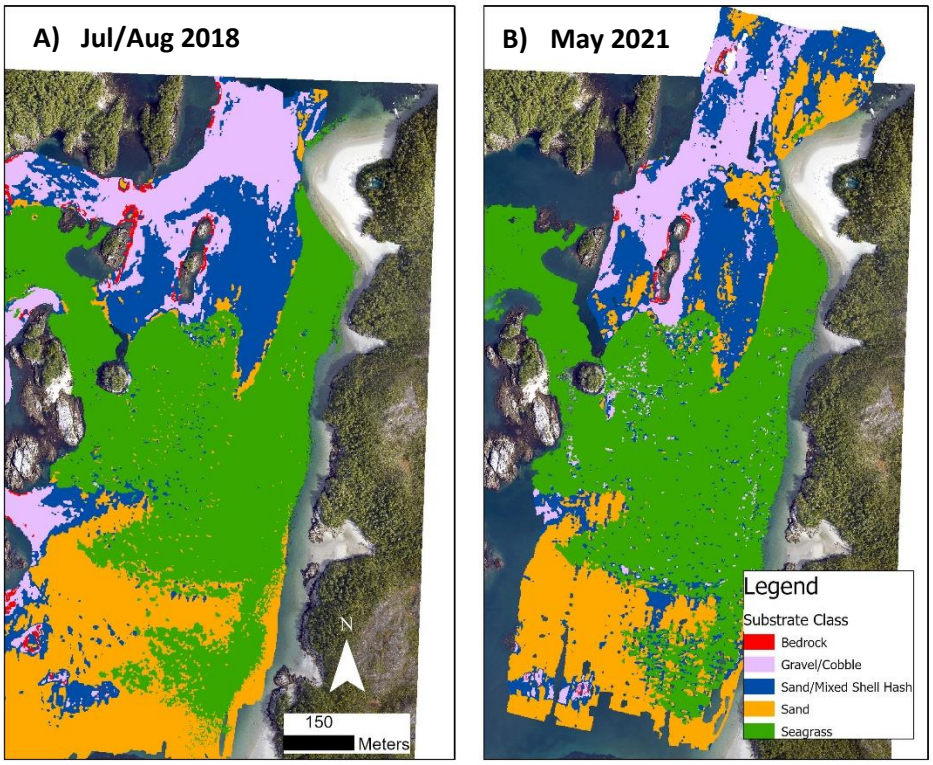

Figure 5 - Substrate classification map of four sedimentary classes and seagrass derived from acoustic multibeam backscatter for A) July/August 2021 and B) May 2021. Imagery provided by the Hakai Institute.

2.44 Zonal differentiation

Choked Passage was segmented into four different zones based on the results of surface differencing, seagrass loss/gain, and general physical setting (Figure 7). Zone 1 experienced the greatest significant erosion and seagrass loss. Zone 2 experienced minor changes, with seagrass growth and a few small patches of erosion and deposition. Zone 3 experienced significant erosion and both seagrass loss and gain within the meadow. Zone 4 encompasses the southern meadow, which lost a significant amount of seagrass coverage but with almost no erosion or deposition.

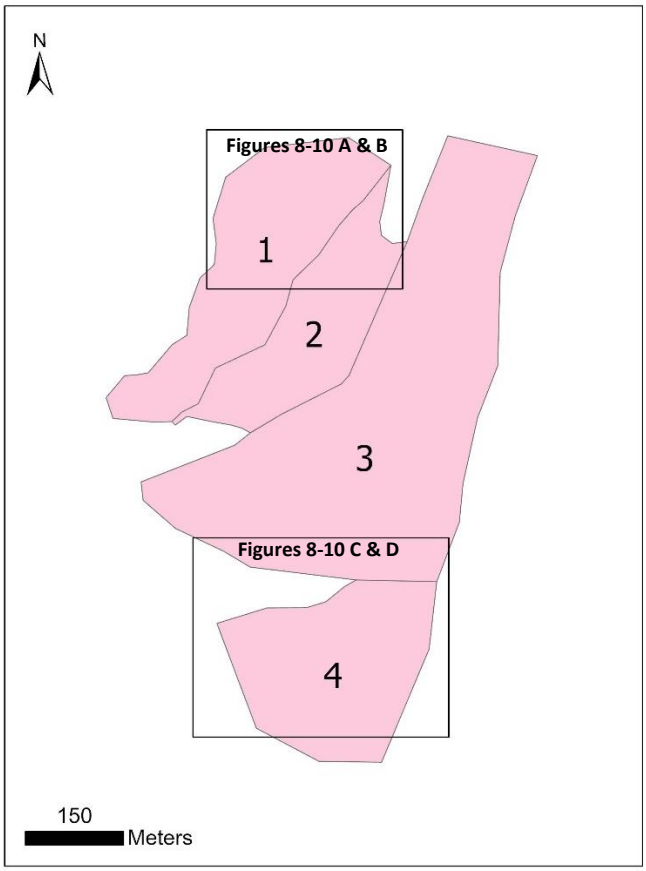

Figure 6 - Map of Choked Passage zones 1-4. Zones are divided based on regions of surface difference and seagrass coverage change from 2018 to 2021.

2.45 Seagrass spatial patterns and seabed surface difference

The spatial pattern metrics for seagrass delineations collected in August 2018 and 2021 are presented in Table 3 along with the significant surface differences for each zone from Jul/Aug 2018 - August 2021. Zone 1 has the highest Patch Shape Index in 2021, followed by Zone 4; Zones 2 and 3 have similar, lower values. All but Zone 2 experienced an increase in Patch Shape Index from 2018 to 2021. Zones 1 and 3 have the greatest Fractal Dimension Index in 2021, followed by Zone 2 and 4. All zones experienced a decrease is Fractal Dimension Index from 2018 to 2021. All four zones experienced overall net surface loss (i.e., erosion). Zone 1 had the greatest amount of erosion per square meter, while Zone 4 had the least amount of surface change. Zone 3 experienced more erosion than Zone 2.

Table 3 – Mean depth (m), spatial pattern metrics from seagrass delineation for July/August 2018 and August 2021, and significant surface differences (95% confidence interval) from 2018 to 2021 for Zones 1-4 in Choked Passage.

Zone	Mean depth (m)	Patch Shape Index Aug 2018	Patch Shape Index Aug 2021	Fractal Dimension Index Aug 2018	Fractal Dimension Index Aug 2021	Total volume of erosion (m^3)	Erosion per area ($m^3\,m^{-2}$)	Total volume of deposition (m^3)	Deposition per area ($m^3\,m^{-2}$)	Net surface volume change ($m^3\,m^2$)
1	-6.43	1.56	2.61	1.26	1.36	-12244.98	-0.18	416.26	0.01	-0.17
2	-7.65	1.93	1.83	1.18	1.05	-1013.56	-0.02	425.60	0.009	-0.012
3	-7.04	1.42	1.86	1.28	1.37	-12801.06	-0.07	23.52	0.0001	-0.07
4	-7.24	1.94	2.26	0.83	1.3	-180.60	-0.003	6.20	0.0001	-0.003

2.46 Seabed morphology and substrate classification

The erosion observed in Zone 1 coincided with the appearance and/or enlargement of blowouts in the North-West, which were visible in the multibeam surface as unvegetated, smooth patches within dense vegetation, and ranged from 5 m – 25 m in diameter (Figure 8 A & B). In the northern-most area of Zone 1, smooth sand waves appear, ranging from 5 m – 25 m in length, and become larger in areas of erosion and seagrass loss (Figure 9 A & B). In Zone 4, the southern meadow, seagrass generally appears to be less dense and patchier than in Zone 1. It appears that seagrass loss led to greater patchiness, without the formation of blowouts or erosion in Zone 4 (Figure 8 & 9 C & D). In the southern edge of Zone 3, a few blowouts appear from 2018 to 2021 (Figure 8 & 9 C & D).

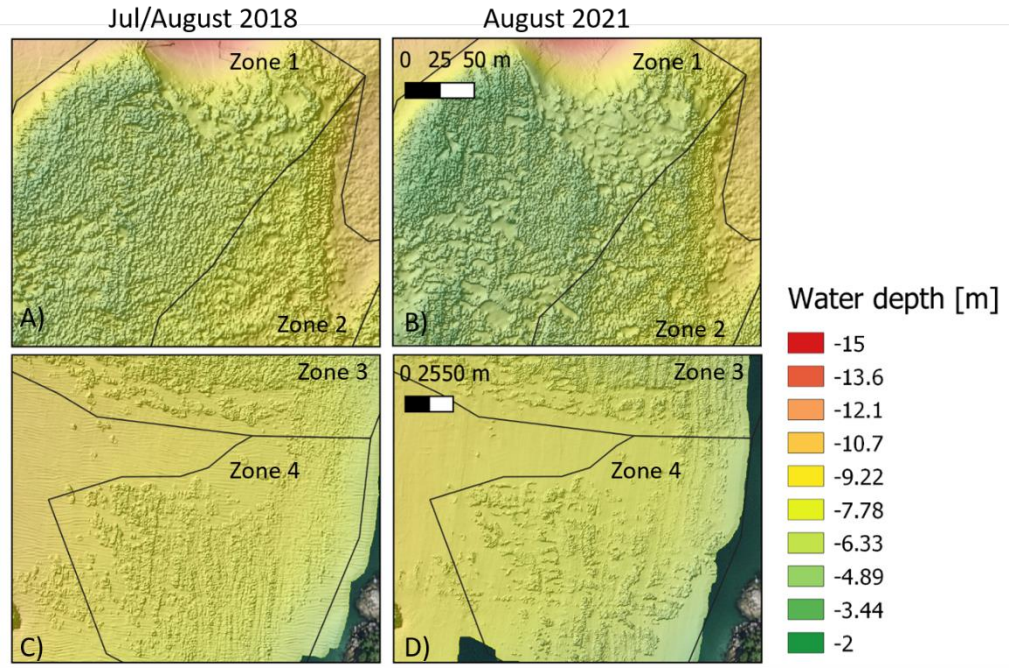

Figure 7 - Morphology of the Choked Passage seagrass meadow for Zone 1 (A and B) and 4 (C and D) in Jul/Aug 2018 and Aug 2021.

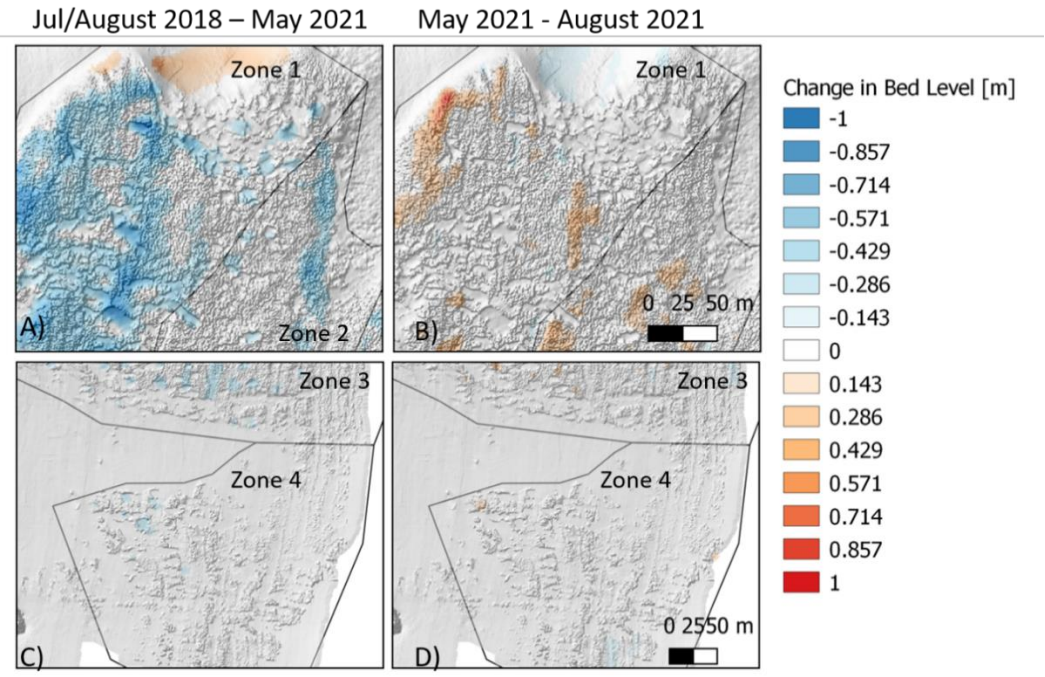

Figure 8 - Significant surface differences (m) at a 95% confidence interval for Zone 1 & 2 in A) July/August 2018 – May 2021, B) May 2021 – August 2021, and Zone 4 in C) July/August 2018 – May 2021, and D) May 2021 – August 2021. Surface difference raster is overlain on hillshade surfaces from May 2021 (A and C) and August 2021 (B and D) surfaces.

The seabed substrate classification (Figure 10 A & B) shows coarse material in the blowouts in the North-West region and a range of grain sizes with some shells around the sand waves. In the South (Figure 8 A & B), the gravel/bolder class is absent and sand and sand/mixed shells material persist. The southern portion of the main meadow shows more shell material in August 2021 than in July/August 2018.

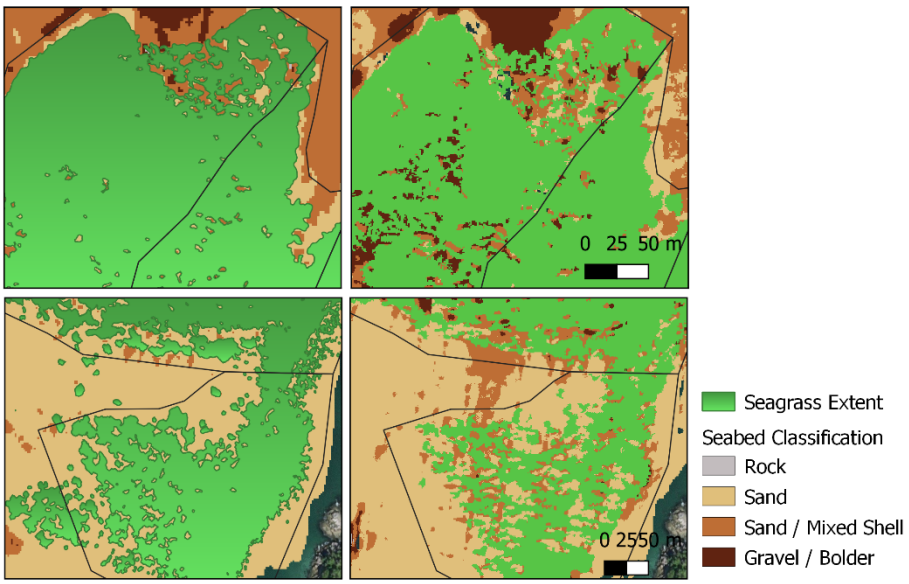

Figure 9 - Substrate and seagrass classification map for Zone 1 (A and B) and 4 (C and D) in July/Aug 2018 and Aug 2021.

2.50 Discussion

2.51 Seabed and seagrass response to storm events

Significant seabed erosion occurred in the seagrass meadow of Choked Passage from July/August 2018 to May 2021, which persists in August 2021. The meadow, which had been expanding since 2016, was reduced by 10% in area from 2020 to 2021. The winter of 2020/21 was a moderate La Niña event, which in British Columbia are associated with extreme winds, wave heights, and storm intensity (Abeysirigunawardena & Walker, 2008; Allan & Komar, 2006; Heathfield, 2013). A particular record-breaking storm was reported in the media in November 2020 (Fretwell, 2020), which caused extreme water levels and wave heights due to coincidence of a King tide and the storm surge. Under severe storms, seagrass shoots can be uprooted in exposed meadows (Fourqurean & Rutten, 2004; Oprandi et al., 2020; Peralta et al., 2005), and seabed sediment can be mobilised (Ferret *et al.*, 2010). Because the few years prior to

this winter were less energetic (Figure 4), we assume that the erosion and loss of seagrass occurred during this stormy winter, whether in a single event or through a sequence of strong storms is not clear. This assumption is supported by a considerable amount of research which have found seagrass loss after storms events and erosion following seagrass loss (De Falco et al., 2000; Oprandi et al., 2020; Rasheed et al., 2014; Walter, 2020). Alternatively, other examples of seagrass loss have been attributed to the 'seagrass-sediment-light feedback', where the loss of seagrass increases resuspension, reduces water clarity, and inhibits seagrass growth (Lawson et al., 2012; Moksnes et al., 2018). However, this process has been found primarily in shallow protected and/or estuarine systems (Carr et al., 2016; Hansen & Reidenbach, 2013; Hansen & Reidenbach, 2012; Nardin et al., 2018), as opposed to the relatively deep and exposed Choked Passage meadow. Due to the relatively coarse grain sizes, low turbidity (Hakai Institute, 2021), and lack of nearby river systems, this feedback cycle cannot explain the observed seagrass-sediment dynamics. We argue that significant storm activity led to erosion and seagrass loss in Choked Passage. No other study has examined the cumulative effects of storm activity on erosion, bed morphology, and seagrass in this region.

The response of the seabed and meadow to storms was not spatially uniform and not always directly coupled. Specifically, erosion is greatest in the shallowest parts of the shoal, which experiences seagrass loss, but the largest seagrass loss occurs in the South, where no detectable bed level changes occur. We will refer to the former area as 'morphologically active', whereas the southern meadow will be described as 'morphologically inactive'. In the morphologically active area of the meadow, seabed erosion and seagrass loss are coupled to the appearance and expansion of morphological features such as blowouts and sand waves (Figure 7 C& D). Blowouts are grass-free depressions with pronounced vertical relief along their margins common to hydrodynamically exposed meadows (Fonseca & Bell, 1998; Koch et al., 2006), and are primarily formed through physical disturbances (Kirkman & Kuo, 1990). Blowouts often consist of coarser sediment than the surrounding areas as increased flow velocities in the grass-free area prevent finer sediments from settling (Bos et al., 2007). This agrees with our observation of particularly coarse sediment in the blowout regions. It is reasonable to presume these features were formed or expanded due to the increased hydrodynamic forces during the 2020/2021 winter storms. In Choked Passage, they occur around rocky islands and shores. It is possible that storm energy would have been the greatest or most chaotically distributed near

these shallow, rocky boundaries, where wave reflection, refraction and turbulence can occur. During periods of reduced disturbances, blowouts can recover (i.e. infill) through re-colonization of seagrass and coalescence of patches to form a more continuous meadow (Walker et al., 2006). Sand waves have also been previously observed in exposed meadows (Fonseca & Bell, 1998; Koch et al., 2006) and are indicative of bedload transport. In Choked Passage, sand waves are concentrated in a single area near the northern slope of the shoal in shallowest water. Significant erosion is focused on the southern margin of this sand wave area, increasing the areas extent, while seagrass loss and growth occurs within the interior of this area (Figure 8A &B). Based on the observed severe significant wave heights, seagrass loss, erosion, and minimal suspended sediment (Prentice et al., 2019), we postulate that sediment transport is predominately limited to extreme conditions, removing both sediment and seagrass blades, and through small-scale bedload transport in select areas. Given that there is no overall bed-level change in the southern meadow, this loss could be related to the ongoing transport of material through the patch, rather than an actual loss of substrate material. The center region of the morphologically active main meadow exhibits only few blowouts, little bed level change and seagrass gain in many areas. Because seagrass meadows are spatially complex and exposed to varying levels of disturbances, they can experience loss/gain and erosion/deposition simultaneously within a single meadow (Allaoui et al., 2016; Carr et al., 2016; Kendrick et al., 2000).

The morphologically inactive, southern meadow had large seagrass losses from 2018 to 2021, but minimal erosion and no blowouts, which suggests that this area within Choked Passage responds to extreme disturbances with increased seagrass patchiness and fragmentation independent of bed level changes. Some of the finest grain sizes and substrate classes within Choked Passage are found in the southern meadow, which suggests reduced exposure to currents and wave energy compared to the main meadow (Hjulstrom, 1939; Orton & Reading, 1993). For flow coming from the North (ebb direction), the southern meadow is in the flow ‘shadow’ of the main meadow and in a region of flow deceleration due to flow expansion into deeper water (Best & Kostaschuk, 2002). For flow coming from the South-West (flood direction), obstruction by rocky islands and increased roughness reduces the incoming flow. The southern meadow is bordered by Wolf Beach to the South and may experience frequent exchange of sediment with the beach. Given these background conditions, a few possible explanations for our observations in the southern meadow include: 1) bed level changes did occur, but where already reversed by

May 2021, 2) seagrass loss occurred without bed level change due to increased turbidity (Moksnes et al., 2018) from eroded materials in the main meadow, 3) the seagrass loss in the main meadow negatively affected seagrass growth in the southern meadow (e.g. Grech et al., 2018; Mari et al., 2021), or 4) seagrass loss occurred through independent stressors (e.g. heat stress, pollution, animal burrowing/grazing; Guerrero-Meseguer et al., 2017; Walter, 2020) only affecting the southern meadow.

2.52 Meadow cycling and recovery

Seagrass ecosystems are resilient to disturbances and can recover given that intensity and duration of the disturbance does not exceed a certain threshold that inhibits recovery (Nowicki et al., 2017; Nyström et al., 2012). Strong seedbanks and adapted reproductive strategies enable recovery after plants are removed (Orth et al., 2006; Vercaemer et al., 2021). The seven years of seagrass delineations available suggest a general trend of a reduction in seagrass coverage following winters with a high number of storm events and/or high recorded storm intensity. Following the very strong El Niño year in 2016, when the meadow measured its smallest recorded extent, the Choked Pass meadow entered a period of recovery. In 2020, it reached maximum coverage area and was reduced following the 2020-2021 moderate La Niña year. Our results indicate a significant bio-geomorphic response of seagrass meadows and their sediments to extreme storm events in this study area. Given that there is no available bathymetry data prior to 2018, we cannot determine whether this bio-geomorphic response occurs in previous ENSO years with significant storm activities and whether the seabed undergoes recovery during more quiescent years. We observed potential recovery through sediment deposition from May – August 2021 in areas that had experienced erosion.

We speculate that there is a bio-geomorphic cycle of seagrass coverage and morphodynamics guided by ENSO activity in Choked Pass. Increased storm magnitude and/or frequency associated with ENSO events induce sediment erosion, seagrass loss, increased patchiness, and the expansion of blowouts and sand waves. The meadow can recover during weak ENSO years, through seagrass growth and expansion, which may promote deposition and sediment retention (de Boer, 2007), until the next significant ENSO year. Future research should continue to survey the Choked Passage bathymetry annually to pair changes in seagrass coverage with bed-level changes over a longer time series to confirm whether this bio-geomorphic cycle

exists. Climate change is expected to increase the frequency of La Niña events (Cai et al., 2015). The cumulative effects of increased storm activity and anthropogenic impacts (*e.g.* coastal development, pollution, dredging) could push seagrass systems past a threshold in an alternative state of erosion, seagrass loss, and limited recovery (Unsworth et al., 2015).

2.60 Conclusion

This study used bathymetry, sediment backscatter, and seagrass delineations from repeat MBES and drone surveys to examine the relationship between the Choked Pass seagrass meadow and bed morphology over time and determine whether changes are linked to storm activity and climate variability. From 2018 to 2021, the meadow experienced significant erosion and loss of seagrass, which we attribute to the preceding winter storm activity driven by moderate La Niña conditions. Spatial patterns in bed level and seagrass changes were not uniform and at times decoupled. We found concentrated erosion along the meadow edges, which are the shallowest and closest to rocky margins. Seagrass loss occurred in these regions, but was highest in the southern meadow, where the bed appears stable. Coupled erosion and seagrass loss resulted in the generation or expansion of blowouts. Despite the significant loss of seagrass near the meadow edge, the interior of the meadow continues to infill seagrass gaps. In locations where seagrass loss was decoupled from bed level changes, we observed increased fragmentation without blowout formation, however, it is unclear why. Future research should aim to identify the drivers of these observed differences in the southern vs northern meadow. We believe the Choked Pass seagrass meadow undergoes cyclic behaviour with reduction in seagrass coverage during energetic ENSO years, followed by a recovery period. The observed recovery of the eroded bed material suggests the meadow has entered this period of seagrass and sediment recovery, until the next significant ENSO year, creating a bio-geomorphic cycle.

Seagrass meadows provide valuable ecosystem services and provide critical habitat for a diversity of species. This study demonstrated linkages between extreme storms (during ENSO years), seabed morphology, seagrass loss and patch complexity on the Central Coast of British Columbia. Ultimately, we have answered our two research questions: increased storm activity may result in seagrass loss, bed-level reductions (i.e. erosion), and creation of morphological features (i.e. blowouts and sand waves), and bed-level reductions are linked to changes in seagrass coverage, however, both of these results depend on the location within the meadow.

Geomorphic processes and disturbances have an important influence on the ecosystem structure and function over time (Corenblit et al., 2011), therefore, it is important to understand how these processes operate and are modified by external drivers. Climate variability is predicted to increase, while seagrasses continue to decline worldwide (Cai et al., 2015; Orth et al., 2006), and effort should be made to understand how seagrass will respond to the changing climate. The results of this study have significant implications on seagrass conservation, restoration, and the evolution of coastal landscapes.

2.70 Bibliography

Abeysirigunawardena, D. S., & Walker, I. J. (2008). Sea level responses to climatic variability and change in northern British Columbia. Atmosphere-Ocean, 46(3), 277–296. https://doi.org/10.3137/ao.460301

Allan, J. C., & Komar, P. D. (2006). Climate Controls on US West Coast Erosion Processes. Journal of Coastal Research, 223, 511–529. https://doi.org/10.2112/03-0108.1

Allaoui, N. E., Serra, T., Colomer, J., Soler, M., Casamitjana, X., & Oldham, C. (2016). Interactions between Fragmented Seagrass Canopies and the Local Hydrodynamics. PLOS ONE, 11(5), e0156264. https://doi.org/10.1371/journal.pone.0156264

ASTM, A. (2017). D7928: Standard test method for particle-size distribution (gradation) of fine-grained soil using the sedimentation (hydrometer) analysis. *ASTM International: West Conshohocken (PA)*.

Barnard, P. L., Hoover, D., Hubbard, D. M., Snyder, A., Ludka, B. C., Allan, J., Kaminsky, G. M., Ruggiero, P., Gallien, T. W., Gabel, L., McCandless, D., Weiner, H. M., Cohn, N., Anderson, D. L., & Serafin, K. A. (2017). Extreme oceanographic forcing and coastal response due to the 2015–2016 El Niño. Nature Communications, 8(1), 14365. https://doi.org/10.1038/ncomms14365

Barnard, P. L., Short, A. D., Harley, M. D., Splinter, K. D., Vitousek, S., Turner, I. L., Allan, J., Banno, M., Bryan, K. R., Doria, A., Hansen, J. E., Kato, S., Kuriyama, Y., Randall-Goodwin, E., Ruggiero, P., Walker, I. J., & Heathfield, D. K. (2015). Coastal vulnerability across the Pacific dominated by El Niño/Southern Oscillation. Nature Geoscience, 8(10), 801–807. https://doi.org/10.1038/ngeo2539

Bell, S. S. (1999). Gap Dynamics in a Seagrass Landscape. Ecosystems, 2(6), 493–504. https://doi.org/10.1007/s100219900097

Best, J., & Kostaschuk, R. (2002). An experimental study of turbulent flow over a low-angle dune. Journal of Geophysical Research: Oceans, 107(C9), 18-1-18–19. https://doi.org/10.1029/2000JC000294

Bos, A. R., Bouma, T. J., de Kort, G. L. J., & van Katwijk, M. M. (2007). Ecosystem engineering by annual intertidal seagrass beds: Sediment accretion and modification.

Estuarine, Coastal and Shelf Science, 74(1–2), 344–348. https://doi.org/10.1016/j.ecss.2007.04.006

Bosma, C. (2019). Multibeam & Backscatter Classification: A methodology for producing theoretical substrate rasters from multibeam echosounder data.

Brown, C. J., Beaudoin, J., Brissette, M., & Gazzola, V. (2019). Multispectral Multibeam Echo Sounder Backscatter as a Tool for Improved Seafloor Characterization. Geosciences, 9(3), 126. https://doi.org/10.3390/geosciences9030126

Cabaço, S., Santos, R., & Duarte, C. M. (2008). The impact of sediment burial and erosion on seagrasses: A review. Estuarine, Coastal and Shelf Science, 79(3), 354–366. https://doi.org/10.1016/j.ecss.2008.04.021

Cai, W., Wang, G., Santoso, A., McPhaden, M. J., Wu, L., Jin, F.-F., Timmermann, A., Collins, M., Vecchi, G., Lengaigne, M., England, M. H., Dommenget, D., Takahashi, K., & Guilyardi, E. (2015). Increased frequency of extreme La Niña events under greenhouse warming. Nature Climate Change, 5(2), 132–137. https://doi.org/10.1038/nclimate2492

Carr, J. A., D'Odorico, P., McGlathery, K. J., & Wiberg, P. L. (2016). Spatially explicit feedbacks between seagrass meadow structure, sediment and light: Habitat suitability for seagrass growth. Advances in Water Resources, 93, 315–325. https://doi.org/10.1016/j.advwatres.2015.09.001

Corenblit, D., Baas, A. C. W., Bornette, G., Darrozes, J., Delmotte, S., Francis, R. A., Gurnell, A. M., Julien, F., Naiman, R. J., & Steiger, J. (2011). Feedbacks between geomorphology and biota controlling Earth surface processes and landforms: A review of foundation concepts and current understandings. Earth-Science Reviews, 106(3–4), 307–331. https://doi.org/10.1016/j.earscirev.2011.03.002

de Boer, W. F. (2007). Seagrass–sediment interactions, positive feedbacks and critical thresholds for occurrence: A review. Hydrobiologia, 591(1), 5–24. https://doi.org/10.1007/s10750-007-0780-9

De Falco, G., Ferrari, S., Cancemi, G., & Baroli, M. (2000). Relationship between sediment distribution and Posidonia oceanica seagrass. Geo-Marine Letters, 20(1), 50–57. https://doi.org/10.1007/s003670000030

Duarte, C. M. (2002). The future of seagrass meadows. Environmental Conservation, 29(2), 192–206. https://doi.org/10.1017/S0376892902000127

Duarte, C. M., & Chiscano, C. L. (1999). Seagrass biomass and production: A reassessment. Aquatic Botany, 65(1–4), 159–174. https://doi.org/10.1016/S0304-3770(99)00038-8

Fonseca, M., & Bell, S. (1998). Influence of physical setting on seagrass landscapes near Beaufort, North Carolina, USA. Marine Ecology Progress Series, 171, 109–121. https://doi.org/10.3354/meps171109

Fourqurean, J. W., & Rutten, L. M. (2004). THE IMPACT OF HURRICANE GEORGES ON SOFT-BOTTOM, BACK REEF COMMUNITIES: SITE- AND SPECIES-SPECIFIC EFFECTS IN SOUTH FLORIDA SEAGRASS BEDS. BULLETIN OF MARINE SCIENCE, 75(2), 20.

Frederiksen, M., Krause-Jensen, D., Holmer, M., & Laursen, J. S. (2004). Spatial and temporal variation in eelgrass (Zostera marina) landscapes: Influence of physical setting. Aquatic Botany, 78(2), 147–165. https://doi.org/10.1016/j.aquabot.2003.10.003

Fretwell, K. (2020). A king tide storms ashore. Hakai Institute. Retrieved from https://hakai.org/a-king-tide-storms-ashore/

Grech, A., Hanert, E., McKenzie, L., Rasheed, M., Thomas, C., Tol, S., Wang, M., Waycott, M., Wolter, J., & Coles, R. (2018). Predicting the cumulative effect of multiple disturbances on seagrass connectivity. Global Change Biology, 24(7), 3093–3104. https://doi.org/10.1111/gcb.14127

Guerrero-Meseguer, L., Marín, A., & Sanz-Lázaro, C. (2017). Future heat waves due to climate change threaten the survival of Posidonia oceanica seedlings. Environmental Pollution, 230, 40–45. https://doi.org/10.1016/j.envpol.2017.06.039

Gumusay, M. U., Bakirman, T., Tuney Kizilkaya, I., & Aykut, N. O. (2019). A review of seagrass detection, mapping and monitoring applications using acoustic systems. European Journal of Remote Sensing, 52(1), 1–29. https://doi.org/10.1080/22797254.2018.1544838

Hansen, J. C. R., & Reidenbach, M. A. (2013). Seasonal Growth and Senescence of a Zostera marina Seagrass Meadow Alters Wave-Dominated Flow and Sediment Suspension Within a Coastal Bay. Estuaries and Coasts, 36(6), 1099–1114. https://doi.org/10.1007/s12237-013-9620-5

Hansen, J., & Reidenbach, M. (2012). Wave and tidally driven flows in eelgrass beds and their effect on sediment suspension. Marine Ecology Progress Series, 448, 271–287. https://doi.org/10.3354/meps09225

Heathfield, D. K. (2013). Erosive water levels and beach-dune morphodynamics, Wickaninnish Bay, Pacific Rim National Park Reserve, British Columbia, Canada [Thesis]. https://dspace.library.uvic.ca/handle/1828/4925

Hjulstrom, F. (1939). Transportation of Detritus by Moving Water: Part 1. Transportation. 142, 5–31.

Hossain, M. S., Islam, M. A., Badhon, F. F., & Imtiaz, T. (2021). Hydrometer Analysis. Properties and Behavior of Soil-Online Lab Manual.

Kalra, Y. P., & Maynard, D. G. (1991). Methods manual for forest soil and plant analysis (Vol. 319).

Kendrick, G. A., Hegge, B. J., Wyllie, A., Davidson, A., & Lord, D. A. (2000). Changes in Seagrass Cover on Success and Parmelia Banks, Western Australia Between 1965 and 1995. Estuarine, Coastal and Shelf Science, 50(3), 341–353. https://doi.org/10.1006/ecss.1999.0569

Kirkman, H., & Kuo, J. (1990). Pattern and process in southern Western Australian seagrasses. Aquatic Botany, 37(4), 367–382. https://doi.org/10.1016/0304-3770(90)90022-D

Koch, E. W., Ackerman, J. D., Verduin, J., & Keulen, M. van. (2006). Fluid Dynamics in Seagrass Ecology—From Molecules to Ecosystems. In A. W. D. LARKUM, R. J. ORTH, & C. M. DUARTE (Eds.), SEAGRASSES: BIOLOGY, ECOLOGYAND CONSERVATION (pp. 193–225). Springer Netherlands. https://doi.org/10.1007/978-1-4020-2983-7_8

Lague, D., Brodu, N., & Leroux, J. (2013). Accurate 3D comparison of complex topography with terrestrial laser scanner: Application to the Rangitikei canyon (N-Z). ISPRS Journal of Photogrammetry and Remote Sensing, 82, 10–26. https://doi.org/10.1016/j.isprsjprs.2013.04.009

Lamarche, G., & Lurton, X. (2018). Recommendations for improved and coherent acquisition and processing of backscatter data from seafloor-mapping sonars. Marine Geophysical Research, 39(1), 5–22. https://doi.org/10.1007/s11001-017-9315-6

Mari, L., Melià, P., Gatto, M., & Casagrandi, R. (2021). Identification of Ecological Hotspots for the Seagrass Posidonia oceanica via Metapopulation Modeling. Frontiers in Marine Science, 8. https://www.frontiersin.org/articles/10.3389/fmars.2021.628976

Moksnes, P.-O., Eriander, L., Infantes, E., & Holmer, M. (2018). Local Regime Shifts Prevent Natural Recovery and Restoration of Lost Eelgrass Beds Along the Swedish West Coast. Estuaries and Coasts, 41(6), 1712–1731. https://doi.org/10.1007/s12237-018-0382-y

Nahirnick, N. K., Reshitnyk, L., Campbell, M., Hessing-Lewis, M., Costa, M., Yakimishyn, J., & Lee, L. (2019). Mapping with confidence; delineating seagrass habitats using Unoccupied Aerial Systems (UAS). Remote Sensing in Ecology and Conservation, 5(2), 121–135. https://doi.org/10.1002/rse2.98

Nardin, W., Larsen, L., Fagherazzi, S., & Wiberg, P. (2018). Tradeoffs among hydrodynamics, sediment fluxes and vegetation community in the Virginia Coast Reserve, USA. Estuarine, Coastal and Shelf Science, 210, 98–108. https://doi.org/10.1016/j.ecss.2018.06.009

National Oceanic and Atmospheric Administration (2022). Cold & Warm Episodes by Season. Retrieved from https://origin.cpc.ncep.noaa.gov/products/analysis_monitoring/ensostuff/ONI_v5.php

Nowicki, R., Thomson, J., Burkholder, D., Fourqurean, J., & Heithaus, M. (2017). Predicting seagrass recovery times and their implications following an extreme climate event. Marine Ecology Progress Series, 567, 79–93. https://doi.org/10.3354/meps12029

Nyström, M., Norström, A. V., Blenckner, T., de la Torre-Castro, M., Eklöf, J. S., Folke, C., Österblom, H., Steneck, R. S., Thyresson, M., & Troell, M. (2012). Confronting Feedbacks of Degraded Marine Ecosystems. Ecosystems, 15(5), 695–710. https://doi.org/10.1007/s10021-012-9530-6

Olson, A. M., Hessing-Lewis, M., Haggarty, D., & Juanes, F. (2019). Nearshore seascape connectivity enhances seagrass meadow nursery function. Ecological Applications, 29(5). https://doi.org/10.1002/eap.1897

Oprandi, A., Mucerino, L., De Leo, F., Bianchi, C. N., Morri, C., Azzola, A., Benelli, F., Besio, G., Ferrari, M., & Montefalcone, M. (2020). Effects of a severe storm on seagrass meadows. Science of The Total Environment, 748, 141373. https://doi.org/10.1016/j.scitotenv.2020.141373

Orth, R. J., Carruthers, T. J. B., Dennison, W. C., Duarte, C. M., Fourqurean, J. W., Heck, K. L., Hughes, A. R., Kendrick, G. A., Kenworthy, W. J., Olyarnik, S., Short, F. T., Waycott, M., & Williams, S. L. (2006). A Global Crisis for Seagrass Ecosystems. BioScience, 56(12), 987. https://doi.org/10.1641/0006-3568(2006)56[987:AGCFSE]2.0.CO;2

Orton, G. J., & Reading, H. G. (1993). Variability of deltaic processes in terms of sediment supply, with particular emphasis on grain size. Sedimentology, 40(3), 475–512. https://doi.org/10.1111/j.1365-3091.1993.tb01347.x

Pace, M., Borg, J. A., Galdies, C., & Malhotra, A. (2017). Influence of wave climate on architecture and landscape characteristics of Posidonia oceanica meadows. Marine Ecology, 38(1), e12387. https://doi.org/10.1111/maec.12387

Parnum, I. M., & Gavrilov, A. N. (2011). High-frequency multibeam echo-sounder measurements of seafloor backscatter in shallow water: Part 1 – Data acquisition and processing. Underwater Technology, 30(1), 3–12. https://doi.org/10.3723/ut.30.003

Peralta, G., Brun, F. G., Hernández, I., Vergara, J. J., & Pérez-Lloréns, J. L. (2005). Morphometric variations as acclimation mechanisms in Zostera noltii beds. Estuarine, Coastal and Shelf Science, 64(2–3), 347–356. https://doi.org/10.1016/j.ecss.2005.02.027

Prentice C., Smith R., & Hessing-Lewis M. (2019). Summary of Chalk Blocks and Sediment Traps from Calvert Seagrass Sites. Hakai Institute.

Prentice, C., Hessing-Lewis, M., Sanders-Smith, R., & Salomon, A. K. (2019). Reduced water motion enhances organic carbon stocks in temperate eelgrass meadows. Limnology and Oceanography, 64(6), 2389–2404. https://doi.org/10.1002/lno.11191

Rasheed, M. A., McKenna, S. A., Carter, A. B., & Coles, R. G. (2014). Contrasting recovery of shallow and deep water seagrass communities following climate associated losses in tropical north Queensland, Australia. Marine Pollution Bulletin, 83(2), 491–499. https://doi.org/10.1016/j.marpolbul.2014.02.013

Robbins, B. D., & Bell, S. S. (2000). Dynamics of a Subtidal Seagrass Landscape: Seasonal and Annual Change in Relation to Water Depth. Ecology, 81(5), 1193–1205. https://doi.org/10.1890/0012-9658(2000)081[1193:DOASSL]2.0.CO;2

Short, F., Carruthers, T., Dennison, W., & Waycott, M. (2007). Global seagrass distribution and diversity: A bioregional model. Journal of Experimental Marine Biology and Ecology, 350(1–2), 3–20. https://doi.org/10.1016/j.jembe.2007.06.012

Short, F. T., & Wyllie-Echeverria, S. (1996). Natural and human-induced disturbance of seagrasses. Environmental Conservation, 23(1), 17–27. https://doi.org/10.1017/S0376892900038212

Stevens, A. W., & Lacy, J. R. (2012). The Influence of Wave Energy and Sediment Transport on Seagrass Distribution. Estuaries and Coasts, 35(1), 92–108. https://doi.org/10.1007/s12237-011-9435-1

Unsworth, R. K. F., Collier, C. J., Waycott, M., Mckenzie, L. J., & Cullen-Unsworth, L. C. (2015). A framework for the resilience of seagrass ecosystems. Marine Pollution Bulletin, 100(1), 34–46. https://doi.org/10.1016/j.marpolbul.2015.08.016

Vercaemer, B. M., Scarrow, M. A., Roethlisberger, B., Krumhansl, K. A., & Wong, M. C. (2021). Reproductive ecology of Zostera marina L. (eelgrass) across varying environmental conditions. Aquatic Botany, 175, 103444. https://doi.org/10.1016/j.aquabot.2021.103444

Walker, D. I., Kendrick, G. A., & McComb, A. J. (2006). Decline and Recovery of Seagrass Ecosystems—The Dynamics of Change. In A. W. D. LARKUM, R. J. ORTH, & C. M. DUARTE (Eds.), SEAGRASSES: BIOLOGY, ECOLOGYAND CONSERVATION (pp. 551–565). Springer Netherlands. https://doi.org/10.1007/978-1-4020-2983-7_23

Walter, R. K. (2020). Large-scale erosion driven by intertidal eelgrass loss in an estuarine environment. 7.

Waycott, M., Duarte, C. M., Carruthers, T. J. B., Orth, R. J., Dennison, W. C., Olyarnik, S., Calladine, A., Fourqurean, J. W., Heck, K. L., Hughes, A. R., Kendrick, G. A., Kenworthy, W. J., Short, F. T., & Williams, S. L. (2009). Accelerating loss of seagrasses across the globe threatens coastal ecosystems. Proceedings of the National Academy of Sciences, 106(30), 12377–12381. https://doi.org/10.1073/pnas.0905620106

Zhang, W., Qi, J., Wan, P., Wang, H., Xie, D., Wang, X., & Yan, G. (2016). An Easy-to-Use Airborne LiDAR Data Filtering Method Based on Cloth Simulation. Remote Sensing, 8(6), 501. https://doi.org/10.3390/rs8060501

3.0 Tidal flow over seagrass beds on the Central Coast of British Columbia

3.10 Introduction

Seagrasses are known as ecosystem engineers because they modify their physical environment to create highly productive nearshore ecosystems (Bos et al., 2007; Orth et al., 2006). Seagrasses induce drag on flow to attenuate mean flow and near-bed velocities (Hansen & Reidenbach, 2012; Koch et al., 2006). This process can shield the seabed from shear stress, erosion, and sediment suspension. However, the influence of seagrass on flow and sediment transport depends on the magnitude of currents and waves, seagrass characteristics (i.e. density and blade height), grain size, and local topography (Nepf, 2012; van Katwijk et al., 2010; Yager & Schmeeckle, 2013). The stable conditions generated by seagrasses serve as critical habitat for a diversity of ecologically and economically important species (Kennedy et al., 2018; Orth et al., 2006). Moreover, seagrasses help protect our coasts from erosion, improve water quality, and

sequester carbon (Mcleod et al., 2011; Mtwana Nordlund et al., 2016). Therefore, it is important to understand how seagrass influences flow and sediment in different locations across a meadow.

In seagrass and other submerged aquatic vegetation (SAV), velocity profiles typically show three layers: a logarithmic flow layer above the canopy and an attenuated layer below, separated by a mixing layer with an inflection point of maximum shear directly above the canopy (Lacy & Wyllie-Echeverria, 2011; Nepf, 2012). Sediment transport is driven by flow velocity and the production of bed-shear stress and turbulence (Le Bouteiller & Venditti, 2014). Applying the logarithmic relationship between velocity and different roughness elements to measured velocity profiles can be used to estimate shear velocity and bed shear stress. By knowing grain size properties, the critical shear stress thresholds can be estimated to determine the potential for sediment transport (Rijn, 2007). Typically, the seagrass canopy creates drag on the flow to reduce velocity and decreases bed shear stress, which inhibits bed load transport and resuspension (de Boer, 2007; Folkard, 2019). Flow velocity varies spatially due to heterogenous canopy characteristics (e.g. blade height and density), differences in exposure and topographic steering, therefore, the magnitude of this process can be highly variable within a single meadow.

Although the general hydrodynamics of seagrass meadows are relatively well-understood, there are only a few field studies which have examined the relationship between flow, seagrass, and sediment transport (de Boer, 2007; Folkard, 2019). Much of the knowledge of seagrass hydrodynamics has come from simplified laboratory studies, or field studies in relatively protected and similar physical settings (Folkard, 2019; Hansen & Reidenbach, 2012; Koch et al., 2006; Nepf, 2012). Seagrasses have diverse morphologies, exist in many different coastal regions, and are exposed to different biophysical processes (Hughes et al., 2009; Koch et al., 2006; Short et al., 2007). More field studies examining seagrass hydrodynamics in different environments that capture the complex bio-physical conditions within a single meadow are needed to improve our overall understanding of seagrass hydrodynamics, refine modelling effort, and contribute to seagrass conservation and restoration.

Acoustic Doppler Current Profilers (ADCP) allow for precise and high-resolution flow measurements across a relatively large spatial area, and can detect seagrass canopy height (Warren & Peterson, 2007). Off the Central Coast of British Columbia, Canada, the seagrass meadow within Choked Pass is exposed to significant current and wave energy (Prentice et al.,

2019), and is relatively free from human disturbance. Therefore, this site presents a unique opportunity to study seagrass hydrodynamics within an undeveloped and hydrodynamically exposed environment. For this study, we aim to examine the interaction between current flow and seagrass and how it varies spatially across a relatively exposed meadow. Specifically, we will answer two questions: 1) How does tidal flow behave at different locations within and outside of the meadow? and 2) Do tidal currents drive sediment transport in Choked Passage? To answer these questions, we analyzed flow data from a 1200 kHz ADCP deployed on the bed looking up and along transects mounted to a vessel looking down.

3.20 Study Area

Choked Passage is located on Calvert Island, approximately 60 km North of Vancouver Island, British Columbia (Figure 1). The Choked Passage *Zostera marina* seagrass meadow is situated on a shallow shoal in water depths of -2.0 m to -11.0 m. The meadow is one of the largest in the region with near-contiguous area of 367,300 m^2 (Olson et al., 2019), an average blade density of 81 m^2, and blade length of 1.65 m (Monteith et al., 2021). Seagrass densities vary at different locations within the meadow (Figure 2). This meadow is situated between Calvert Island (334 km^2) to the east and exposed islets to the west. The bottom substrate is predominately coarse to fine sand with high shell content. This area is highly dynamic, with minimal freshwater input, in a macro-tidal setting with high-current tidal exchanges (Prentice et al., 2019; Hakai, 2021). Choked Passage is ebb dominated which flows from the north to the south. Flood currents travel north through the meadow from the southwest (Hakai, 2021).

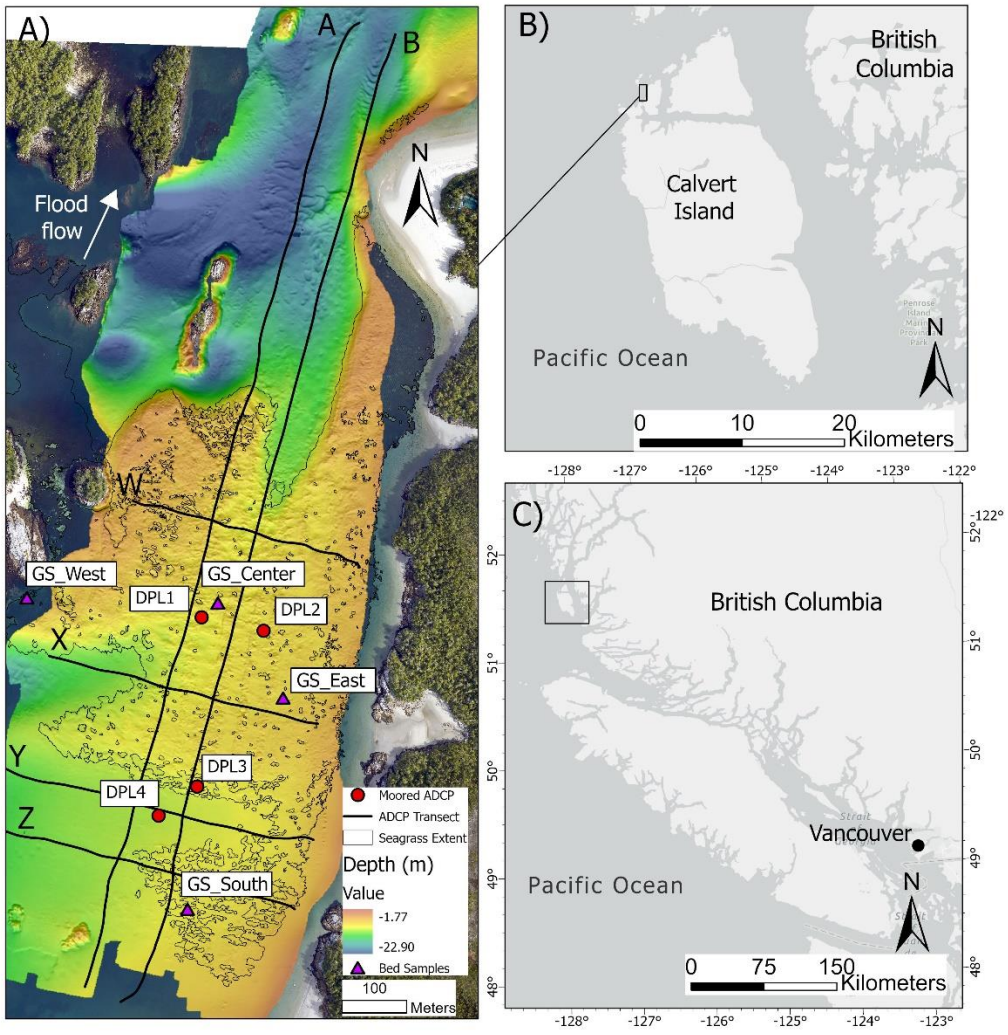

Figure 1 - Choked Passage study area showing (A) ADCP longitudinal and cross-passage transect lines over bathymetry seagrass extent, moored ADCP, and seabed sample sites from May 2021, (B) location of Choked Passage off Calvert Island, C) on the Central Coast of British Columbia, Canada.

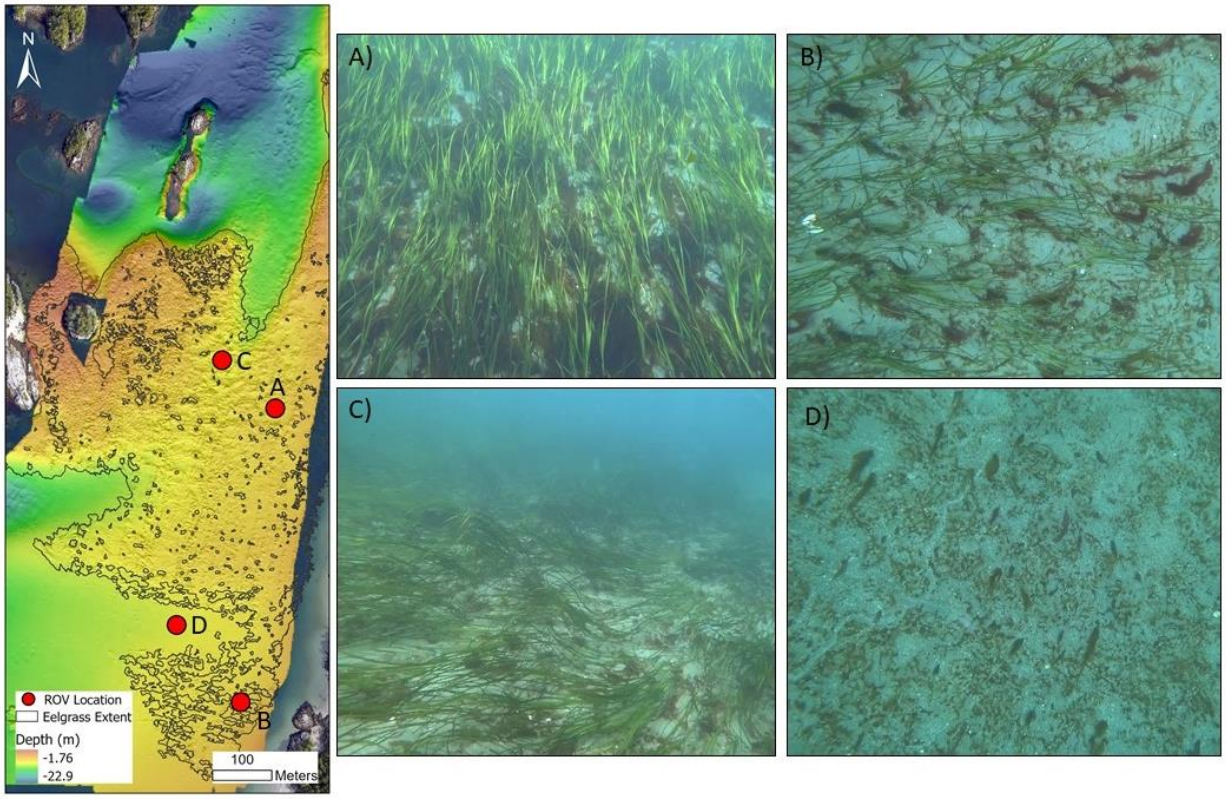

Figure 2 - ROV acquired images of seagrass canopy at different locations within the Choked Passage meadow. A) Dense interior canopy in the north-eastern section towards the shoreline with epiphytes and drift algae, B) Less-dense southern meadow patch, C) Moderately dense interior towards northern meadow edge, and D) un-vegetated sand outside of the meadow with biofilm and drifting algae.

3.30 Methods

3.31 Data Collection

A 1200 kHz Teledyne Workhorse Sentinel ADCP was deployed on the seabed at four different locations for 6-7 hours during the ebb tide May 6th to 10th, 2021 (for location see Figure 1). The instrument was set to send out five pings per ensemble at a 0.37 ping rate and recorded measurements into 0.25 m bins. On May 12, 2021, a 1200 kHz Teledyne Workhorse Sentinel ADCP was mounted to a 23 ft aluminum research vessel (Hakai Blue) to survey transects A and B (Figure 1). One ping was sent out every 0.84 seconds at 0.25 m depth bins and set to water mode 1. It took approximately 15 min to complete one line and lines were surveyed every 20 min. The cross-sectional transects (Figure 1) were surveyed on May 13th, 2021, which took

approximately five minutes to complete. All transects were surveyed during flood tide and early-mid ebb. A total of 35 transects were surveyed from May 12-13, 2021.

3.32 Water Sampling

To quantify suspended sediment concentrations, water samples were collected at various sites along the transects A and B (see Appendix F). A 5 L Niskin bottle was deployed to collect water samples and estimate total suspended material (TSM) at different times a tidal cycle. Samples were collected near slack low and high tide to prevent the Niskin bottle from drifting under high currents and interfering with the sample collection. Water samples were transferred to clear Nalgene sample bottles and brought to the lab for processing.

Prior to sampling, approximately 40 MF-Millipore Membrane Filters with a 0.45 µm pore size and a 47 mm diameter were rinsed with 10 mL of DI water through a mild vacuum (See Appendix F for detailed steps). The filters were then transferred into an oven for 24 hours at 60 ºC. Filters were weighed three times to the nearest 3rd decimal of a gram using a Mettler Toledo NewClassic MF ML104 and averaged to determine the filter weight. The filters were placed on filtering apparatus and 3L of the sample were filtered under a mild vacuum and transferred to an oven to dry for 24 hours at 60 ºC. The initial weight of each filter was subtracted from the post-filtered weight and divided by the volume of sample filtered to determine the total suspended material per volume.

3.33 Grain Size Analysis

Nine sediment samples were collected by divers from the seabed in Choked Pass in August 2021 (See 6.3 Appendix C Figure 9). However, only the four in closest proximity to the moored ADCP deployments were assessed for this study (Figure 1). Samples were retrieved by hand and stored in Ziploc bags. Samples were immediately frozen and transported to the lab for grain size analysis (See Appendix C for detailed steps). The frozen samples were thawed at room temperature for 24 hrs, and then oven dried at 110°C for 24 hrs. Fragments of organic material (e.g. macro-algae, invertebrates) were removed from the sample prior to drying. The dry samples were then burned at 500°C for 1 hr to combust any other organics within the sample. Due to the high shell-content of Choked Pass sediments, clumps and aggregations were broken up by hand, rather than a mortar and pestle to prevent damaging the shells and altering their size.

Approximately 500 g of each sample were collected for sieve grain analysis. The finest grain sediments within the receiving pan were collected for hydrometer analysis of fine sands, silt, and clays (ASTM, 2017; Hossain et al., 2021; Kalra and Manard, 1991).

3.34 ADCP Data Processing

All ADCP data was processed in MATLAB (see Appendix E for detailed steps). First, GPS coordinates were converted to local east, north, up (ENU) coordinates (Gilcoto, Jones, and Luis Fariña-Busto, 2009). The flow velocity measurements were corrected for boat motion using bottomtrack, internal time delay, and magnetic declination (Rennie & Millar, 2004). All bins below the bed profile and/or above the water surface were removed, and any missing bed or surface values were interpolated (Wild, 2020). In addition, the first and last 6% of the bins in the dataset were removed, as these bins typically contain sidelobe interference at 20° beam positioning (Yorke and Oberg, 2002).

The location of each ADCP transect deviated at times slightly from the planned transect line. For better comparison between different measurement times and to remove data at the start and the end of a transect when the line was approached, a linear fit was conducted through all position measurements of all transects for each line. Equidistant position values along the linear fit where extracted every 10 m to create an 'average' transect line, which represents the average route travelled by the vessel. Each ADCP transects was then shifted onto the average transect by finding the ensemble closest to each equidistant point, but never more than 10 m away. All other ensembles were discarded as they were collected too far away from the other data. Of the 35 ADCP transects surveyed (see Appendix E Figure 19), only those collected during peak flood velocity, strongest ebb flow, and low tide were used for spatial flow analysis and canopy detection. The tidal stage and water height of each transect used for spatial flow analysis are shown in Figure 3 and Table 1. All longitudinal transects (A&B) were surveyed on May 12, 2021, between mid-flood to mid-ebb. All cross-passage transects (W, X,Y, Z) were surveyed on May 13, 2021, between mid-flood to mid-ebb. A total of 5 transects were used for each tidal stage group (i.e. peak flood, strongest ebb, and low tide). Because no transects were surveyed during peak ebb conditions, those taken during the strongest ebb conditions of our survey window were grouped together.

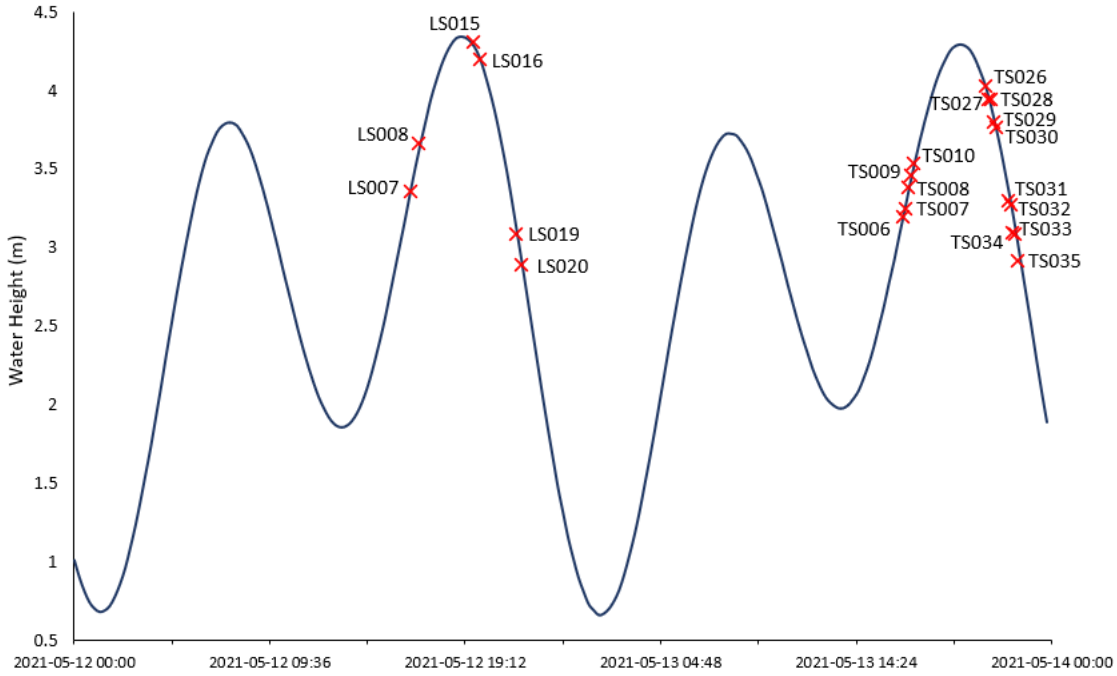

Figure 13 – Tidal heights during ADCP transect start times used for flow spatial analysis during peak flood, strongest ebb flow, and low-tide from May 12 – 14, 2021 over the Choked Passage seagrass meadow.

Table 11 – Summary of ADCP transects surveyed on May 12-13 over the Choked Passage seagrass meadow.

Transect ID	Line	Tidal Stage
TS006	W	Peak flood
TS007	X	Peak flood
TS009	Y	Peak flood
TS010	Z	Peak flood
LS007	A	Peak flood
LS008	B	Peak flood
TS031	W	Strongest ebb flow
TS032	X	Strongest ebb flow
TS033	Y	Strongest ebb flow
TS034	Z	Strongest ebb flow
LS019	A	Strongest ebb flow
LS020	B	Strongest ebb flow
TS026	W	Low tide
TS027	X	Low tide
TS028	Y	Low tide
TS029	Z	Low tide
LS015	A	Low tide
LS016	B	Low tide

Backscatter was used to detect the canopy for each low tide transect. For each vertical profile, the difference between each ADCP depth bin was calculated to find the maximum

difference (i.e. spike). If the maximum difference was greater than 30 dB that signalled the top of the seagrass canopy. All velocity measurements at or below the canopy were removed. Figure 3 illustrates the canopy detection and removal process, where spikes in backscatter are shown as bright dots in panels A and D. All values below these bright dots were removed from the velocity profiles in panels B and D (Figure 3).

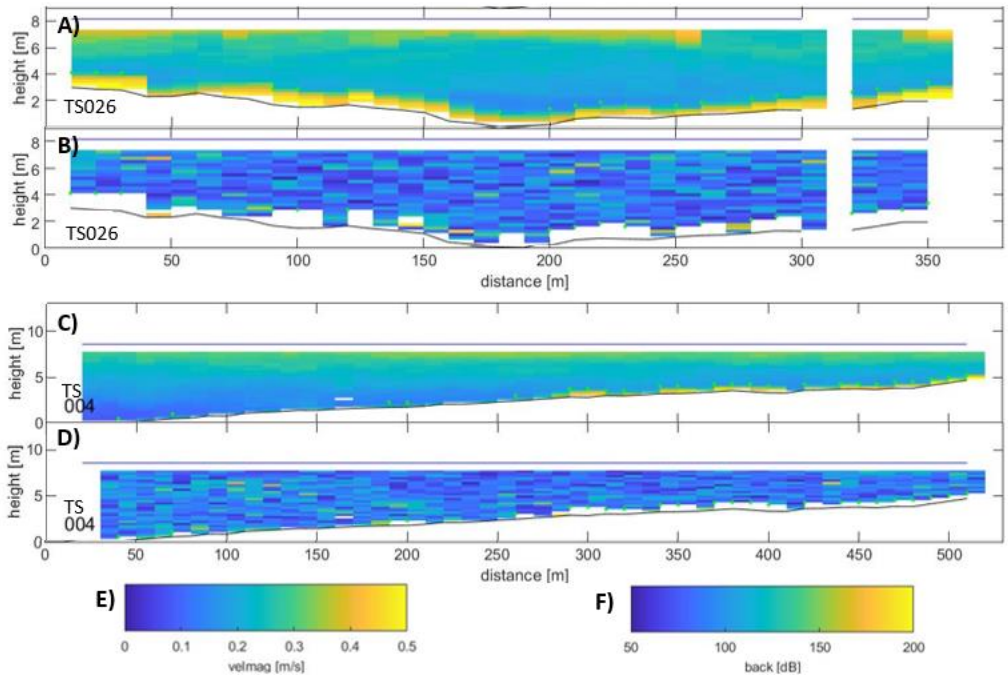

Figure 4 – Example of ADCP profiles used to calculate canopy height and remove values below the seagrass canopy. A) Backscatter profile (dB) of transect TS026 with location of seagrass canopy shown as bright spheres and B) velocity profile (m/s) after removal of measurements below canopy. C) Backscatter profile (dB) of transect TS004 with location of seagrass canopy shown as bright spheres and B) velocity profile (m/s) after removal of measurements below canopy. Scale bars for transect profiles are E) velocity in m/s and F) backscatter in dB.

3.35 Shear Velocity & Critical Threshold for Sediment Transport

Shear velocity (u_*) was calculated for each moored ADCP deployment following Lefebvre (2010) and Wilkinson (1984), which fits a logarithmic profile to one or several layers in the ADCP velocity profile if the velocity profile follows the law of the wall (here given for heights above the bed (z) normalised by water depth (h)):

$$u\left(\frac{z}{h}\right) = \frac{u_*}{\kappa}\ln\frac{z}{h} - \frac{u_*}{\kappa}\ln\frac{z_0}{h}$$

Where u is the flow velocity at height z/h, κ is the von Kármán constant (0.41) and z_0 is the roughness length (Spalding, 1961). Ebb flow is strongest in Choked Passage, therefore, we only used ebb velocity measurements above 0.38 m/s to estimate maximum shear velocities and stress. This yielded a measurement period of 30 – 80 min. Tests were conducted to determine the best height of fit (i.e. water column depth with the highest goodness of fit of the logarithmic profile) for a range of averaging windows. In this approach, a moving average over the velocity profiles is applied and the best height for a fit for each averaged profile is calculated by determining the height that yielded the highest R-squared. The best fit height that occurred most often at each site and with an R-squared > 0.95 for all averaged profiles was recorded and the above steps were repeated for the next averaging window. The best fit heights were then examined with typical average velocity profiles to determine final fits. Once, u_* was known, shear stress was derived with the formula below, where ρ_w is water density.

$$\tau = u_*^2 * \rho_w$$

Based on the number of log-segments needed to adequately represent the velocity profile, interpretations can be made as to what roughness layer (and log segment) represents each roughness element. Total shear stress over a vegetated, sandy sediment can be partitioned into shear stress contributions from vegetation, bed form roughness, and grain roughness, where only the shear stress related to grain roughness is responsible for sediment transport.

$$\tau_{tot} = \tau_{veg} + \tau_{morph} + \tau_{grain}$$

We assumed that bed form roughness was minimal at the deployment locations (τ_{morph} = 0). The grain size distributions of four sample sites were used to estimate the critical shear stress for incipient motion and suspension of bed material. The non-dimensional critical shear stress of incipient motion $\tau^*_{cr,mot}$ for the D10, D50, and D90 of all sites was estimated using the Brownlie (1981) formulation of the Shields curve as modified by Parker et al (2003):

$$\tau^*_{cr,mot} = 0.5(0.22\ {Re_p}^{-0.6} + 0.06 * 10^{(-7.7{Re_p}^{-0.6})}$$

Where $Re_p = \frac{\sqrt{\gamma_s g D}\, D}{\nu}$ is the Particle Reynolds Number, γ_s is the submerged specific gravity of sediment (1.65), g is gravitational acceleration, D is the grain diameter, and ν is the kinematic viscosity of water (1.00×10^{-6} $m^2\ s^{-1}$). Next, the non-dimensional critical shear stress for

suspension of particles $\tau^*_{cr,sus}$ was calculated using the Bagnold (1966) criterion for the relation between critical shear velocity of suspension $u^*_{cr,sus}$and sediment fall velocity v_s:

$$\tau^*_{cr,sus} = \frac{{u^*_{cr,sus}}^2}{\gamma_s g D} = \frac{{v_s}^2}{\gamma_s g D}$$

Where v_s was determined using the relation by Dietrich (1982) as specified by Parker (2016). For grain sizes < 0.1 mm $\tau^*_{cr,sus} = \tau^*_{cr,mot}$ since all material eroded immediately goes into suspension.

3.40 Results & Discussion

3.42 Longitudinal Transect ADCP Profiles

Detailed velocity profiles for Transect A are shown in Figure 7. All profiles generally show flow acceleration towards the north during the flood and deceleration towards the south during the ebb caused by topographic steering. Moreover, there is a low flow area near the bed over the northern slope of the meadow shoal during all tidal times, separating the high flows in the northern most end of the transect and the meadow. Approaching peak flood (Figure 7 B&C), flow accelerated in the northern and southern meadow, but less in the meadow interior, rather the interior meadow velocity remains consistently high until slack high conditions. During the transition from flood to ebb around slack, (Figure 7 C&D) flow velocity remained heightened for a longer duration in the southern meadow than the main meadow. In other words, it appears the deceleration in the southern meadow lags the main meadow interior and northern sections of Choked Passage as ebb flow enters the passage from the north. The effect of flow steering by topography over the southern end of the main meadow and the meadow interior to the north is more pronounced during the ebb (Figure 7 F& G), where flow decelerates and accelerates with changes in water depth. However, during this study period, the transects were not surveyed during peak ebb conditions. Future work should continue to survey both transects at both peak ebb and flood conditions, however, that may require surveying peak ebb and flood on different days, as peak conditions may arise during the evening, when surveying is hazardous.

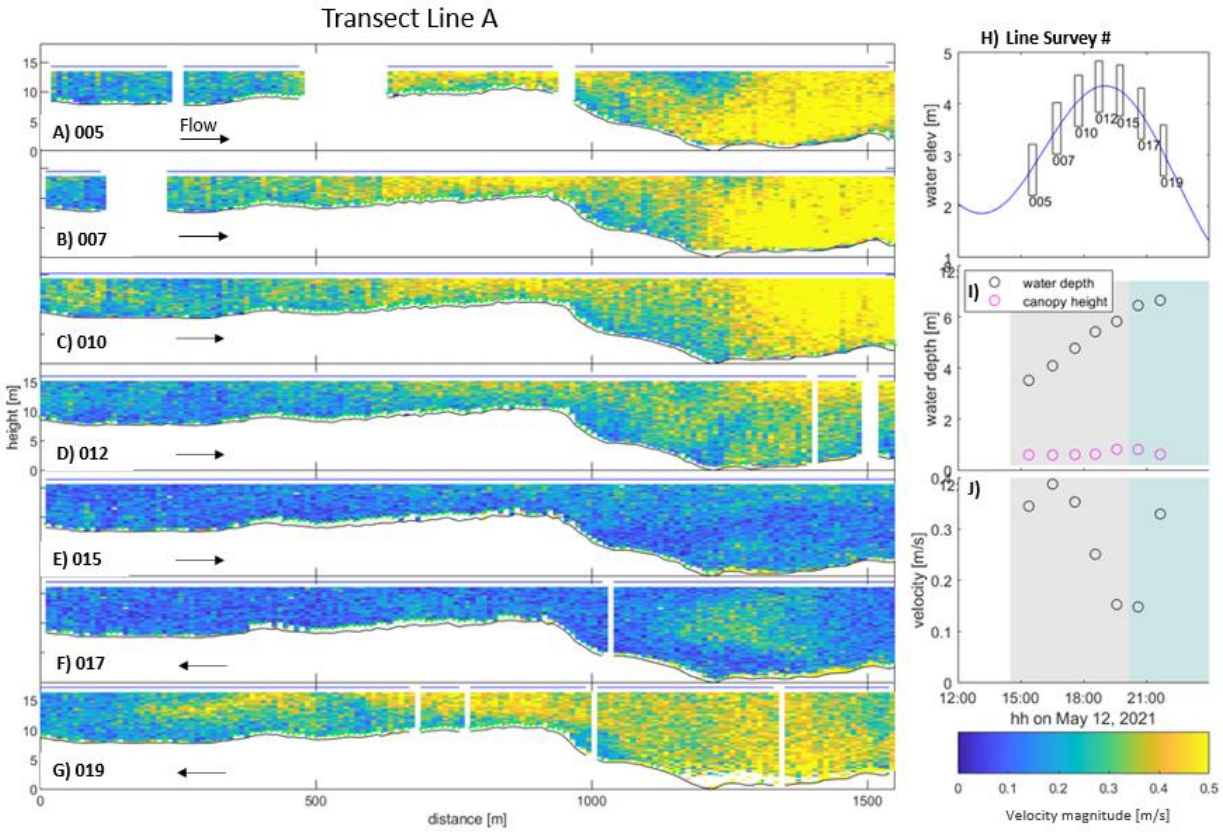

Figure 5 – Velocity magnitude profiles of longitudinal transect Line A surveyed seven times on May 12, 201. A) 005, B) 007, C) 010, D) 012, E) 015, F) 017, G) 019. I) Water level and tidal stage of each transect. J) Average flow velocity (m/s) over time during transect survey period.

Velocity profiles for Transect B are shown in Figure 8. Similar, to Transect A, all profiles show the trend of flow acceleration towards the northern meadow portion during the flood and deceleration towards the south during the ebb. The flow captured along these lines north of the meadow is influenced by a sharp morphological feature. All profiles, expect for 006 (Figure 8 A) show flow reductions on the lee side of the sharp feature, which varies based on the direction of flow between flood and ebb. Near peak flood (Figure 8 A & B), flow appears to accelerate within the interior and northern meadow and beyond the meadow, despite an increase in water depth. As seen along Transect A (Figure 7 C&D), during the transition from flood to ebb around slack (Figure 8 B-D), flow decelerated first in the north and the interior, while the southern meadow remained heightened for longer and lagged the other sections. However, due to the missing values from the vessel departing too much from the transect line, this process was less visible in Transect B than A. As flow transitions into ebb, flow first accelerates in the north and the northern most edge of the meadow, as it travels from north to south. The low-flow zone on

the lee side of the sharp feature is pronounced during the strongest ebb time period, and flow begins to accelerate into the interior meadow towards the south.

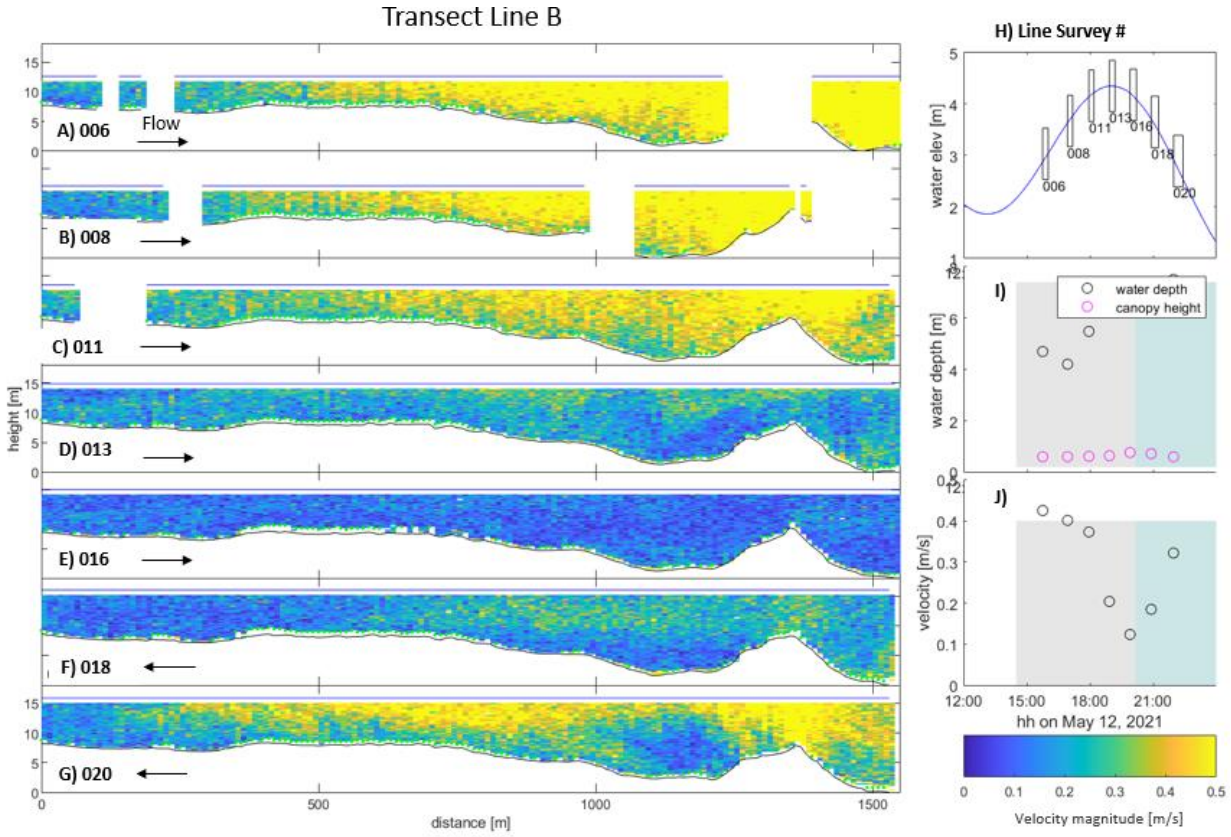

Figure 6 – Velocity magnitude profiles of longitudinal transect Line B surveyed seven times on May 12, 201. A) 006, B) 008, C) 011, D) 013, E) 016, F) 018, G) 20. I) Water level and tidal stage of each transect. J) Average flow velocity over time during transect survey period.

3.41 ADCP Measured Seagrass Canopy & Flow Velocity

The measured seagrass canopy heights along ADCP transects agree well with the mapped distribution within Choked Passage (Figure 5). This method successfully depicted the patchiness of the southern meadow, the relatively dense and high canopy interior, as well as the increasing patchiness at the northern margin of the interior meadow. Percentage of seagrass canopy within the water column was greatest during low tide transects and reached up to 1.2 m in the interior meadow. During strong tidal currents, canopy height was lower and reached a maximum of 0.8 m, due to blade bending. At water depths around 7.5-8.5 m during the strongest measured ebb flow over the main meadow, seagrass canopies occupy between 5-10% of the water depth. Within the interior, there were several areas that seagrass was not detected, this may

have resulted from the sparse seagrass in certain areas of the interior, or simply may reflect a gap within the seagrass canopy. Moreover, there are several instances of seagrass detection outside of the meadow extent. These detections may be caused by kelp, drifting algae, or other material near the bed, causing a similar spike in backscatter. Given the strict depth limits of *Z. marina* (Duarte, 1991), most of these seagrass detections outside of the meadow extent and in deeper sections likely do not reflect actual seagrass.

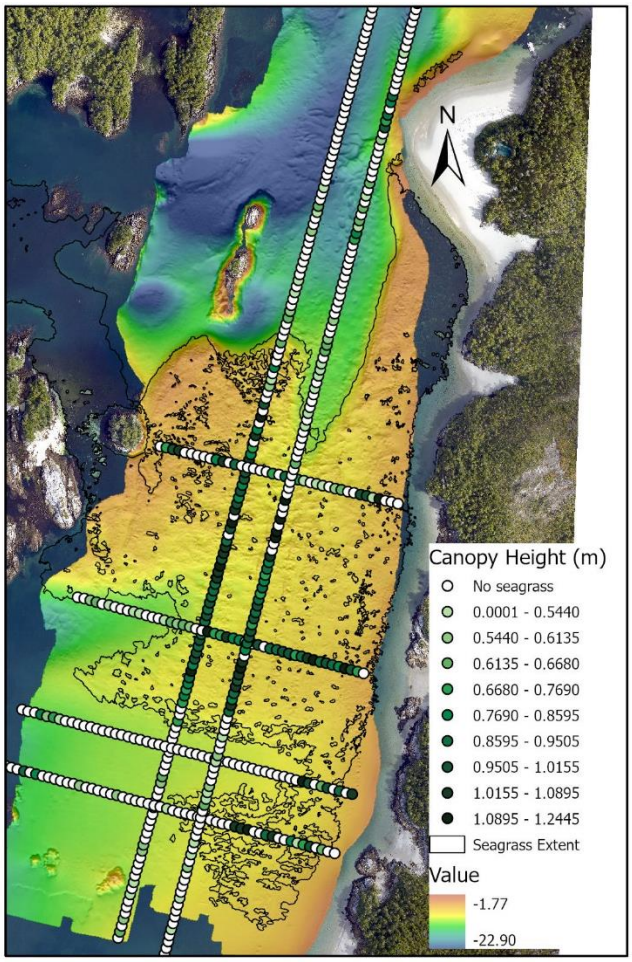

Figure 7 – A) Seagrass canopy height (m) detected from low-tide ADCP transects on May 2021 in Choked Passage, British Columbia.

During both peak flood and strongest ebb conditions, flow velocity is greatest in the northern section of Choked Passage outside of the meadow and reduced in the southern section (Figure 6). During peak flood, flow accelerates as it flows from the south towards the north-west corner of the meadow, adjacent to rocky islands, and over the meadow interior (Figure 6 A). The fastest flood flow over the main meadow occurs in the region of increased seagrass patchiness in

the northwest. The strongest ebb tides measured during this study showed overall similar spatial trends as peak flood conditions (Figure 6 B). Flow is fastest over the northern margin of the main meadow, decelerates in the meadow center to accelerate again over the southern end of the main meadow. The lowest ebb flow velocities occur over the southern meadow. The cross-sections were collected slightly earlier during the ebbing tide and show overall lower flow velocities, that are inconsistent with the longitudinal profiles.

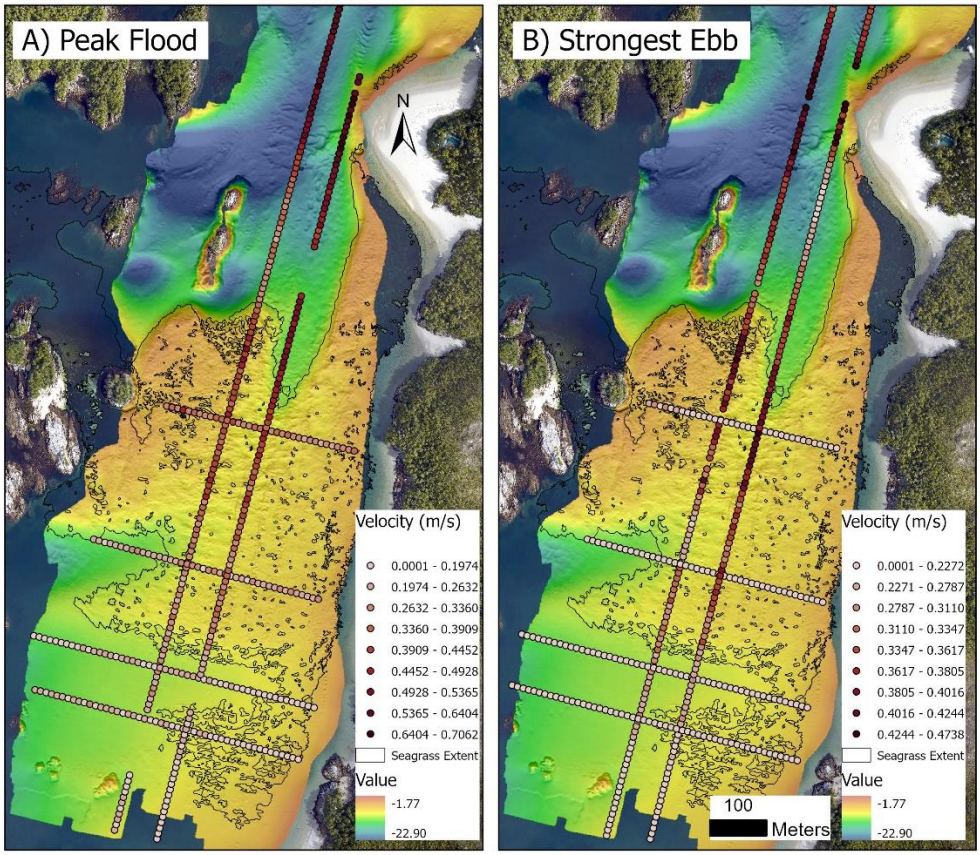

Figure 8 – A) Peak flood depth-average velocity (m/s) measurements and B) strongest ebb depth-averaged velocity (m/s) measurements from May 2021 ADCP transects in Choked Passage, British Columbia.

3.43 Total Suspended Material

The average total suspended material (TSM) was 1.45 mg/L ± 0.33 mg/L. Overall, the measured TSM were low for nearshore coastal systems (Loos & Costa, 2010), and were consistent among slack low and high tide conditions, different water depths, and locations within the meadow. This indicates that there is minimal suspended sediment in the water column during these times in Choked Passage, however, this method of TSM measurement can capture micro-

organisms and organic material (Röttgers et al., 2014), therefore actual concentrations of suspended sediment may be lower, and are likely higher during periods of stronger current speeds. In the future, a Loss on Ignition should be performed to collected water samples to remove all organic material and quantify the amount of suspended sediment and organic material in the water column. In Choked Passage, material maybe temporarily transported as bed-load, which requires lower sustained shear stress and velocity for relatively coarse sand grains (Fernandez Luque & Van Beek, 1976).

Table 12 - Total suspended material (mg/L) measured from water samples at different locations, tidal stage, and depth in Choked Passage. See 6.6 Appendix F Figure 20 for map of water sample locations.

Sample ID	Site ID	Tidal Stage	Depth (m)	TSM (mg/L)
A1-L	A1	Low	6	1.64
A2-L	A2	Low	2.5	1.03
A3-L	A3	Low	3	1.61
A4-L	A4	Low	4	1.09
B1-L	B1	Low	6	2.16
B2-L	B2	Low	3	1.43
B3-L	B3	Low	3	0.99
B4-L	B4	Low	4	1.19
A1-H	A1	High	7	1.27
A2-H	A2	High	4	1.54
A3-H	A3	High	5	1.29
A4-H	A4	High	6	1.66
B1-H	B1	High	10	1.46
B2-H	B2	High	5	1.32
B3-H	B3	High	5	2.06
B4-H	B4	High	5	1.41

3.44 Critical Threshold for Incipient Motion, Shear Velocity & Shear Stress

The grain size distributions of bed samples for four locations within the meadow were used to estimate critical shear stress for incipient motion and suspension of bed material. The location of bed samples are shown in Figure 1; D10, D50, and D90 of the four samples are given in Table 3. All samples consist mostly of sand, with the finest material found at GS_South and coarsest material at GS_Centre. A significant amount of shell fragments were present in most

sediment samples, ranging from whole shells in largest clast size to fine fragments in the smallest clast size. The greatest proportions of shell fragments were found in GS_West and GS_Center, while the lowest proportions and smallest sizes were found in GS_South. The critical shear stress required to initiate motion of the D50 at GS_South is largest, while the other sites have similar $\boldsymbol{\tau^*_{cr,mot}}$. The critical shear stress for suspension of the D50, however, is largest at GS_Centre and smallest at GS_South. Once initiation of motion begins at GS_South, it only requires a small increase in shear stress to suspend the grains, while bedload continues for a while at the other locations.

Table 13 – Grain size diameters, dimensionless critical shear stress for sediment motion, and suspension for bed samples in Choked Pass.

Bed Sample	**D10 (mm)**	**D50 (mm)**	**D90 (mm)**	$\boldsymbol{\tau^*_{cr,mot}}$ **D10**	$\boldsymbol{\tau^*_{cr,mot}}$ **D50**	$\boldsymbol{\tau^*_{cr,mot}}$ **D90**	$\boldsymbol{\tau^*_{cr,sus}}$ **D10**	$\boldsymbol{\tau^*_{cr,sus}}$ **D50**	$\boldsymbol{\tau^*_{cr,sus}}$ **D90**
GS_West	0.084	0.21	0.55	0.056	0.025	0.016	0.056	0.166	0.767
GS_East	0.086	0.20	0.41	0.055	0.026	0.017	0.055	0.152	0.511
GS_Centre	0.090	0.24	0.42	0.052	0.023	0.017	0.052	0.213	0.530
GS_South	0.090	0.13	0.4	0.052	0.038	0.017	0.052	0.063	0.493

The stationary flow data revealed that DPL 2 is located in the shallowest water, experienced the strongest flow, and consequently the longest peak ebb (flow > 0.38 m/s) duration (~80 min) (Table 4). All other sites experience peak ebb for approximately 33 – 43 minutes. DPL 4 was situated in the deepest water and outside the meadow. Water level fluctuated by 0.34-0.44 m during peak ebb for DPL 1, DPL 3, and DPL 4, and by 0.62 m for DPL 2.

Table 14 – Maximum depth-average ebb flow velocity, high tide water depth at start of ebb, low tide water depth at the end of ebb, duration of peak ebb, and change in water level during peak ebb for each deployment (DPL1-4).

	DPL 1	**DPL 2**	**DPL 3**	**DPL 4**
Max. d.a. ebb flow [m/s]	0.40	0.43	0.39	0.41
HT water depth [m]	9.14	8.22	8.98	9.62
LT water depth [m]	6.96	5.88	6.70	6.30
Duration [min] of peak ebb	33.2	81.8	37.1	43.1
Δ water level during peak ebb	0.34	0.62	0.38	0.44

[m]				

Figure 9 demonstrates the effect of the averaging window on the distribution of best fit heights for velocity profiles during peak ebb at each deployment site. 10-minute averages showed a range of best fit heights, often clustering around certain heights (e.g., DPL 1 and 4 around 0.4). 30-minute averages over almost entirely all profiles collected during peak ebb for DPL 1, 3, and 4, reduced the cluster and showed the emergence of one dominant fit height mid water column. For the longer DPL 2, two dominant peaks remain, even with a 30-min averaging window. Example average velocity profiles are shown in Figure 10. Next to the dominant peaks emerging from 30-minute averaging, additional inflection points can be seen for DPL 1, 2, and 3 that occur at the secondary histogram peaks visible in the top panels of Figure 9. Based on these observations, it appears that all three deployments 1, 2, and 3 are best represented by three log linear segments, converging between z/h = 0.31 – 0.4 and z/h = 0.58-0.61. DPL 4 appears to be best represented by two log linear segments, converging at z/h = 0.4 (Figure 10

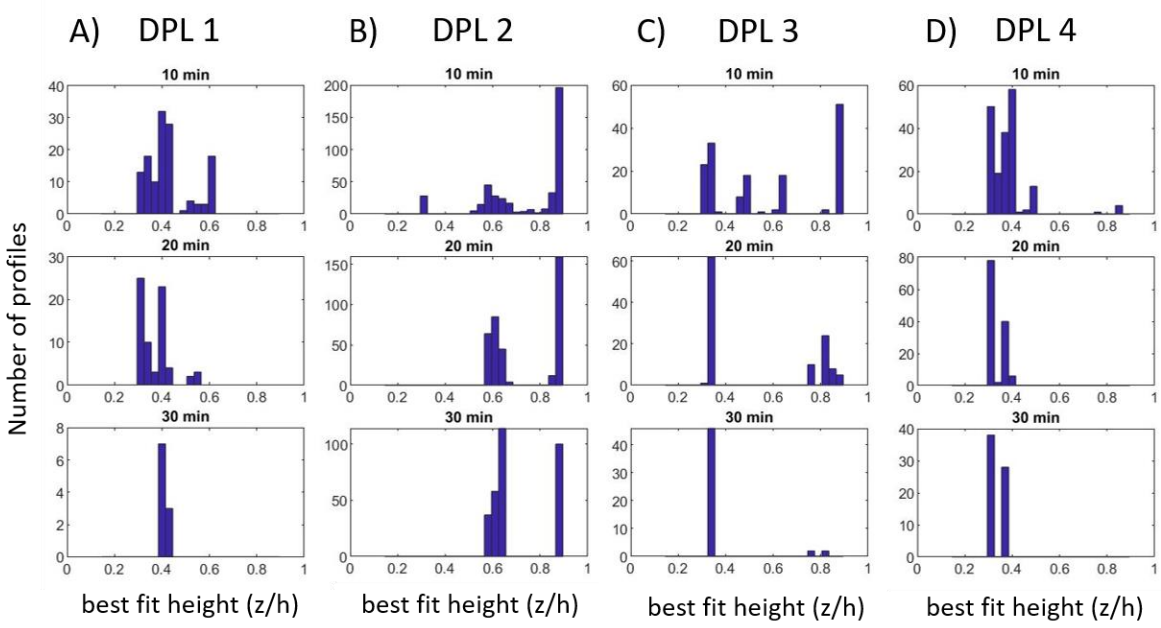

Figure 14 - Distribution of best fit heights (z/h) for average velocity profiles collected during peak flood flow. A) – D) show results for DPL 1 to DPL 4, top to bottom show different averaging windows (10, 20, and 30 min).

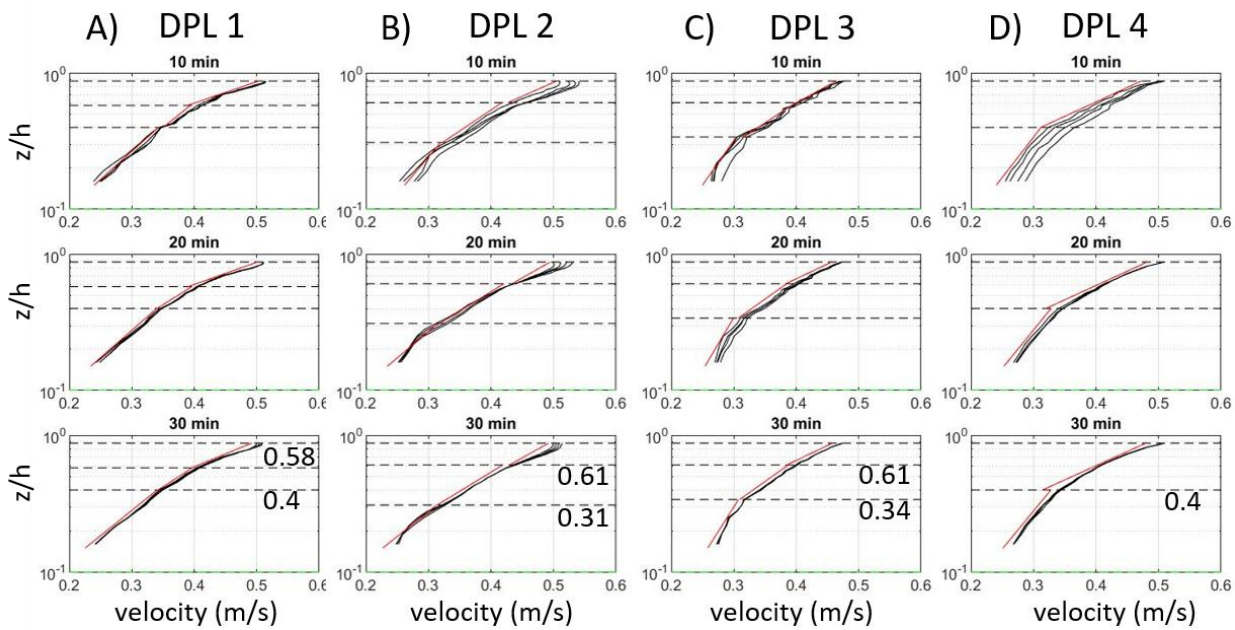

Figure 15 – Example averaged velocity profile for ebb flow > 0.38 m/s from moored ADCP deployments in May 2021. Red lines show three (two for DPL 4) log fit segments derived for the example profiles from which shear velocity was derived. Dashed lines show heights for logfits used in shear velocity estimates. Maximum height of the canopy is indicated in green (z/h = 0.1). Top to bottom: 10-minute to 30-minute averages.

Given that all velocity profiles from deployments inside the meadow are best approximated by three log-linear segments, and the one deployment outside the meadow by two segments, we assume the following: the upper inflection point, ranging from between 0.58 – 0.61 reflects the top of the vegetation roughness layer, while the lower inflection point represents the top of the grain roughness layer. This assumes that bedform roughness is negligible. The shear stress available for sediment movement should then be equal to the shear stress derived from the lower log fit segments. Shear velocities derived from each log-linear segment, roughness lengths, and calculated shear stresses are given in Table 5. Accordingly, the shear stress available for sediment movement during this peak ebb period is largest at DPL 1 and lowest in DPL 3.

Table 15 - Average shear velocities u_* and roughness height *z0* derived from 30-minute moving average velocity profiles under ebb flow > 0.38 m/s. Log fits were conducted for the grain roughness layer, the vegetation roughness layer, and the full water column (z/h = 0.88). Shear stress as calculated from shear velocity is also given.

	DPL 1	**DPL 2**	**DPL 3**	**DPL 4**
$u_*, grain$ [m/s]	0.0482	0.0403	0.0239	0.032
u_*, veg [m/s]	0.0592	0.0696	0.0547	-
$u_*, full$ [m/s]	0.0978	0.0929	0.0784	0.083
$z0, grain$ [m]	0.1858	0.1264	0.0142	0.05
$z0, veg$ [m]	0.3158	0.4059	0.2768	-
$z0, full$ [m]	0.9394	0.7162	0.6779	0.76
$\boldsymbol{\tau, grain}$ **[Pa]**	**2.32**	**1.62**	**0.57**	**1.02**
τ, veg [Pa]	3.50	4.84	2.99	-
$\tau, full$ [Pa]	9.56	8.63	6.15	6.89

Using the D50 of the four bed samples, the dimensionless bed shear stress τ^* is calculated as.

$$\tau^* = \frac{\tau}{(\rho_s - \rho_w) g D_{50}})$$

The D50 of the main meadow sediment ranged between 0.2 - 0.24 mm, which resulted in dimensionless bed shear stresses between 0.15 – 0.72 for the three deployments within the main meadow. Critical shear stress thresholds for motion of the D50 ranged from 0.23-0.26. The range of dimensionless bed shear stress values are all above the critical shear stresses needed for initiation of motion of the D50, however, the maximum value of dimensionless shear stress is insufficient to cause suspension at DPL 3.

3.50 Conclusion

This study examined spatial patterns of canopy height and flow during peak flood and strong ebb, as well as examined whether sediment transport can occur under peak ebb flow velocities at different locations within the Choked Passage seagrass meadow using ADCP data. We investigated how tidal flow behaves over the seagrass meadow and whether tidal flow is responsible for sediment transport. Flow is very dynamic and spatially variable within the meadow. Overall, flow is fastest in the northern section of the main meadow, particularly in the north-west corner where the meadow is patchy. Moreover, flow appears to accelerate above the canopy through the meadow interior, which suggests that topographic steering and the strength

of incoming currents exceeds the ability of seagrass to dampen flow velocity. During the transition from peak flood to ebb, flow velocity remained heightened for longer above the southern meadow and was lagged relative to the other sections. Shear stress results indicate that sediment can be transport as bedload and in suspension under peak flow velocities at some of the sites examined within the meadow. Shear stress is largest in the meadow center and lower towards the southern margin of the main meadow. At this location, peak shear stresses are insufficient to cause suspension of the D50. Our shear stress estimates stem from peak ebbing conditions and are representative of a short (~30 minute) time window during a tidal cycle (except for DPL 2, which experienced fastest flow over a longer duration). Suspension may therefore be generally limited, which agrees with observation of low total suspended matter in water samples.

There may be other biophysical factors limiting sediment transport, such as algae and biofilm, which may increase the shear strength of the seabed (Fang et al., 2014) and could explain further the low suspended sediment concentrations observed in Choked Passage. Flow above the southern meadow is larger during peak tidal flows when compared to the main meadow. The finer bed sediment at this location requires larger bed shear stress to go into motion than bed sediment of the main meadow, but the critical shear stress for suspension is lower than in the main meadow. For example, the shear stress at DPL 3 would be sufficient to entrain and suspend those grains. Unfortunately, we do not have a deployment in the southern meadow to determine bed shear stress during peak ebb.

Additional research is needed to fully understand the flow dynamics within the Choked Passage seagrass meadow. Future studies should aim to compare the differences between peak ebb and peak flood, as well as seasonal differences between winter and summer seagrass condition. Moreover, acoustic backscatter could be calibrated to quantify suspended sediment concentrations across different locations within the meadow and over a tidal cycle. The results from this study provide insight on the complex morphodynamics within Choked Passage and indicate the need for more research on hydrodynamically exposed seagrass meadows.

3.60 Bibliography

Bos, A. R., Bouma, T. J., de Kort, G. L. J., & van Katwijk, M. M. (2007). Ecosystem engineering by annual intertidal seagrass beds: Sediment accretion and modification.

Estuarine, Coastal and Shelf Science, 74(1–2), 344–348. https://doi.org/10.1016/j.ecss.2007.04.006

Bouma, T. J., Friedrichs, M., van Wesenbeeck, B. K., Temmerman, S., Graf, G., & Herman, P. M. J. (2009). Density-dependent linkage of scale-dependent feedbacks: A flume study on the intertidal macrophyte Spartina anglica. Oikos, 118(2), 260–268. https://doi.org/10.1111/j.1600-0706.2008.16892.x

de Boer, W. F. (2007). Seagrass–sediment interactions, positive feedbacks and critical thresholds for occurrence: A review. Hydrobiologia, 591(1), 5–24. https://doi.org/10.1007/s10750-007-0780-9

Fang, H., Shang, Q., Chen, M., & He, G. (2014). Changes in the critical erosion velocity for sediment colonized by biofilm. Sedimentology, 61(3), 648–659. https://doi.org/10.1111/sed.12065

Fernandez Luque, R., & Van Beek, R. (1976). Erosion And Transport Of Bed-Load Sediment. Journal of Hydraulic Research, 14(2), 127–144. https://doi.org/10.1080/00221687609499677

Folkard, A. M. (2019). Biophysical Interactions in Fragmented Marine Canopies: Fundamental Processes, Consequences, and Upscaling. Frontiers in Marine Science, 6. https://doi.org/10.3389/fmars.2019.00279

Hansen, J., & Reidenbach, M. (2012). Wave and tidally driven flows in eelgrass beds and their effect on sediment suspension. Marine Ecology Progress Series, 448, 271–287. https://doi.org/10.3354/meps09225

Hughes, A. R., Stachowicz, J. J., & Williams, S. L. (2009). Morphological and physiological variation among seagrass (Zostera marina) genotypes. Oecologia, 159(4), 725–733. https://doi.org/10.1007/s00442-008-1251-3

Kennedy, L. A., Juanes, F., & El-Sabaawi, R. (2018). Eelgrass as Valuable Nearshore Foraging Habitat for Juvenile Pacific Salmon in the Early Marine Period. Marine and Coastal Fisheries, 10(2), 190–203. https://doi.org/10.1002/mcf2.10018

Koch, E. W., Ackerman, J. D., Verduin, J., & Keulen, M. van. (2006). Fluid Dynamics in Seagrass Ecology—From Molecules to Ecosystems. In A. W. D. LARKUM, R. J. ORTH, & C. M. DUARTE (Eds.), SEAGRASSES: BIOLOGY, ECOLOGYAND CONSERVATION (pp. 193–225). Springer Netherlands. https://doi.org/10.1007/978-1-4020-2983-7_8

Lacy, J. R., & Wyllie-Echeverria, S. (2011). The influence of current speed and vegetation density on flow structure in two macrotidal eelgrass canopies: A field study of eelgrass hydrodynamics. Limnology and Oceanography: Fluids and Environments, 1(1), 38–55. https://doi.org/10.1215/21573698-1152489

Le Bouteiller, C., & Venditti, J. G. (2014). Vegetation-driven morphodynamic adjustments of a sand bed. Geophysical Research Letters, 41(11), 3876–3883. https://doi.org/10.1002/2014GL060155

Lefebvre, A., Thompson, C. E. L., & Amos, C. L. (2010). Influence of Zostera marina canopies on unidirectional flow, hydraulic roughness and sediment movement. *Continental Shelf Research*, 30(16), 1783-1794.

Loos, E. A., & Costa, M. (2010). Inherent optical properties and optical mass classification of the waters of the Strait of Georgia, British Columbia, Canada. *Progress in Oceanography*, 87(1-4), 144-156.

Mcleod, E., Chmura, G. L., Bouillon, S., Salm, R., Björk, M., Duarte, C. M., Lovelock, C. E., Schlesinger, W. H., & Silliman, B. R. (2011). A blueprint for blue carbon: Toward an improved understanding of the role of vegetated coastal habitats in sequestering CO 2. Frontiers in Ecology and the Environment, 9(10), 552–560. https://doi.org/10.1890/110004

Mtwana Nordlund, L., Koch, E. W., Barbier, E. B., & Creed, J. C. (2016). Seagrass Ecosystem Services and Their Variability across Genera and Geographical Regions. PLOS ONE, 11(10), e0163091. https://doi.org/10.1371/journal.pone.0163091

Nepf, H. M. (2012). Hydrodynamics of vegetated channels. Journal of Hydraulic Research, 50(3), 262–279. https://doi.org/10.1080/00221686.2012.696559

Olson, A. M., Hessing-Lewis, M., Haggarty, D., & Juanes, F. (2019). Nearshore seascape connectivity enhances seagrass meadow nursery function. Ecological Applications, 29(5). https://doi.org/10.1002/eap.1897

Orth, R. J., Carruthers, T. J. B., Dennison, W. C., Duarte, C. M., Fourqurean, J. W., Heck, K. L., Hughes, A. R., Kendrick, G. A., Kenworthy, W. J., Olyarnik, S., Short, F. T., Waycott, M., & Williams, S. L. (2006). A Global Crisis for Seagrass Ecosystems. BioScience, 56(12), 987. https://doi.org/10.1641/0006-3568(2006)56[987:AGCFSE]2.0.CO;2

Prentice, C., Hessing-Lewis, M., Sanders-Smith, R., & Salomon, A. K. (2019). Reduced water motion enhances organic carbon stocks in temperate eelgrass meadows. Limnology and Oceanography, 64(6), 2389–2404. https://doi.org/10.1002/lno.11191

Rennie, C. D., & Millar, R. G. (2004). Measurement of the spatial distribution of fluvial bedload transport velocity in both sand and gravel. Earth Surface Processes and Landforms, 29(10), 1173–1193. https://doi.org/10.1002/esp.1074

Rijn, V., & C, L. (2007). Unified View of Sediment Transport by Currents and Waves. I: Initiation of Motion, Bed Roughness, and Bed-Load Transport. Journal of Hydraulic Engineering, 133(6), 649–667. https://doi.org/10.1061/(ASCE)0733-9429(2007)133:6(649)

Röttgers, R., Heymann, K., & Krasemann, H. (2014). Suspended matter concentrations in coastal waters: Methodological improvements to quantify individual measurement uncertainty. Estuarine, Coastal and Shelf Science, 151, 148–155. https://doi.org/10.1016/j.ecss.2014.10.010

Short, F., Carruthers, T., Dennison, W., & Waycott, M. (2007). Global seagrass distribution and diversity: A bioregional model. Journal of Experimental Marine Biology and Ecology, 350(1–2), 3–20. https://doi.org/10.1016/j.jembe.2007.06.012

Spalding, D. B. (1961). A single formula for the law of the wall. *Journal of Applied Mechanics*, *28*(3), 455-458.

van Katwijk, M. M., Bos, A. R., Hermus, D. C. R., & Suykerbuyk, W. (2010). Sediment modification by seagrass beds: Muddification and sandification induced by plant cover and environmental conditions. Estuarine, Coastal and Shelf Science, 89(2), 175–181. https://doi.org/10.1016/j.ecss.2010.06.008

Warren, J. D., & Peterson, B. J. (2007). Use of a 600-kHz Acoustic Doppler Current Profiler to measure estuarine bottom type, relative abundance of submerged aquatic vegetation, and eelgrass canopy height. Estuarine, Coastal and Shelf Science, 72(1–2), 53–62. https://doi.org/10.1016/j.ecss.2006.10.026

Widdows, J., Pope, N., Brinsley, M., Asmus, H., & Asmus, R. (2008). Effects of seagrass beds (Zostera noltii and Z. marina) on near-bed hydrodynamics and sediment resuspension. Marine Ecology Progress Series, 358, 125–136. https://doi.org/10.3354/meps07338

Wilkinson, R. H. (1983). A method for evaluating statistical errors associated with logarithmic velocity profiles. *Geo-marine letters*, 3(1), 49-52.

Yager, E. M., & Schmeeckle, M. W. (2013). The influence of vegetation on turbulence and bed load transport. Journal of Geophysical Research: Earth Surface, 118(3), 1585–1601. https://doi.org/10.1002/jgrf.20085

4.0 Conclusion

This research examined the morphodynamics (i.e. the interaction between flow, sediment transport, and bed morphology) of the Choked Passage seagrass meadow, on the Central Coast of British Columbia. Each chapter examined a different component of the morphodynamic drivers within Choked Passage (climate variability, storm events, and tidal cycles).

In chapter two , I used bathymetry, sediment backscatter, and seagrass delineations from repeat MBES and drone surveys to examine the relationship between the Choked Passage seagrass meadow and bed morphology over time and determine whether changes are linked to storm activity and climate variability. From 2018 to 2021, the meadow experienced significant

erosion (net surface lowering of -18,768 m^3) and loss of seagrass (10% reduction), which we attribute to the preceding winter storm activity driven by moderate La Niña conditions. The spatial patterns of erosion and seagrass loss was non-uniform across the meadow. Coupled erosion and seagrass loss resulted in the generation or expansion of blowouts. In locations where seagrass loss was decoupled from bed level changes, we observed increased fragmentation without blowout formation. Future research should aim to understand why seagrass loss and blowout formation/expansion is coupled in some areas but not all, and whether these features form during or are lagged after a storm event. We observed a trend of reduction in seagrass coverage following winters with a high number of storm events and/or high recorded storm intensity from 2014 to 2021. We expect the Choked Passage seagrass meadow undergoes cyclic behaviour with reduction in seagrass coverage during energetic ENSO years, followed by a recovery period. The observed recovery of the eroded bed material suggests the meadow has entered this period of seagrass and sediment recovery, until the next significant ENSO year, creating a bio-geomorphic cycle. However, the current timeseries is unable to resolve whether this cycle truly occurs in Choked Passage. Future research should continue to survey the Choked Passage seagrass to develop a longer time series in order to uncover the significance of the proposed bio-geomorphic cycle.

In chapter three, an ADCP was moored to the seafloor to measure flow overtime at different sites and was mounted to a vessel to survey transects lines across the meadow. The objective of this research section was to examine how flow behaves within and outside the seagrass meadow, and whether tidal currents drive sediment transport. The ADCP measured canopy height, flow velocity and direction along transect lines. The moored ADCP data were used to estimate shear stress. Overall, flow is fastest in the northern section of above the canopy of the main meadow, particularly in the north-west corner where the meadow is patchy. Moreover, flow appears to accelerate through above the canopy in the meadow interior, which suggests that topographic steering and the strength of incoming currents exceeds the ability of seagrass to dampen flow velocity. During the transition from peak flood to ebb, flow velocity remained heightened for longer above the southern meadow and lagged the other sections. Shear stress results suggest that sediment can be transport as bedload and in suspension under peak flow velocities at some of the sites examined within the meadow. Shear stress is largest in the meadow center and lower towards the southern margin of the main meadow, due to reduced flow

in the south. Total suspended material is relatively low within Choked Passage under low and high tide conditions. Shear stress results indicate that sediment can be transport as bedload and suspension under peak flow velocities at most of the sites examined. When initiated, sediment is likely primarily transported as bedload, creating the observed sand wave and blowout bedforms in chapter two. Future research should collect ADCP flow data during the winter storm period to determine how storm events modify flow and sediment transport. Moreover, future research should aim to quantify the concentration of suspended sediment using the ADCP acoustic backscatter.

This research provides a comprehensive overview of the morphodynamics of the Choked Passage seagrass meadow on the Central Coast of British Columbia. By studying a highly dynamic and relatively exposed seagrass meadow, we improve the overall understanding of physical processes of seagrass meadows. Morphodynamics have an important influence on the ecosystem structure and function over time (Corenblit et al., 2011), therefore, it is important to better understand these processes. Climate variability is predicted to increase, while seagrasses continue to decline worldwide (Cai et al., 2015; Orth et al., 2006), and effort should be made to understand how seagrass will respond to the changing climate and physical environment. The results of this study have significant implications on seagrass conservation, restoration, and the evolution of coastal landscapes.

5.0 Bibliography

Abeysirigunawardena, D. S., & Walker, I. J. (2008). Sea level responses to climatic variability and change in northern British Columbia. Atmosphere-Ocean, 46(3), 277–296. https://doi.org/10.3137/ao.460301

Allan, J. C., & Komar, P. D. (2006). Climate Controls on US West Coast Erosion Processes. Journal of Coastal Research, 223, 511–529. https://doi.org/10.2112/03-0108.1

Allaoui, N. E., Serra, T., Colomer, J., Soler, M., Casamitjana, X., & Oldham, C. (2016). Interactions between Fragmented Seagrass Canopies and the Local Hydrodynamics. *PLOS ONE*, *11*(5), e0156264. https://doi.org/10.1371/journal.pone.0156264

Anthony Stallins, J., & Corenblit, D. (2018). Interdependence of geomorphic and ecologic resilience properties in a geographic context. *Geomorphology*, *305*, 76–93. https://doi.org/10.1016/j.geomorph.2017.09.012

ASTM, A. (2017). D7928: Standard test method for particle-size distribution (gradation) of fine-grained soil using the sedimentation (hydrometer) analysis. *ASTM International: West Conshohocken (PA)*.

Barnard, P. L., Hoover, D., Hubbard, D. M., Snyder, A., Ludka, B. C., Allan, J., Kaminsky, G. M., Ruggiero, P., Gallien, T. W., Gabel, L., McCandless, D., Weiner, H. M., Cohn, N., Anderson, D. L., & Serafin, K. A. (2017). Extreme oceanographic forcing and coastal response due to the 2015–2016 El Niño. Nature Communications, 8(1), 14365. https://doi.org/10.1038/ncomms14365

Belcher, S. E., Jerram, N., & Hunt, J. C. R. (2003). Adjustment of a turbulent boundary layer to a canopy of roughness elements. *Journal of Fluid Mechanics*, *488*, 369–398. https://doi.org/10.1017/S0022112003005019

Bell, S. S. (1999). Gap Dynamics in a Seagrass Landscape. *Ecosystems*, *2*(6), 493–504. https://doi.org/10.1007/s100219900097

Beudin, A., Kalra, T. S., Ganju, N. K., & Warner, J. C. (2017). Development of a coupled wave-flow-vegetation interaction model. *Computers & Geosciences*, *100*, 76–86. https://doi.org/10.1016/j.cageo.2016.12.010

Best, J., & Kostaschuk, R. (2002). An experimental study of turbulent flow over a low-angle dune. Journal of Geophysical Research: Oceans, 107(C9), 18-1-18–19. https://doi.org/10.1029/2000JC000294

Bos, A. R., Bouma, T. J., de Kort, G. L. J., & van Katwijk, M. M. (2007). Ecosystem engineering by annual intertidal seagrass beds: Sediment accretion and modification. *Estuarine, Coastal and Shelf Science*, *74*(1–2), 344–348. https://doi.org/10.1016/j.ecss.2007.04.006

Bosma, C. (2019). Multibeam & Backscatter Classification: A methodology for producing theoretical substrate rasters from multibeam echosounder data.

Boström, C., Baden, S., Bockelmann, A.-C., Dromph, K., Fredriksen, S., Gustafsson, C., Krause-Jensen, D., Möller, T., Nielsen, S. L., Olesen, B., Olsen, J., Pihl, L., & Rinde, E. (2014).

Distribution, structure and function of Nordic eelgrass (Zostera marina) ecosystems: Implications for coastal management and conservation. *Aquatic Conservation: Marine and Freshwater Ecosystems*, *24*(3), 410–434. https://doi.org/10.1002/aqc.2424

Boström, C., Pittman, S., Simenstad, C., & Kneib, R. (2011). Seascape ecology of coastal biogenic habitats: Advances, gaps, and challenges. *Marine Ecology Progress Series*, *427*, 191–217. https://doi.org/10.3354/meps09051

Bouma, T. J., van Duren, L. A., Temmerman, S., Claverie, T., Blanco-Garcia, A., Ysebaert, T., & Herman, P. M. J. (2007). Spatial flow and sedimentation patterns within patches of epibenthic structures: Combining field, flume and modelling experiments. *Continental Shelf Research*, *27*(8), 1020–1045. https://doi.org/10.1016/j.csr.2005.12.019

Bradley, K., & Houser, C. (2009). Relative velocity of seagrass blades: Implications for wave attenuation in low-energy environments. *Journal of Geophysical Research: Earth Surface*, *114*(F1). https://doi.org/10.1029/2007JF000951

Brown, C. J., Beaudoin, J., Brissette, M., & Gazzola, V. (2019). Multispectral Multibeam Echo Sounder Backscatter as a Tool for Improved Seafloor Characterization. Geosciences, 9(3), 126. https://doi.org/10.3390/geosciences9030126

Cabaço, S., Santos, R., & Duarte, C. M. (2008). The impact of sediment burial and erosion on seagrasses: A review. Estuarine, Coastal and Shelf Science, 79(3), 354–366. https://doi.org/10.1016/j.ecss.2008.04.021

Cai, W., Wang, G., Santoso, A., McPhaden, M. J., Wu, L., Jin, F.-F., Timmermann, A., Collins, M., Vecchi, G., Lengaigne, M., England, M. H., Dommenget, D., Takahashi, K., & Guilyardi, E. (2015). Increased frequency of extreme La Niña events under greenhouse warming. Nature Climate Change, 5(2), 132–137. https://doi.org/10.1038/nclimate2492

Carr, J. A., D'Odorico, P., McGlathery, K. J., & Wiberg, P. L. (2016). Spatially explicit feedbacks between seagrass meadow structure, sediment and light: Habitat suitability for seagrass growth. *Advances in Water Resources*, *93*, 315–325. https://doi.org/10.1016/j.advwatres.2015.09.001

Chen, S.-N., Sanford, L. P., Koch, E. W., Shi, F., & North, E. W. (2007). A nearshore model to investigate the effects of seagrass bed geometry on wave attenuation and suspended sediment transport. *Estuaries and Coasts*, *30*(2), 296–310. https://doi.org/10.1007/BF02700172

Colomer, J., Soler, M., Serra, T., Casamitjana, X., & Oldham, C. (2017). Impact of anthropogenically created canopy gaps on wave attenuation in a Posidonia oceanica seagrass meadow. *Marine Ecology Progress Series*, *569*, 103–116. https://doi.org/10.3354/meps12090

Corenblit, D., Baas, A. C. W., Bornette, G., Darrozes, J., Delmotte, S., Francis, R. A., Gurnell, A. M., Julien, F., Naiman, R. J., & Steiger, J. (2011). Feedbacks between geomorphology and biota controlling Earth surface processes and landforms: A review of foundation concepts and current understandings. Earth-Science Reviews, 106(3–4), 307–331. https://doi.org/10.1016/j.earscirev.2011.03.002

de Boer, W. F. (2007). Seagrass–sediment interactions, positive feedbacks and critical thresholds for occurrence: A review. *Hydrobiologia*, *591*(1), 5–24. https://doi.org/10.1007/s10750-007-0780-9

De Falco, G., Ferrari, S., Cancemi, G., & Baroli, M. (2000). Relationship between sediment distribution and Posidonia oceanica seagrass. Geo-Marine Letters, 20(1), 50–57. https://doi.org/10.1007/s003670000030

de los Santos, C. B., Krause-Jensen, D., Alcoverro, T., Marbà, N., Duarte, C. M., van Katwijk, M. M., Pérez, M., Romero, J., Sánchez-Lizaso, J. L., Roca, G., Jankowska, E., Pérez-Lloréns, J. L., Fournier, J., Montefalcone, M., Pergent, G., Ruiz, J. M., Cabaço, S., Cook, K., Wilkes, R. J., … Santos, R. (2019). Recent trend reversal for declining European seagrass meadows. *Nature Communications*, *10*(1), 3356. https://doi.org/10.1038/s41467-019-11340-4

Duarte, C. M. (1991). Seagrass depth limits. *Aquatic Botany*, *40*(4), 363–377. https://doi.org/10.1016/0304-3770(91)90081-F

Duarte, C. M., & Chiscano, C. L. (1999). Seagrass biomass and production: A reassessment. Aquatic Botany, 65(1–4), 159–174. https://doi.org/10.1016/S0304-3770(99)00038-8

Duarte, C. M. (2002). The future of seagrass meadows. Environmental Conservation, 29(2), 192–206. https://doi.org/10.1017/S0376892902000127

Duarte, C. M., Fourqurean, J. W., Krause-Jensen, D., & Olesen, B. (2006). Dynamics of Seagrass Stability and Change. In A. W. D. LARKUM, R. J. ORTH, & C. M. DUARTE (Eds.), *SEAGRASSES: BIOLOGY, ECOLOGYAND CONSERVATION* (pp. 271–294). Springer Netherlands. https://doi.org/10.1007/978-1-4020-2983-7_11

Durán, O., Andreotti, B., & Claudin, P. (2012). Numerical simulation of turbulent sediment transport, from bed load to saltation. *Physics of Fluids*, *24*(10), 103306. https://doi.org/10.1063/1.4757662

Dyer, K. R., & New, A. L. (1986). INTERMITTENCY IN ESTUARINE MIXING. In D. A. Wolfe (Ed.), *Estuarine Variability* (pp. 321–339). Academic Press. https://doi.org/10.1016/B978-0-12-761890-6.50025-3

Fang, H., Shang, Q., Chen, M., & He, G. (2014). Changes in the critical erosion velocity for sediment colonized by biofilm. Sedimentology, 61(3), 648–659. https://doi.org/10.1111/sed.12065

Fahrig, L. (2003). Effects of Habitat Fragmentation on Biodiversity. *Annual Review of Ecology, Evolution, and Systematics*, *34*(1), 487–515. https://doi.org/10.1146/annurev.ecolsys.34.011802.132419

Fernandez Luque, R., & Van Beek, R. (1976). Erosion And Transport Of Bed-Load Sediment. Journal of Hydraulic Research, 14(2), 127–144. https://doi.org/10.1080/00221687609499677

Finnigan, J. (n.d.). Turbulence in plant canopies. *Ann. Rev. Fluid Mech*, 519–571.

Folkard, A. M. (2005). Hydrodynamics of model Posidonia oceanica patches in shallow water. *Limnology and Oceanography*, *50*(5), 1592–1600. https://doi.org/10.4319/lo.2005.50.5.1592

Folkard, A. M. (2019). Biophysical Interactions in Fragmented Marine Canopies: Fundamental Processes, Consequences, and Upscaling. *Frontiers in Marine Science*, *6*. https://doi.org/10.3389/fmars.2019.00279

Follett, E. M., & Nepf, H. M. (2012). Sediment patterns near a model patch of reedy emergent vegetation. *Geomorphology*, *179*, 141–151.https://doi.org/10.1016/j.geomorph.2012.08.006

Fonseca, M. S., Koehl, M. A. R., & Kopp, B. S. (2007). Biomechanical factors contributing to self-organization in seagrass landscapes. *Journal of Experimental Marine Biology and Ecology*, *340*(2), 227–246. https://doi.org/10.1016/j.jembe.2006.09.015

Fourqurean, J. W., & Rutten, L. M. (2004). THE IMPACT OF HURRICANE GEORGES ON SOFT-BOTTOM, BACK REEF COMMUNITIES: SITE- AND SPECIES-SPECIFIC EFFECTS IN SOUTH FLORIDA SEAGRASS BEDS. BULLETIN OF MARINE SCIENCE, 75(2), 20.

Frederiksen, M., Krause-Jensen, D., Holmer, M., & Laursen, J. S. (2004). Spatial and temporal variation in eelgrass (Zostera marina) landscapes: Influence of physical setting. *Aquatic Botany*, *78*(2), 147–165. https://doi.org/10.1016/j.aquabot.2003.10.003

Fretwell, K. (2020). A king tide storms ashore. Hakai Institute. Retrieved from https://hakai.org/a-king-tide-storms-ashore/

Ganthy, F., Sottolichio, A., & Verney, R. (2013). Seasonal modification of tidal flat sediment dynamics by seagrass meadows of Zostera noltii (Bassin d'Arcachon, France). *Journal of Marine Systems*, *109–110*, S233–S240. https://doi.org/10.1016/j.jmarsys.2011.11.027

Ghisalberti, M., & Nepf, H. M. (2002). Mixing layers and coherent structures in vegetated aquatic flows. *Journal of Geophysical Research: Oceans*, *107*(C2), 3-1-3–11. https://doi.org/10.1029/2001JC000871

Gilcoto, M., Jones, E., & Fariña-Busto, L. (2009). Robust estimations of current velocities with four-beam broadband ADCPs. *Journal of Atmospheric and Oceanic Technology*, *26*(12), 2642-2654.

Grech, A., Hanert, E., McKenzie, L., Rasheed, M., Thomas, C., Tol, S., Wang, M., Waycott, M., Wolter, J., & Coles, R. (2018). Predicting the cumulative effect of multiple disturbances on seagrass connectivity. Global Change Biology, 24(7), 3093–3104. https://doi.org/10.1111/gcb.14127

Gruber, R. K., & Kemp, W. M. (2010). Feedback effects in a coastal canopy-forming submersed plant bed. *Limnology and Oceanography*, *55*(6), 2285–2298. https://doi.org/10.4319/lo.2010.55.6.2285

Gordon, R. L. (1996). Acoustic Doppler current profiler-Principles of operation: A practical primer. *RD Instruments*.

Guerrero-Meseguer, L., Marín, A., & Sanz-Lázaro, C. (2017). Future heat waves due to climate change threaten the survival of Posidonia oceanica seedlings. Environmental Pollution, 230, 40–45. https://doi.org/10.1016/j.envpol.2017.06.039

Hansen, J., & Reidenbach, M. (2012). Wave and tidally driven flows in eelgrass beds and their effect on sediment suspension. Marine Ecology Progress Series, 448, 271–287. https://doi.org/10.3354/meps09225

Hansen, J. C. R., & Reidenbach, M. A. (2013). Seasonal Growth and Senescence of a Zostera marina Seagrass Meadow Alters Wave-Dominated Flow and Sediment Suspension Within a Coastal Bay. *Estuaries and Coasts*, *36*(6), 1099–1114. https://doi.org/10.1007/s12237-013-9620-5

Hansen, J. C. R., & Reidenbach, M. A. (2017). Turbulent mixing and fluid transport within Florida Bay seagrass meadows. *Advances in Water Resources*, *108*, 205–215. https://doi.org/10.1016/j.advwatres.2017.08.001

Hasegawa, N., Hori, M., & Mukai, H. (2008). Seasonal changes in eelgrass functions: Current velocity reduction, prevention of sediment resuspension, and control of sediment–water column nutrient flux in relation to eelgrass dynamics. *Hydrobiologia*, *596*(1), 387–399. https://doi.org/10.1007/s10750-007-9111-4

Heathfield, D. K. (2013). Erosive water levels and beach-dune morphodynamics, Wickaninnish Bay, Pacific Rim National Park Reserve, British Columbia, Canada [Thesis]. https://dspace.library.uvic.ca/handle/1828/4925

Heide, T. van der, Bouma, T. J., Nes, E. H. van, Koppel, J. van de, Scheffer, M., Roelofs, J. G. M., Katwijk, M. M. van, & Smolders, A. J. P. (2010). Spatial self-organized patterning in seagrasses along a depth gradient of an intertidal ecosystem. *Ecology*, *91*(2), 362–369. https://doi.org/10.1890/08-1567.1

Herman, P. M. J., Middelburg, J. J., & Heip, C. H. R. (2001). Benthic community structure and sediment processes on an intertidal flat: Results from the ECOFLAT project. *Continental Shelf Research*, *21*(18), 2055–2071. https://doi.org/10.1016/S0278-4343(01)00042-5

Hjulstrom, F. (1939). *Transportation of Detritus by Moving Water: Part 1. Transportation*. *142*, 5–31.

Hossain, M. S., Islam, M. A., Badhon, F. F., & Imtiaz, T. (2021). Hydrometer Analysis. Properties and Behavior of Soil-Online Lab Manual.

Hughes, A. R., Stachowicz, J. J., & Williams, S. L. (2009). Morphological and physiological variation among seagrass (Zostera marina) genotypes. Oecologia, 159(4), 725–733. https://doi.org/10.1007/s00442-008-1251-3

Hughes, B. B., Eby, R., Dyke, E. V., Tinker, M. T., Marks, C. I., Johnson, K. S., & Wasson, K. (2013). Recovery of a top predator mediates negative eutrophic effects on seagrass. *Proceedings of the National Academy of Sciences*, *110*(38), 15313–15318. https://doi.org/10.1073/pnas.1302805110

Jankowska, E., Włodarska-Kowalczuk, M., Kotwicki, L., Balazy, P., & Kuliński, K. (2014). Seasonality in vegetation biometrics and its effects on sediment characteristics and meiofauna in Baltic seagrass meadows. *Estuarine, Coastal and Shelf Science*, *139*, 159–170. https://doi.org/10.1016/j.ecss.2014.01.003

Kalra, Y. P., & Maynard, D. G. (1991). Methods manual for forest soil and plant analysis (Vol. 319).

Kendrick, G. A., Hegge, B. J., Wyllie, A., Davidson, A., & Lord, D. A. (2000). Changes in Seagrass Cover on Success and Parmelia Banks, Western Australia Between 1965 and 1995. Estuarine, Coastal and Shelf Science, 50(3), 341–353. https://doi.org/10.1006/ecss.1999.0569

Kennedy, L. A., Juanes, F., & El-Sabaawi, R. (2018). Eelgrass as Valuable Nearshore Foraging Habitat for Juvenile Pacific Salmon in the Early Marine Period. Marine and Coastal Fisheries, 10(2), 190–203. https://doi.org/10.1002/mcf2.10018

Kirkman, H., & Kuo, J. (1990). Pattern and process in southern Western Australian seagrasses. Aquatic Botany, 37(4), 367–382. https://doi.org/10.1016/0304-3770(90)90022-D

Koch, E. W., Ackerman, J. D., Verduin, J., & Keulen, M. van. (2006). Fluid Dynamics in Seagrass Ecology—From Molecules to Ecosystems. In A. W. D. LARKUM, R. J. ORTH, & C. M. DUARTE (Eds.), *SEAGRASSES: BIOLOGY, ECOLOGYAND CONSERVATION* (pp. 193–225). Springer Netherlands. https://doi.org/10.1007/978-1-4020-2983-7_8

Kundu, P. K., Cohen, I. M., & Dowling, D. R. (2015). *Fluid Mechanics*. Academic Press.

Lacy, J. R., & Wyllie-Echeverria, S. (2011). The influence of current speed and vegetation density on flow structure in two macrotidal eelgrass canopies: A field study of eelgrass hydrodynamics. *Limnology and Oceanography: Fluids and Environments*, *1*(1), 38–55. https://doi.org/10.1215/21573698-1152489

Lague, D., Brodu, N., & Leroux, J. (2013). Accurate 3D comparison of complex topography with terrestrial laser scanner: Application to the Rangitikei canyon (N-Z). ISPRS Journal of Photogrammetry and Remote Sensing, 82, 10–26. https://doi.org/10.1016/j.isprsjprs.2013.04.009

Lamarche, G., & Lurton, X. (2018). Recommendations for improved and coherent acquisition and processing of backscatter data from seafloor-mapping sonars. Marine Geophysical Research, 39(1), 5–22. https://doi.org/10.1007/s11001-017-9315-6

Larsen, L. G., & Harvey, J. W. (2011). Modeling of hydroecological feedbacks predicts distinct classes of landscape pattern, process, and restoration potential in shallow aquatic ecosystems. *Geomorphology*, *126*(3–4), 279–296. https://doi.org/10.1016/j.geomorph.2010.03.015

Lawson, S. E., Wiberg, P. L., McGlathery, K. J., & Fugate, D. C. (2007). Wind-driven sediment suspension controls light availability in a shallow coastal lagoon. *Estuaries and Coasts*, *30*(1), 102–112. https://doi.org/10.1007/BF02782971

Lawson, S., McGlathery, K., & Wiberg, P. (2012). Enhancement of sediment suspension and nutrient flux by benthic macrophytes at low biomass. *Marine Ecology Progress Series*, *448*, 259–270. https://doi.org/10.3354/meps09579

Le Bouteiller, C., & Venditti, J. G. (2014). Vegetation-driven morphodynamic adjustments of a sand bed. Geophysical Research Letters, 41(11), 3876–3883. https://doi.org/10.1002/2014GL060155

Le Roux, J. P. (2004). An integrated law of the wall for hydrodynamically transitional flow over plane beds. *Sedimentary Geology*, *163*(3–4), 311–321. https://doi.org/10.1016/j.sedgeo.2003.07.005

Lefebvre, A., Thompson, C. E. L., & Amos, C. L. (2010). Influence of Zostera marina canopies on unidirectional flow, hydraulic roughness and sediment movement. *Continental Shelf Research*, *30*(16), 1783–1794. https://doi.org/10.1016/j.csr.2010.08.006

Lefebvre, A., Ernstsen, V. B., & Winter, C. (2013). Estimation of roughness lengths and flow separation over compound bedforms in a natural-tidal inlet. *Continental Shelf Research*, *61–62*, 98–111. https://doi.org/10.1016/j.csr.2013.04.030

Lefebvre, A., Paarlberg, A. J., Ernstsen, V. B., & Winter, C. (2014). Flow separation and roughness lengths over large bedforms in a tidal environment: A numerical investigation. *Continental Shelf Research*, *91*, 57–69. https://doi.org/10.1016/j.csr.2014.09.001

Loos, E. A., & Costa, M. (2010). Inherent optical properties and optical mass classification of the waters of the Strait of Georgia, British Columbia, Canada. *Progress in Oceanography*, 87(1-4), 144-156.

Luhar, M., Rominger, J., & Nepf, H. (2008). Interaction between flow, transport and vegetation spatial structure. *Environmental Fluid Mechanics*, *8*(5–6), 423–439. https://doi.org/10.1007/s10652-008-9080-9

Mari, L., Melià, P., Gatto, M., & Casagrandi, R. (2021). Identification of Ecological Hotspots for the Seagrass Posidonia oceanica via Metapopulation Modeling. Frontiers in Marine Science, 8. https://www.frontiersin.org/articles/10.3389/fmars.2021.628976

Mcleod, E., Chmura, G. L., Bouillon, S., Salm, R., Björk, M., Duarte, C. M., Lovelock, C. E., Schlesinger, W. H., & Silliman, B. R. (2011). A blueprint for blue carbon: Toward an improved understanding of the role of vegetated coastal habitats in sequestering CO 2. Frontiers in Ecology and the Environment, 9(10), 552–560. https://doi.org/10.1890/110004

Mills, M., Leon, J. X., Saunders, M. I., Bell, J., Liu, Y., O'Mara, J., Lovelock, C. E., Mumby, P. J., Phinn, S., Possingham, H. P., Tulloch, V. J. D., Mutafoglu, K., Morrison, T., Callaghan, D. P., Baldock, T., Klein, C. J., & Hoegh-Guldberg, O. (2016). Reconciling Development and Conservation under Coastal Squeeze from Rising Sea Level. *Conservation Letters*, *9*(5), 361–368. https://doi.org/10.1111/conl.12213

Moksnes, P.-O., Eriander, L., Infantes, E., & Holmer, M. (2018). Local Regime Shifts Prevent Natural Recovery and Restoration of Lost Eelgrass Beds Along the Swedish West Coast. *Estuaries and Coasts*, *41*(6), 1712–1731. https://doi.org/10.1007/s12237-018-0382-y

Moore, K. A. (2004). Influence of Seagrasses on Water Quality in Shallow Regions of the Lower Chesapeake Bay. *Journal of Coastal Research*, *10045*, 162–178. https://doi.org/10.2112/SI45-162.1

Mtwana Nordlund, L., Koch, E. W., Barbier, E. B., & Creed, J. C. (2016). Seagrass Ecosystem Services and Their Variability across Genera and Geographical Regions. PLOS ONE, 11(10), e0163091. https://doi.org/10.1371/journal.pone.0163091

Mueller, D. S., Wagner, C. R., Rehmel, M. S., Oberg, K. A., & Rainville, F. (2009). *Measuring discharge with acoustic Doppler current profilers from a moving boat* (p. 72). Reston, Virginia (EUA): US Department of the Interior, US Geological Survey.

Nahirnick, N. K., Reshitnyk, L., Campbell, M., Hessing-Lewis, M., Costa, M., Yakimishyn, J., & Lee, L. (2019). Mapping with confidence; delineating seagrass habitats using Unoccupied Aerial Systems (UAS). Remote Sensing in Ecology and Conservation, 5(2), 121–135. https://doi.org/10.1002/rse2.98

Nardin, W., Larsen, L., Fagherazzi, S., & Wiberg, P. (2018). Tradeoffs among hydrodynamics, sediment fluxes and vegetation community in the Virginia Coast Reserve, USA. Estuarine, Coastal and Shelf Science, 210, 98–108. https://doi.org/10.1016/j.ecss.2018.06.009

National Oceanic and Atmospheric Administration (2022). Cold & Warm Episodes by Season. Retrieved from https://origin.cpc.ncep.noaa.gov/products/analysis_monitoring/ensostuff/ONI_v5.php

Nepf, H. M. (1999). Drag, turbulence, and diffusion in flow through emergent vegetation. *Water Resources Research*, *35*(2), 479–489. https://doi.org/10.1029/1998WR90006

Nepf, H. M. (2012). Hydrodynamics of vegetated channels. *Journal of Hydraulic Research*, *50*(3), 262–279. https://doi.org/10.1080/00221686.2012.696559

Nowicki, R., Thomson, J., Burkholder, D., Fourqurean, J., & Heithaus, M. (2017). Predicting seagrass recovery times and their implications following an extreme climate event. Marine Ecology Progress Series, 567, 79–93. https://doi.org/10.3354/meps12029

Nyström, M., Norström, A. V., Blenckner, T., de la Torre-Castro, M., Eklöf, J. S., Folke, C., Österblom, H., Steneck, R. S., Thyresson, M., & Troell, M. (2012). Confronting Feedbacks of Degraded Marine Ecosystems. *Ecosystems*, *15*(5), 695–710. https://doi.org/10.1007/s10021-012-9530-

Olesen, B., & Sand-Jensen, K. (1994). Biomass-density patterns in the temperate seagrass Zostera marina. *Mar. Ecol. Prog. Ser.*, 9.

Olson, A. M., Hessing-Lewis, M., Haggarty, D., & Juanes, F. (2019). Nearshore seascape connectivity enhances seagrass meadow nursery function. Ecological Applications, 29(5). https://doi.org/10.1002/eap.1897

Oprandi, A., Mucerino, L., De Leo, F., Bianchi, C. N., Morri, C., Azzola, A., Benelli, F., Besio, G., Ferrari, M., & Montefalcone, M. (2020). Effects of a severe storm on seagrass meadows. Science of The Total Environment, 748, 141373. https://doi.org/10.1016/j.scitotenv.2020.141373

Oreska, M. P. J., McGlathery, K. J., & Porter, J. H. (2017). Seagrass blue carbon spatial patterns at the meadow-scale. *PLOS ONE*, *12*(4), e0176630. https://doi.org/10.1371/journal.pone.0176630

Orth, R. J., Carruthers, T. J. B., Dennison, W. C., Duarte, C. M., Fourqurean, J. W., Heck, K. L., Hughes, A. R., Kendrick, G. A., Kenworthy, W. J., Olyarnik, S., Short, F. T., Waycott, M., & Williams, S. L. (2006). A Global Crisis for Seagrass Ecosystems. *BioScience*, *56*(12), 987. https://doi.org/10.1641/0006-3568(2006)56[987:AGCFSE]2.0.CO;2

Orth, R. J., Moore, K. A., Marion, S. R., Wilcox, D. J., & Parrish, D. B. (2012). Seed addition facilitates eelgrass recovery in a coastal bay system. *Marine Ecology Progress Series*, *448*, 177–195. https://doi.org/10.3354/meps09522

Orton, G. J., & Reading, H. G. (1993). Variability of deltaic processes in terms of sediment supply, with particular emphasis on grain size. Sedimentology, 40(3), 475–512. https://doi.org/10.1111/j.1365-3091.1993.tb01347.x

Pace, M., Borg, J. A., Galdies, C., & Malhotra, A. (2017). Influence of wave climate on architecture and landscape characteristics of Posidonia oceanica meadows. *Marine Ecology*, *38*(1), e12387. https://doi.org/10.1111/maec.12387

Parnum, I. M., & Gavrilov, A. N. (2011). High-frequency multibeam echo-sounder measurements of seafloor backscatter in shallow water: Part 1 – Data acquisition and processing. Underwater Technology, 30(1), 3–12. https://doi.org/10.3723/ut.30.003

Peralta, G., Brun, F. G., Hernández, I., Vergara, J. J., & Pérez-Lloréns, J. L. (2005). Morphometric variations as acclimation mechanisms in Zostera noltii beds. Estuarine, Coastal and Shelf Science, 64(2–3), 347–356. https://doi.org/10.1016/j.ecss.2005.02.027

Perlin, A., Moum, J. N., Klymak, J. M., Levine, M. D., Boyd, T., & Kosro, P. M. (2005). A modified law-of-the-wall applied to oceanic bottom boundary layers. *Journal of Geophysical Research: Oceans*, *110*(C10). https://doi.org/10.1029/2004JC002310\

Prentice C., Smith R., & Hessing-Lewis M. (2019). Summary of Chalk Blocks and Sediment Traps from Calvert Seagrass Sites. Hakai Institute.

Prentice, C., Hessing-Lewis, M., Sanders-Smith, R., & Salomon, A. K. (2019). Reduced water motion enhances organic carbon stocks in temperate eelgrass meadows. Limnology and Oceanography, 64(6), 2389–2404. https://doi.org/10.1002/lno.11191

Pittman, S. J. (2017). *Seascape Ecology*. John Wiley & Sons.

Rasheed, M. A., McKenna, S. A., Carter, A. B., & Coles, R. G. (2014). Contrasting recovery of shallow and deep water seagrass communities following climate associated losses in tropical north Queensland, Australia. Marine Pollution Bulletin, 83(2), 491–499. https://doi.org/10.1016/j.marpolbul.2014.02.013

Rennie, C. D., & Millar, R. G. (2004). Measurement of the spatial distribution of fluvial bedload transport velocity in both sand and gravel. Earth Surface Processes and Landforms, 29(10), 1173–1193. https://doi.org/10.1002/esp.1074

Ribas, F., Falqués, A., de Swart, H. E., Dodd, N., Garnier, R., & Calvete, D. (2015). Understanding coastal morphodynamic patterns from depth-averaged sediment concentration. *Reviews of Geophysics*, *53*(2), 362–410. https://doi.org/10.1002/2014RG000457

Rijn, V., & C, L. (2007). Unified View of Sediment Transport by Currents and Waves. I: Initiation of Motion, Bed Roughness, and Bed-Load Transport. Journal of Hydraulic Engineering, 133(6), 649–667. https://doi.org/10.1061/(ASCE)0733-9429(2007)133:6(649)

Rippeth, T. P., Williams, E., & Simpson, J. H. (2002). Reynolds Stress and Turbulent Energy Production in a Tidal Channel. *Journal of Physical Oceanography*, *32*(4), 1242–1251. https://doi.org/10.1175/1520-0485(2002)032<1242:RSATEP>2.0.CO;2

Robbins, B. D., & Bell, S. S. (2000). Dynamics of a Subtidal Seagrass Landscape: Seasonal and Annual Change in Relation to Water Depth. Ecology, 81(5), 1193–1205. https://doi.org/10.1890/0012-9658(2000)081[1193:DOASSL]2.0.CO;2

Röttgers, R., Heymann, K., & Krasemann, H. (2014). Suspended matter concentrations in coastal waters: Methodological improvements to quantify individual measurement uncertainty. Estuarine, Coastal and Shelf Science, 151, 148–155. https://doi.org/10.1016/j.ecss.2014.10.010

Short, F., Carruthers, T., Dennison, W., & Waycott, M. (2007). Global seagrass distribution and diversity: A bioregional model. *Journal of Experimental Marine Biology and Ecology*, *350*(1–2), 3–20. https://doi.org/10.1016/j.jembe.2007.06.012

Short, F. T., & Wyllie-Echeverria, S. (1996). Natural and human-induced disturbance of seagrasses. *Environmental Conservation*, *23*(1), 17–27. https://doi.org/10.1017/S0376892900038212

Stevens, A. W., & Lacy, J. R. (2012). The Influence of Wave Energy and Sediment Transport on Seagrass Distribution. Estuaries and Coasts, 35(1), 92–108. https://doi.org/10.1007/s12237-011-9435-1

Tanner, C. E., & Parham, T. (2010). Growing Zostera marina (eelgrass) from Seeds in Land-Based Culture Systems for Use in Restoration Projects. *Restoration Ecology*, *18*(4), 527–537. https://doi.org/10.1111/j.1526-100X.2010.00693.x

Terrados, J., & Duarte, C. M. (2000). Experimental evidence of reduced particle resuspension within a seagrass (Posidonia oceanica L.) meadow. *Journal of Experimental Marine Biology and Ecology*, *243*(1), 45–53. https://doi.org/10.1016/S0022-0981(99)00110-0

Thorne, P. D., & Hanes, D. M. (2002). A review of acoustic measurement of small-scale sediment processes. *Continental Shelf Research*, 22(4), 603–632. https://doi.org/10.1016/S0278-4343(01)00101-7

Tinoco, R. O., Juan, J. E. S., & Mullarney, J. C. (2020). Simplification bias: Lessons from laboratory and field experiments on flow through aquatic vegetation. *Earth Surface Processes and Landforms*, *45*(1), 121–143. https://doi.org/10.1002/esp.4743

Turner, M. G. (2010). Disturbance and landscape dynamics in a changing world. *Ecology*, *91*(10), 2833–2849. https://doi.org/10.1890/10-0097.1

Turner, M. G., & Gardner, R. H. (2015). *Landscape Ecology in Theory and Practice*. Springer New York. https://doi.org/10.1007/978-1-4939-2794-4

Uhrin, A. V., & Turner, M. G. (2018). Physical drivers of seagrass spatial configuration: The role of thresholds. *Landscape Ecology*, *33*(12), 2253–2272. https://doi.org/10.1007/s10980-018-0739-4

Unsworth, R. K. F., Collier, C. J., Waycott, M., Mckenzie, L. J., & Cullen-Unsworth, L. C. (2015). A framework for the resilience of seagrass ecosystems. Marine Pollution Bulletin, 100(1), 34–46. https://doi.org/10.1016/j.marpolbul.2015.08.016

Vacchi, M., Falco, G. D., Simeone, S., Montefalcone, M., Morri, C., Ferrari, M., & Bianchi, C. N. (2017). Biogeomorphology of the Mediterranean Posidonia oceanica seagrass meadows. *Earth Surface Processes and Landforms*, *42*(1), 42–54. https://doi.org/10.1002/esp.3932

van der Heide, T., van Nes, E. H., Geerling, G. W., Smolders, A. J. P., Bouma, T. J., & van Katwijk, M. M. (2007). Positive Feedbacks in Seagrass Ecosystems: Implications for Success in Conservation and Restoration. *Ecosystems*, *10*(8), 1311–1322. https://doi.org/10.1007/s10021-007-9099-7

van Katwijk, M. M., Bos, A. R., Hermus, D. C. R., & Suykerbuyk, W. (2010). Sediment modification by seagrass beds: Muddification and sandification induced by plant cover and environmental conditions. *Estuarine, Coastal and Shelf Science*, *89*(2), 175–181. https://doi.org/10.1016/j.ecss.2010.06.008

van Katwijk, M. M., Thorhaug, A., Marbà, N., Orth, R. J., Duarte, C. M., Kendrick, G. A., Althuizen, I. H. J., Balestri, E., Bernard, G., Cambridge, M. L., Cunha, A., Durance, C., Giesen, W., Han, Q., Hosokawa, S., Kiswara, W., Komatsu, T., Lardicci, C., Lee, K.-S., … Verduin, J. J. (2016). Global analysis of seagrass restoration: The importance of large-scale planting. *Journal of Applied Ecology*, *53*(2), 567–578. https://doi.org/10.1111/1365-2664.1256

Vargas-Luna, A., Crosato, A., & Uijttewaal, W. S. J. (2015). Effects of vegetation on flow and sediment transport: Comparative analyses and validation of predicting models. *Earth Surface Processes and Landforms*, *40*(2), 157–176. https://doi.org/10.1002/esp.363

Vercaemer, B. M., Scarrow, M. A., Roethlisberger, B., Krumhansl, K. A., & Wong, M. C. (2021). Reproductive ecology of Zostera marina L. (eelgrass) across varying environmental conditions. Aquatic Botany, 175, 103444. https://doi.org/10.1016/j.aquabot.2021.103444

Walker, D. I., Kendrick, G. A., & McComb, A. J. (2006). Decline and Recovery of Seagrass Ecosystems—The Dynamics of Change. In A. W. D. LARKUM, R. J. ORTH, & C. M.

DUARTE (Eds.), *SEAGRASSES: BIOLOGY, ECOLOGYAND CONSERVATION* (pp. 551–565). Springer Netherlands. https://doi.org/10.1007/978-1-4020-2983-7_23

Walter, R. K., O'Leary, J. K., Vitousek, S., Taherkhani, M., Geraghty, C., & Kitajima, A. (2020). Large-scale erosion driven by intertidal eelgrass loss in an estuarine environment. *Estuarine, Coastal and Shelf Science*, *243*, 106910. https://doi.org/10.1016/j.ecss.2020.106910

Ward, L. G., Michael Kemp, W., & Boynton, W. R. (1984). The influence of waves and seagrass communities on suspended particulates in an estuarine embayment. *Marine Geology*, *59*(1), 85–103. https://doi.org/10.1016/0025-3227(84)90089-6

Warren, J. D., & Peterson, B. J. (2007). Use of a 600-kHz Acoustic Doppler Current Profiler to measure estuarine bottom type, relative abundance of submerged aquatic vegetation, and eelgrass canopy height. Estuarine, Coastal and Shelf Science, 72(1–2), 53–62. https://doi.org/10.1016/j.ecss.2006.10.026

Waycott, M., Duarte, C. M., Carruthers, T. J. B., Orth, R. J., Dennison, W. C., Olyarnik, S., Calladine, A., Fourqurean, J. W., Heck, K. L., Hughes, A. R., Kendrick, G. A., Kenworthy, W. J., Short, F. T., & Williams, S. L. (2009). Accelerating loss of seagrasses across the globe threatens coastal ecosystems. *Proceedings of the National Academy of Sciences*, *106*(30), 12377–12381. https://doi.org/10.1073/pnas.0905620106

Wedding, L., Lepczyk, C., Pittman, S., Friedlander, A., & Jorgensen, S. (2011). Quantifying seascape structure: Extending terrestrial spatial pattern metrics to the marine realm. *Marine Ecology Progress Series*, *427*, 219–232. https://doi.org/10.3354/meps09119

Widdows, J., Pope, N., Brinsley, M., Asmus, H., & Asmus, R. (2008). Effects of seagrass beds (Zostera noltii and Z. marina) on near-bed hydrodynamics and sediment resuspension. *Marine Ecology Progress Series*, *358*, 125–136. https://doi.org/10.3354/meps07338

Wild, A. L. (2020). *Morphodynamics of a bedrock confined estuary and delta: The Skeena River Estuary* (Masters thesis, University of Victoria).

Williams, S. L. (2007). Introduced species in seagrass ecosystems: Status and concerns. *Journal of Experimental Marine Biology and Ecology*, *350*(1–2), 89–110. https://doi.org/10.1016/j.jembe.2007.05.032

Wilkinson, R. H. (1983). A method for evaluating statistical errors associated with logarithmic velocity profiles. *Geo-marine letters*, 3(1), 49-52.

Yager, E. M., & Schmeeckle, M. W. (2013). The influence of vegetation on turbulence and bed load transport. *Journal of Geophysical Research: Earth Surface*, *118*(3), 1585–1601. https://doi.org/10.1002/jgrf.20085

Yarnall, A. H., Byers, J. E., Yeager, L. A., & Fodrie, F. J. (2022). Comparing edge and fragmentation effects within seagrass communities: A meta-analysis. *Ecology*, *103*(3), e3603. https://doi.org/10.1002/ecy.3603

Yorke, T. H., & Oberg, K. A. (2002). Measuring river velocity and discharge with acoustic Doppler profilers. *Flow Measurement and Instrumentation*, 13(5–6), 191–195. https://doi.org/10.1016/S0955-5986(02)00051-1

Zhang, W., Qi, J., Wan, P., Wang, H., Xie, D., Wang, X., & Yan, G. (2016). An Easy-to-Use Airborne LiDAR Data Filtering Method Based on Cloth Simulation. Remote Sensing, 8(6), 501. https://doi.org/10.3390/rs8060501

Zhu, Q., Wiberg, P. L., & Reidenbach, M. A. (2021). Quantifying Seasonal Seagrass Effects on Flow and Sediment Dynamics in a Back-Barrier Bay. *Journal of Geophysical Research: Oceans*, *126*(2), e2020JC016547. https://doi.org/10.1029/2020JC016547

Zong, L., & Nepf, H. (2011). Spatial distribution of deposition within a patch of vegetation: DEPOSITION PATTERN WITHIN A PATCH. *Water Resources Research*, *47*(3). https://doi.org/10.1029/2010WR009516

6.0 Appendices

6.1 Appendix A: Additional Tables & Figures.

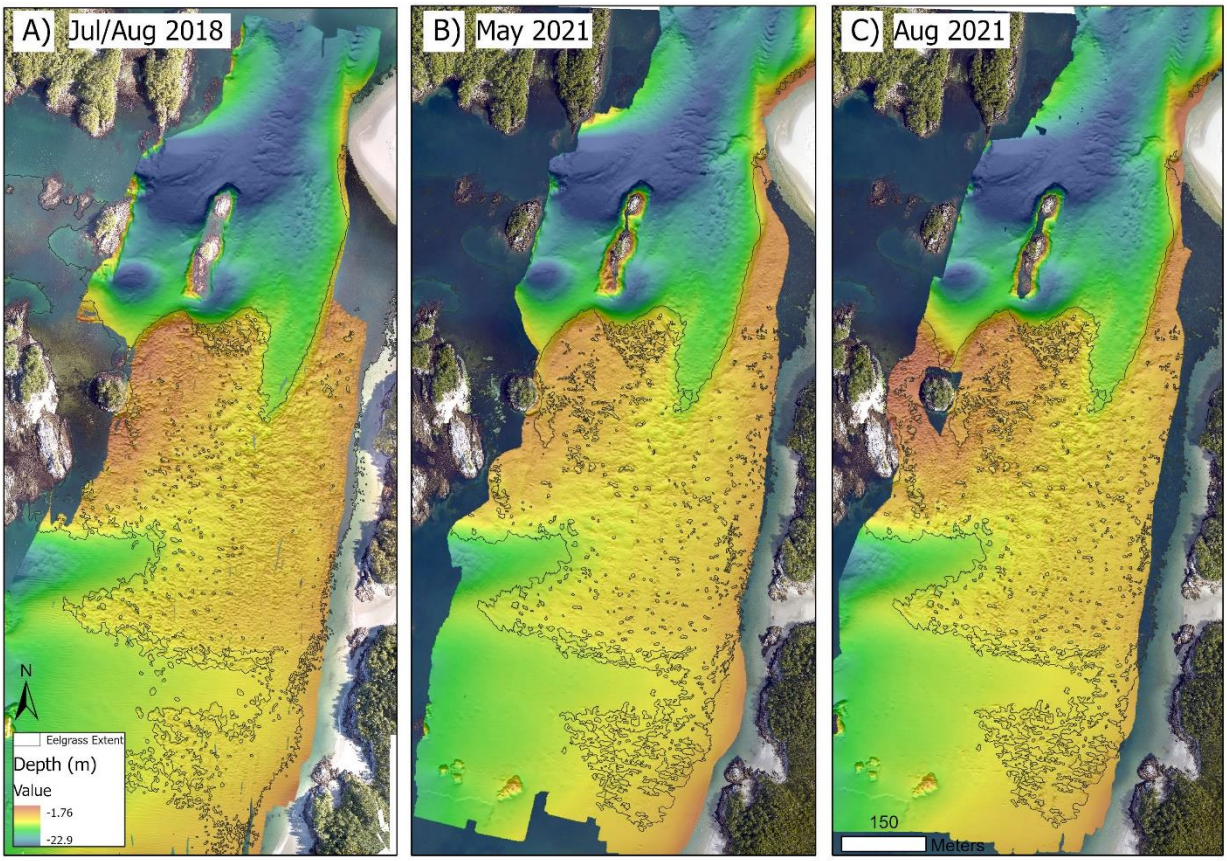

Figure 1 - Multibeam bathymetry (1 m resolution) with seagrass soundings and seagrass extent in (A) in July/August 2018, (B) May 2021, and (C) August 2021.

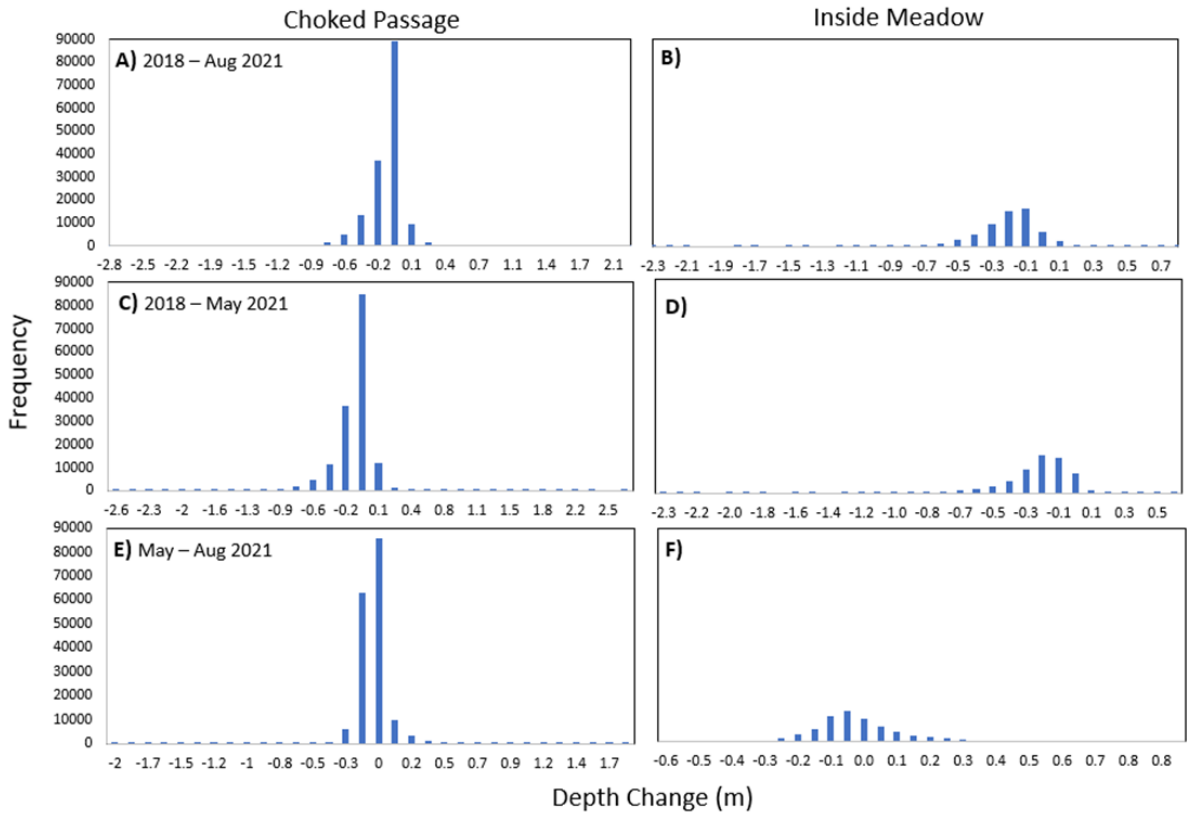

Figure 2 - Frequency of cell-by-cell surface differences between each MBES survey of Choked Passage. (A) All of Choked Passage from 2018-August 2021, (B) inside the meadow from 2018-August 2021, (C) all of Choked Passage from 2018 – May 2021, (D) inside the meadow 2018 – May 2021, (E) all of Choked Passage from May 2021 – August 2021, (F) inside the meadow from May 2021 – August 2021.

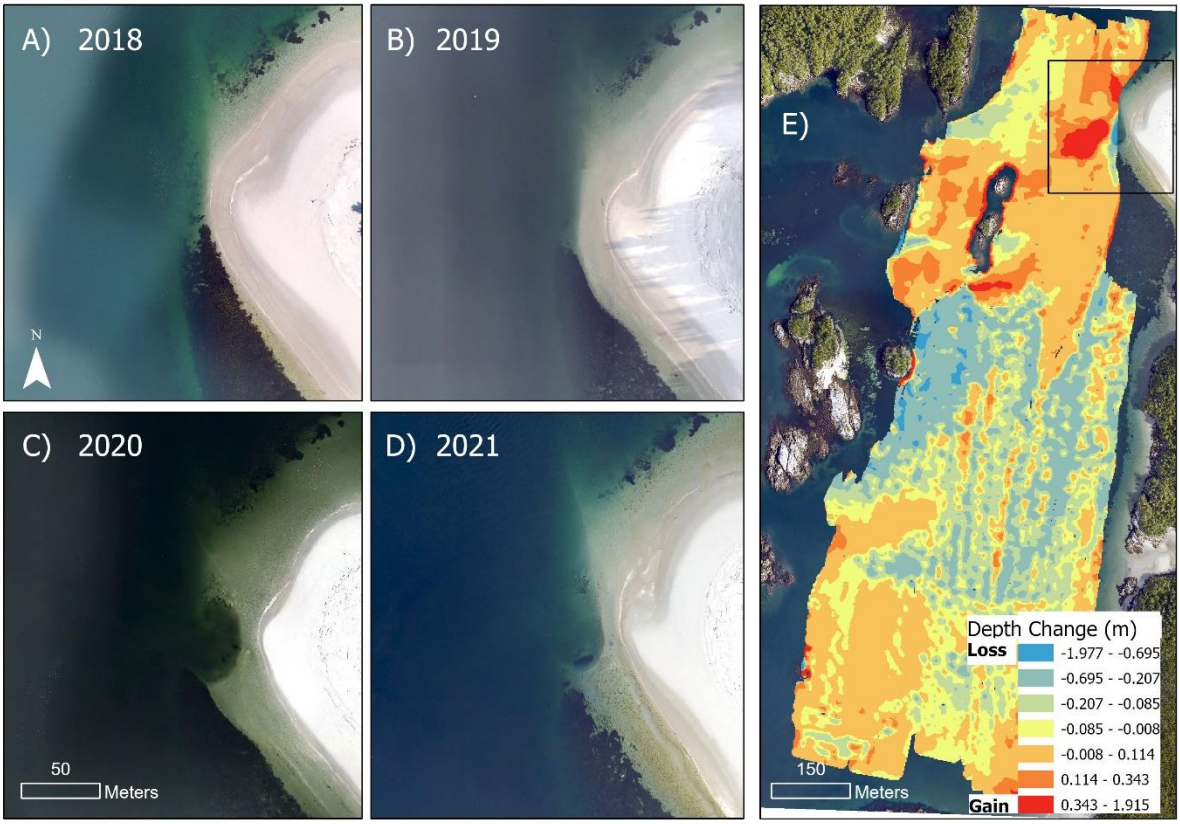

Figure 3 - Aerial imagery of sandspit in A) 2018 and B) 2019, and C) the appearance of an erosional feature in 2020, which persists into D) 2021. E) Map of surface differences (m) from July/August 2018 to August 2021 showing a large depositional feature adject to the sandspit.

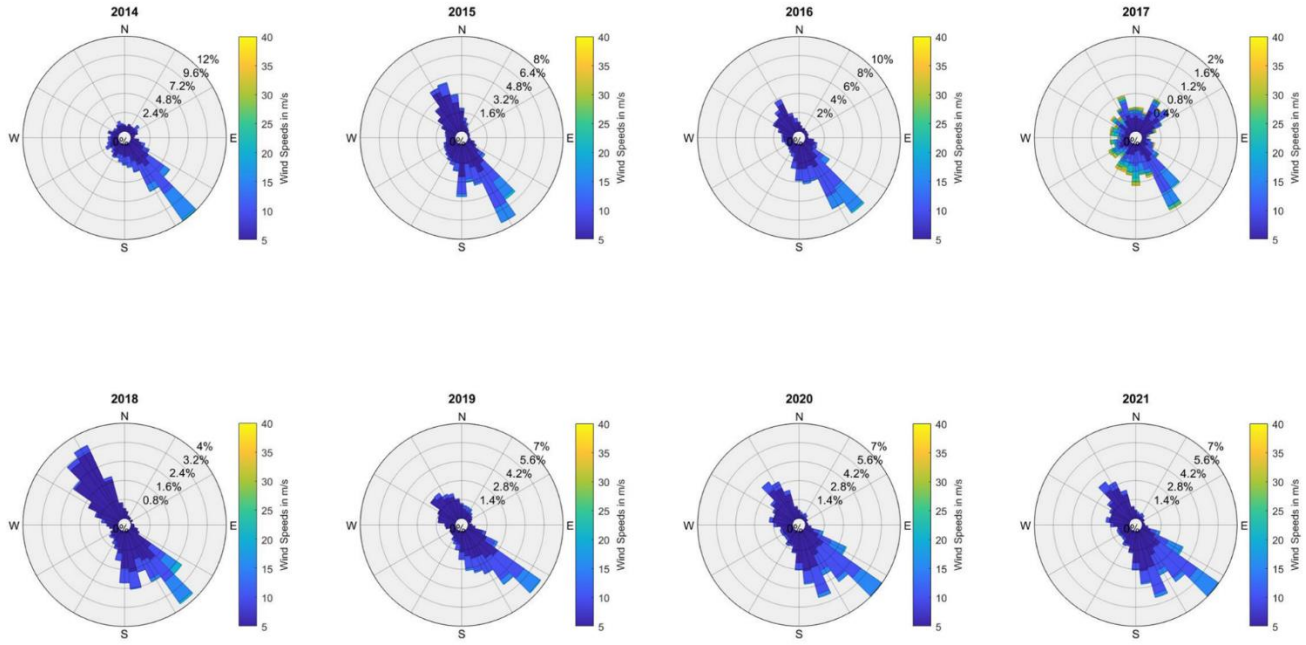

Figure 4 - Annual wind rose showing wind direction (°) and speed (m/s) at West Sea Otter buoy from 2014 to 2021.

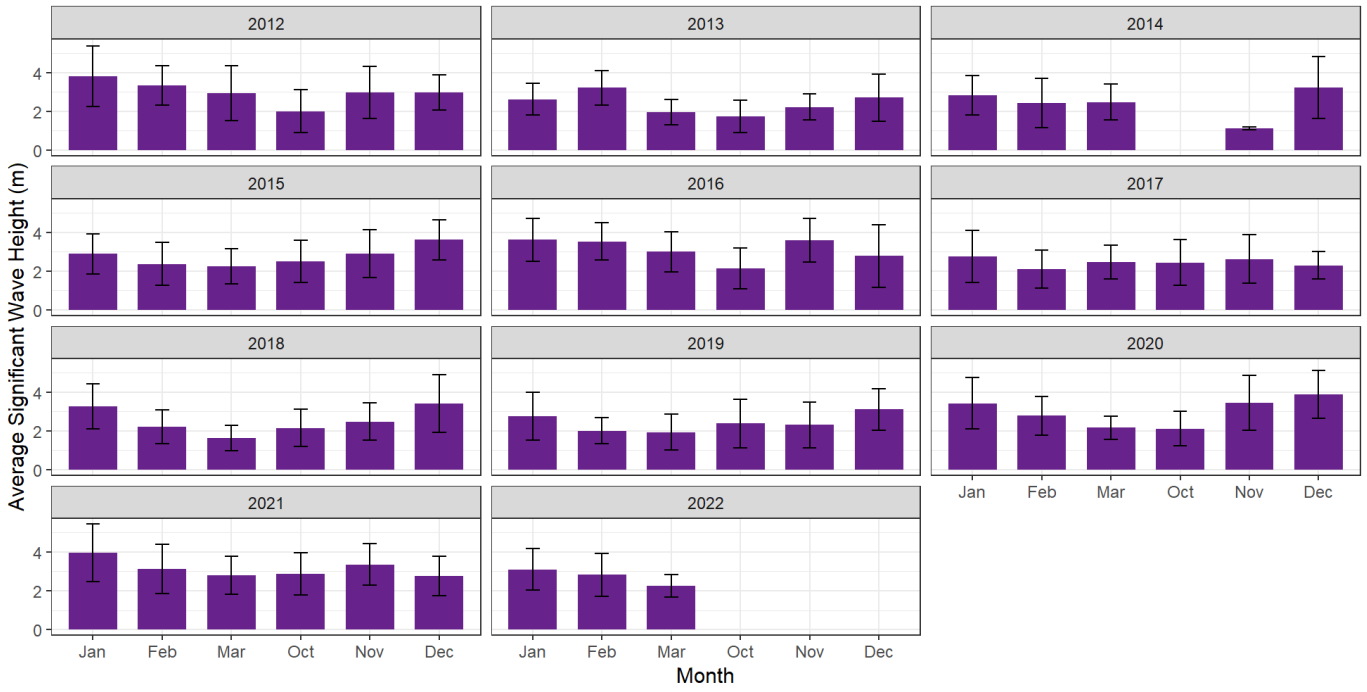

Figure 5 - Average winter monthly significant wave height (m) at West Sea Otter buoy from 2012 2022.

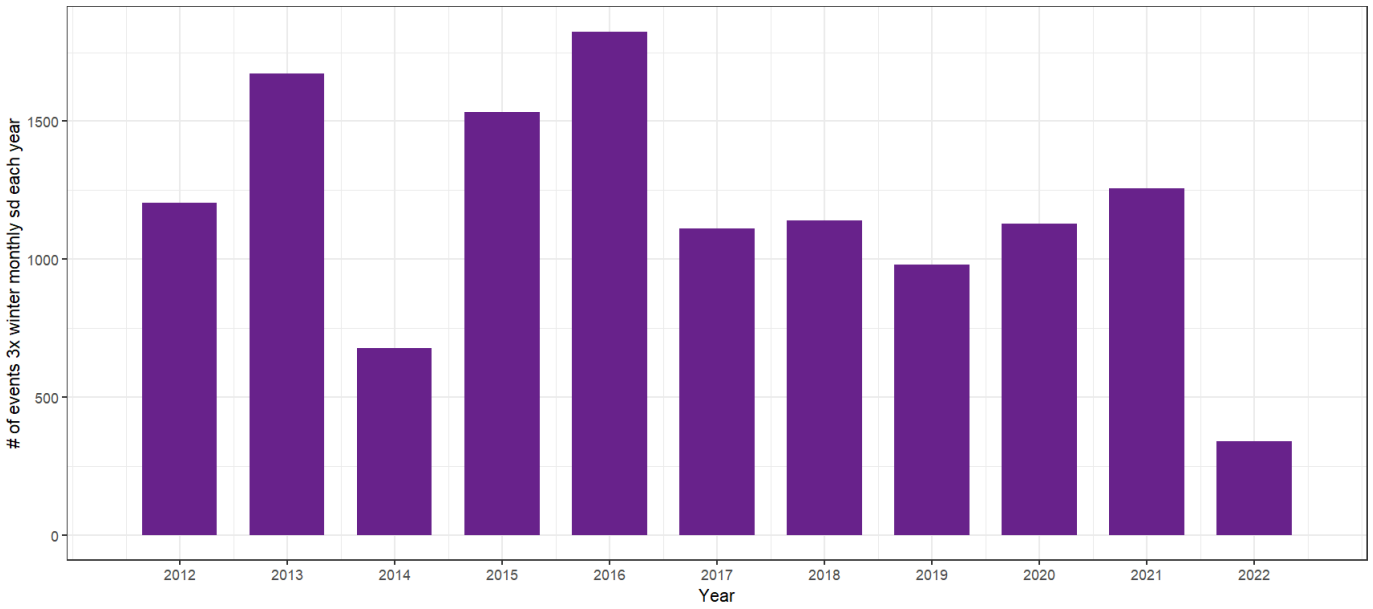

Figure 6 - Number of observations at least 3 times greater than the standard deviation for each month from 2021-2022.

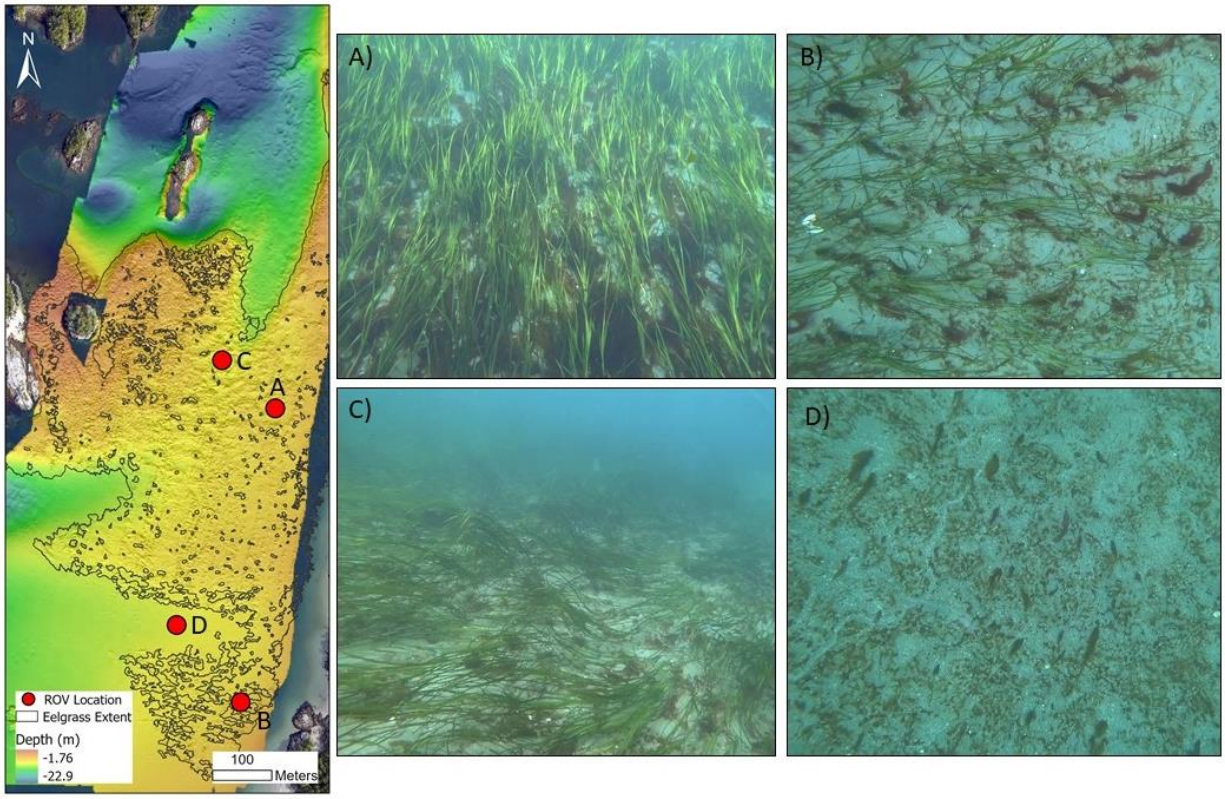

Figure 7 - ROV acquired images of seagrass canopy at different locations within the Choked Passage meadow. A) Dense interior canopy in the North-Eastern section towards the shoreline with epiphytes and drift algae, B) Less-dense southern meadow patch, C) Moderately dense interior towards Northern meadow edge, and D) un-vegetated sand outside of the meadow with biofilm and drifting algae.

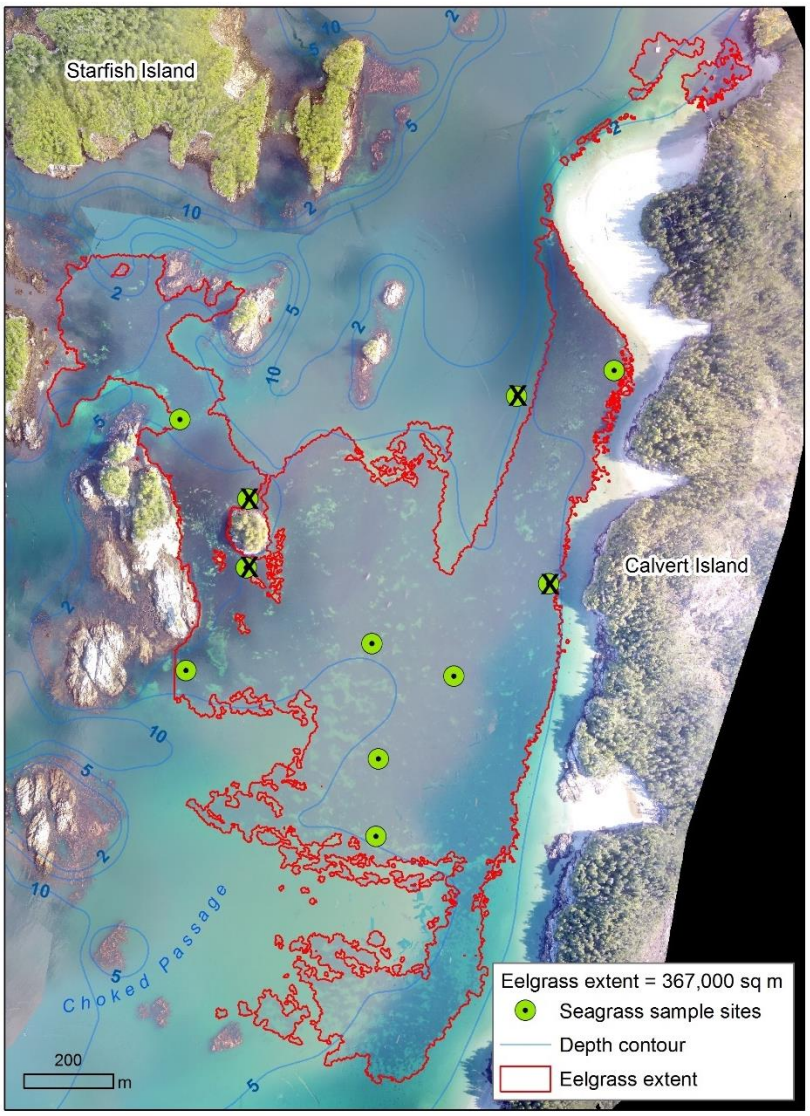

Figure 8 - Map of seagrass density surveys performed by the Hakai Nearshore Ecology Team from in August 2021.

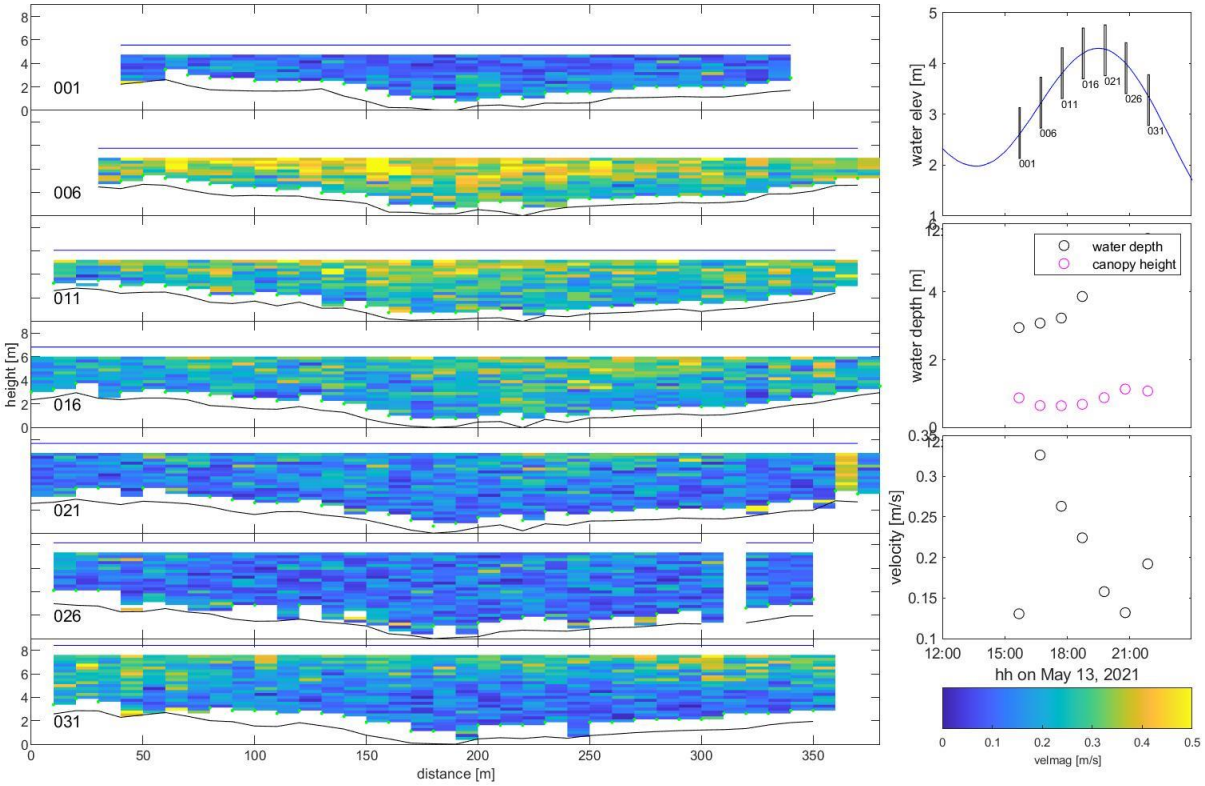

Figure 9 - Velocity profiles for ADCP cross-sectional transect line W surveyed on May 13, 2021, showing water elevation during each transect number, water depth and canopy height, and average flow velocity during each survey

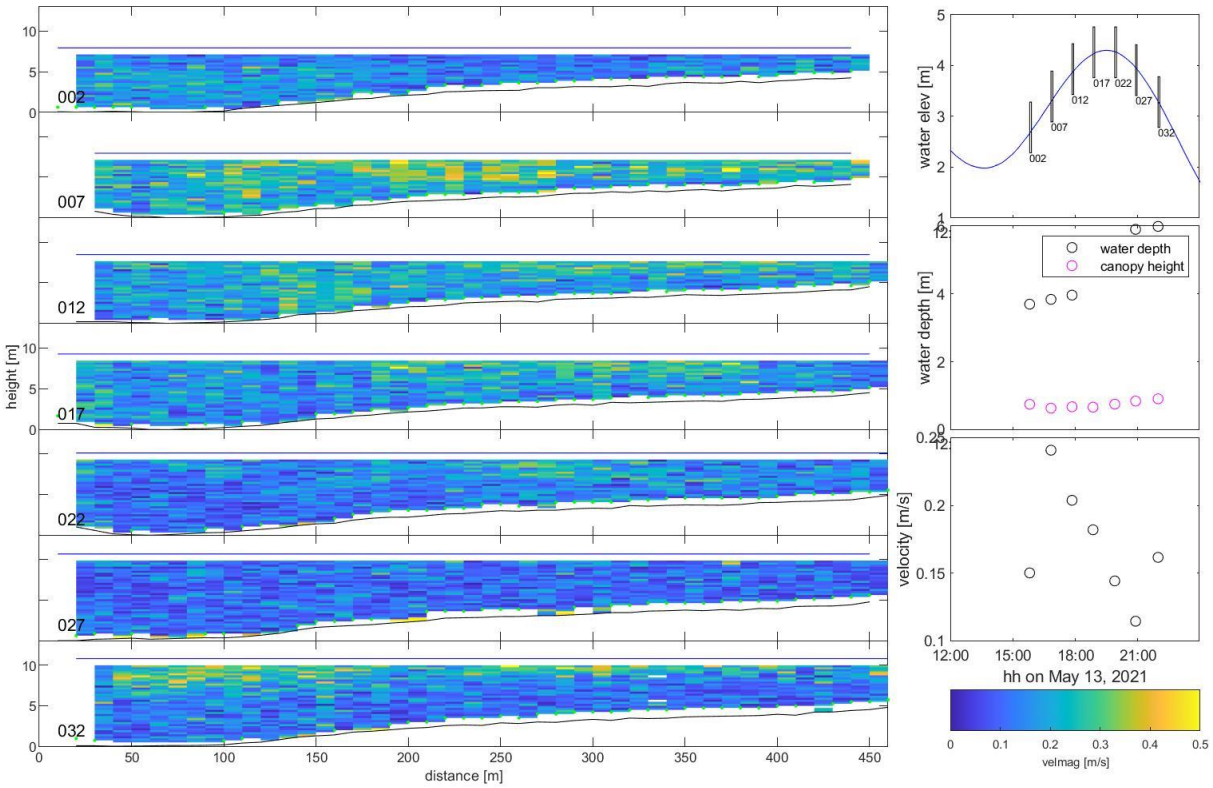

Figure 10 - Velocity profiles for ADCP cross-sectional transect line X surveyed on May 13, 2021, showing water elevation during each transect number, water depth and canopy height, and average flow velocity during each survey.

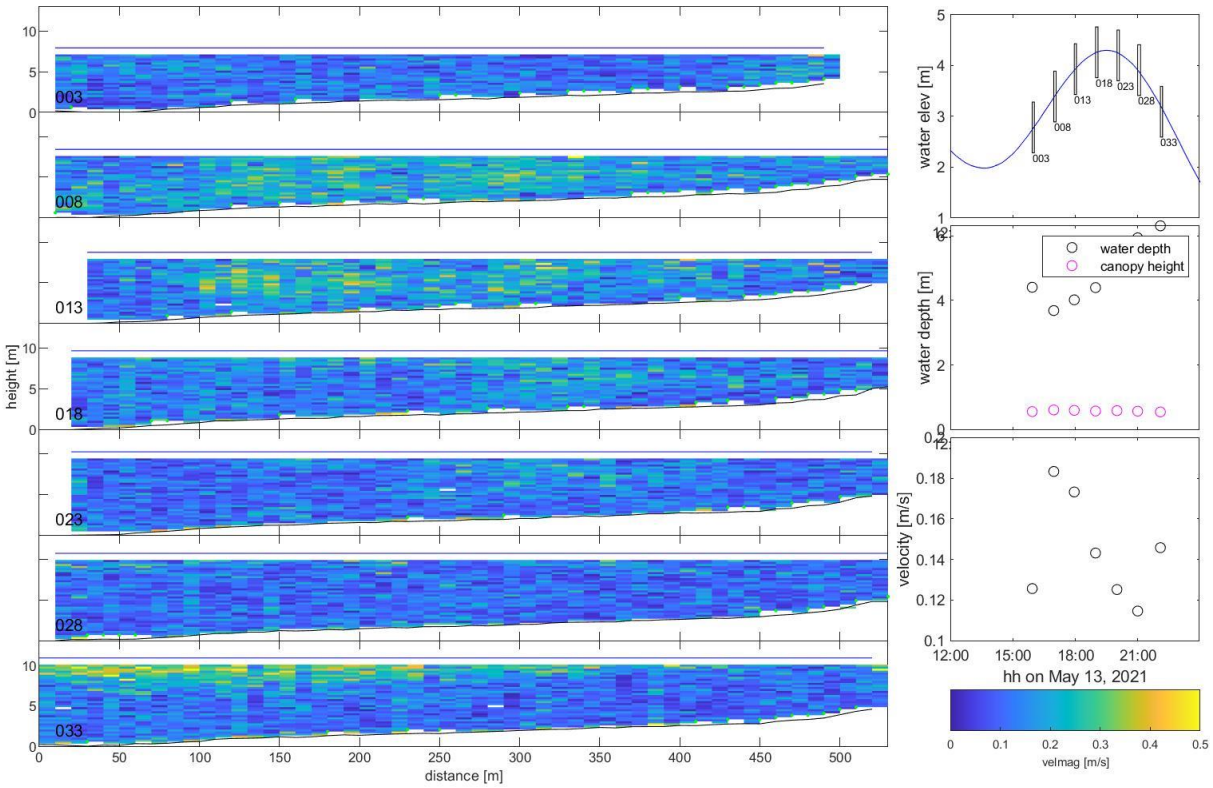

Figure 11 - Velocity profiles for ADCP cross-sectional transect line Y surveyed on May 13, 2021, showing water elevation during each transect number, water depth and canopy height, and average flow velocity during each survey.

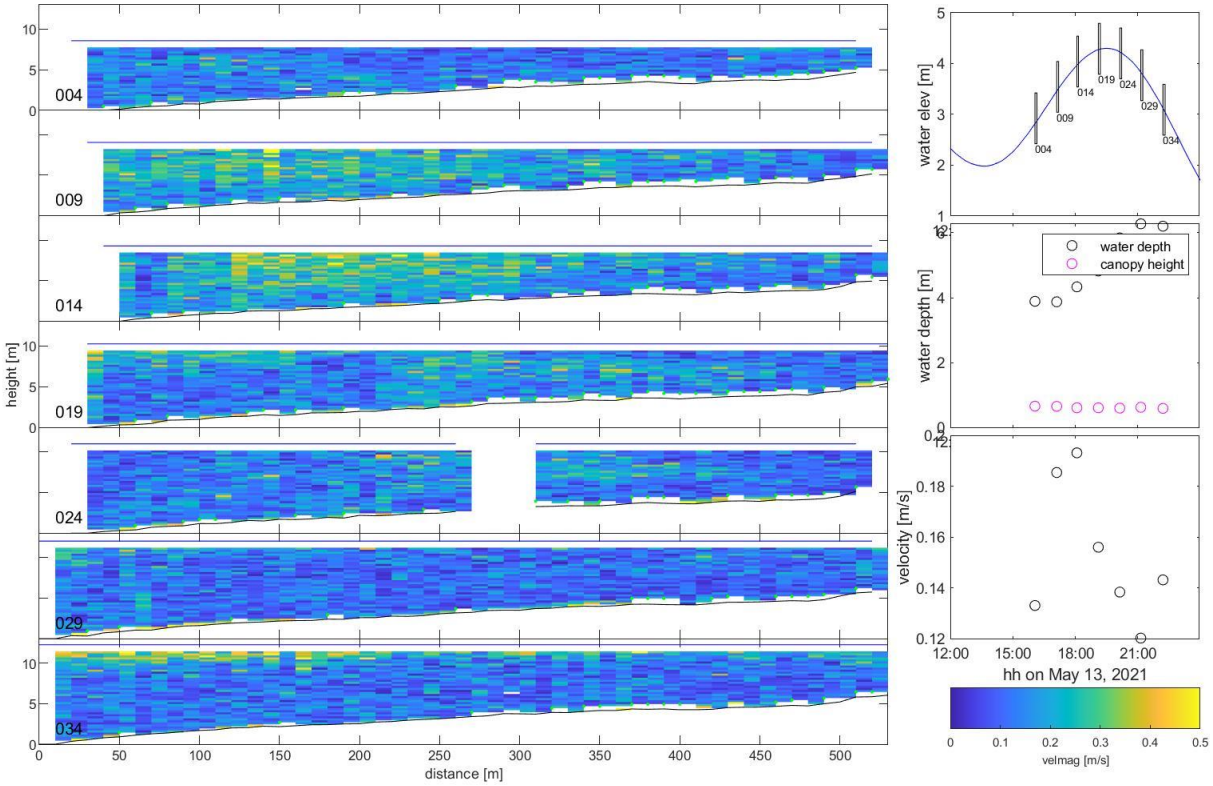

Figure 12 - Velocity profiles for ADCP cross-sectional transect line Z surveyed on May 13, 2021, showing water elevation during each transect number, water depth and canopy height, and average flow velocity during each survey.

6.2 Appendix B: MBES processing of May & August 2021 data

The MBES bathymetry was acquired with QPS Qinsy software and the raw sonar files were stored as Qinsy database files (.dbf). The data was imported into QPS Qimera to clean the soundings and generate a dynamic 3D surface. The data was projected with NAD83 UTM Zone 9N, with the CGVD 2013 vertical datum, and the CGG2013 geoid model.

A dynamic surface with a 0.50 m cell size was generated. Because, the MBES survey ran for multiple days, separate dynamic surfaces were created and cleaned for each survey day and merged after processing and cleaning. First, the data was cleaned with a medium spline filter and additional soundings (*i.e.* multi-detect) were removed from the surface. Outliers were removed from the soundings from each survey line using the swath tool. Due to the large swath width of the Norbit iWBMS, the outer beams away from nadir contained high levels of noise. These noisy outer beams were removed manually with the slice and swath editors and automatically with the reject specific beam(s) filter. Kelp and organic matter were thoroughly cleaned from the static

features (*i.e.* rocks and islands) in order to co-register and detect vertical changes between the surfaces. The dynamic surface interpolation tool (iterations = 3 and minimum neighbours = 3)was used conservatively to fill in gaps.

Finally, the cleaned surfaces were exported as an ASCII ArcView grid file and imported into ArcGIS Pro. The surfaces from each survey day were merged into one with the Raster Calculator from the Spatial Analyst Toolbox. The following expression was used: Con(IsNull(inputRasterWithGaps), inputRasterToFillGaps, inputRasterWithGaps). This expression created a new raster with cells from the first survey day (inputRasterWithGaps) and filled missing cells with values from the following survey day (inputRasterToFillGaps).

In order to examine geomorphic changes within the meadow, the vegetation was removed from the bathymetry surface. Otherwise, natural changes in the seagrass meadow, would be interpreted as changes to the seabed. The point clouds were imported into Cloud Compare, and a Cloth Simulation Filter (CSF) was performed to extract ground points (Zhang et al., 2016). The filtered point cloud was exported as a raster and loaded into ArcGIS. A shapefile of the 2021 meadow extent was used as a mask to clip the meadow from the raster. The clipped raster was aggregated into a 2m resolution with each cell containing the minimum value of each input cell, to ensure the cell value was that of the seabed and not vegetation. Next, the 2m raster of the meadow was merged with a 2m raster of Choked Pass without a CSF filter. Then the .tiff raster files were loaded into Cloud Compare and fine referenced in the z-direction to the August bathymetry surface.

6.3 Appendix C: Grain Size Analysis

Nine sediment samples were collected from by divers from the seabed in Choked Pass in August 2021 (Figure 9). Samples were retrieved by hand and stored in Ziploc bags. Samples were immediately frozen and transported to the University of Victoria. Once in the lab, the frozen samples were thawed at room temperature for 24 hrs, and then oven dried at 110°C for 24 hrs. Large pieces of organic material (e.g. macro-algae, invertebrates) were removed from the sample prior to drying. The dry samples were then burned at 500°C for 1 hr to combust any other organics within the sample. Due to the high shell-content of Choked Pass sediments, clumps and aggregations were broken up by hand, rather than a mortar and pestle to prevent damaging the shells and altering their size.

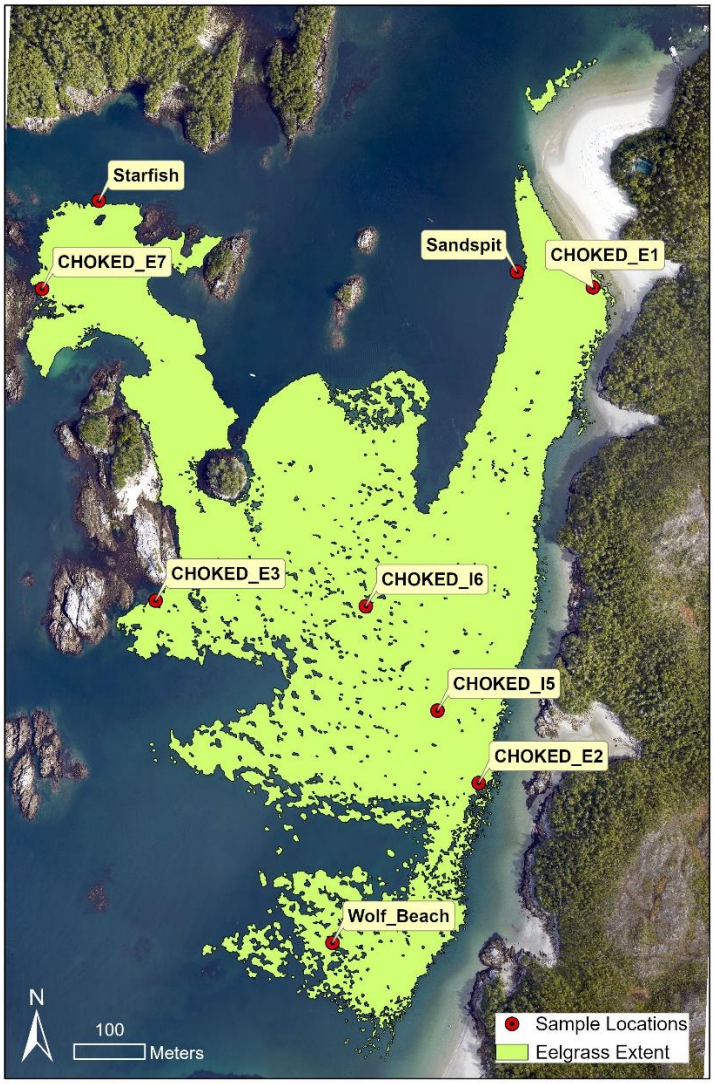

Figure 13 - Map of sediment samples collected from the Choked Pass seagrass meadow. Samples were collected by divers in August of 2021.

Table 16 - Locations of Choked Pass sediment samples collected in August 2021.

Site Name	Substrate	Biotic Community	Latitude	Longitude	Whole Sample Mass (g)	Sieved Mass (g)
Choked_E1	Sand	Zostera marina	51.67881951	-128.1147522	14358.3	536.4
Choked_E2	Sand	Zostera marina	51.67256649	-128.1172077	1059.3	505.8
Choked_E3	Sand	Zostera marina	51.67492689	-128.1237431	857.3	517.4
Choked_E7	Sand	Zostera marina	51.67888847	-128.1259801	961.9	545.3
Choked_I5	Sand	Zostera marina	51.67349206	-128.1180197	924.8	507.1
Choked_I6	Sand	Zostera marina	51.67482341	-128.1194543	1112.3	518.3
Sandspit	Sand	Zostera marina	51.6790354	-128.1163	964.5	500.2
Wolf Beach	Sand	Zostera marina	51.67056667	-128.1202167	940.5	526.5
Starfish	Sand	Zostera marina	51.68	-128.1248	638.2	503.4

Approximately 500 g of each sample were collected for sieve grain analysis (Table 1). Each sieve was cleaned for residues from prior usage. The weight of each sieve and pan were recorded prior to shaking. Sieves were assembled in ascending order (Table 2). The sample was poured into the top sieve and the lid was placed over the stack. Finally, the stack was placed into the sieve shaker for 15 minutes. Once finished, the stack was removed, and each sieve and the receiving pan were weighed.

Table 17 - Sieve number and size (mm) used in grain size analysis of particles greater than 0.075 mm.

Sieve Number	Sieve Size (mm)
5	4
10	2
30	0.6
80	0.18
100	0.15
140	0.106
200	0.075

The finest grain sediments within the receiving pan were collected for hydrometer analysis of fine sands, silts and clays (ASTM, 2017; Hossain et al., 2021; Kalra and Manard, 1991). Due to the small proportion of fine grains within each sample, it was not possible to obtain the 40-50 g of the fine grains that is recommended for hydrometer analysis (Kalra and Manard, 1991; Hossain et al., 2021). Therefore, the mass of fine sediments captured in the receiving pan were used for hydrometer analysis, which ranged from 1.1 – 9.0 g. A 152H hydrometer was used for this part of the analysis. The fines were placed in a beaker with 125 mL of a [40 g/L] Sodium hexametaphosphate (NaPO3) solution. The mixture was stirred until mixed and let rest for 10 minutes. While resting, a control sample was prepared in a 1000 mL graduate cylinder with 125 mL of the a [40 g/L] Sodium hexametaphosphate (NaPO3) solution and 875 mL of distilled. The control sample was mixed thoroughly, and the hydrometer and thermometer were inserted into the control to measure the zero correction, meniscus correction, and the temperature. The zero correction is where the meniscus formed on the hydrometer stem by the control solution. Values less than zero are negative corrections, while values between zero and sixty are positive corrections. The meniscus correction is determined by the difference from the top of the meniscus and the level of control solution graduated cylinder. The hydrometer

readings are corrected with the meniscus correction value and either subtracted or added to the original reading depending on the sign of the zero connection.

After the 10-minute rest period, the soil slurry sample was mixed with distilled water for an additional two minutes, then transferred into a graduated cylinder and filled with distilled water up to create a 1000 mL soil slurry solution. The final solution was inverted 30 times, and the timer began. Once recording, the hydrometer was carefully placed in the sample. Measurements were collected at the top of the meniscus, then removed from the soil slurry solution and placed in the control sample until the next reading. Hydrometer readings and temperature to the nearest 0.5°C were recorded at 10 15 secs, 20 secs, 40 secs, 1 min, 2 min, 4 min, 6 min, 8 min, 15 min, 30 min, 1.5 hr, 2 hrs, and 24 hrs.

After 48 hrs, the meniscus correction was applied to all readings. From the corrected meniscus readings, the effective hydrometer depth (L) was determined using the values in Table 3. To determine the *K* value at specific temperatures, the specific gravity of the soil was assumed to be 2.65 (Table 4). The equivalent particle diameter was calculated for each reading using this formula:

$$D = L \times \sqrt{\frac{L}{t}} \quad \text{(Eq.1)}$$

In equation 1, *t* is time in minutes, *L* is effective hydrometer depth, and *D* is particle diameter in mm. Table 5 was used to determine the temperature correction factor (C_T). Then, Table 6 was used to determine the correction factor *a* for the specific unit weight of solids (g/cm^3). The corrected hydrometer readings were calculated by the following formula:

$$R_c = R_{actual} - Zero\ Correction + C_t \quad \text{(Eq.2)}$$

Using R_c, the percent finer were calculated using the following equation:

$$P = \frac{R_c \times a}{W_s} \times 100 \quad \text{(Eq.3)}$$

In equation 3, W_s is the initial sample weight in grams. Finally, the percent fines is adjusted with the following equation:

$$P_A = \frac{P \times F_{200}}{100} \quad \text{(Eq.4)}$$

In equation 4, F_{200} is the percent finer of the #200 sieve as a percentage.

Table 18 - Vales of effective depth based on hydrometer and sedimentation cylinders of specific sizes for corrections for the Hydrometer 152H (Table 4.1; Hossain et al., 2021).

Corrected Hydrometer Reading	Effective Depth, L (cm)	Corrected Hydrometer Reading	Effective Depth, L (cm)
0	16.3	31	11.2
1	16.1	32	11.1
2	16.0	33	10.9
3	15.8	34	10.7
4	15.6	35	10.6
5	15.5	36	10.4
6	15.3	37	10.2
7	15.2	38	10.1
8	15.0	39	9.9
9	14.8	40	9.7
10	14.7	41	9.6
11	14.5	42	9.4
12	14.3	43	9.2
13	14.2	44	9.1
14	14.0	45	8.9
15	13.8	46	8.8
16	13.7	47	8.6
17	13.5	48	8.4
18	13.3	49	8.3
19	13.2	50	8.1
20	13.0	51	7.9
21	12.9	52	7.8
22	12.7	53	7.6
23	12.5	54	7.4
24	12.4	55	7.3
25	12.2	56	7.1
26	12.0	57	7.0
27	11.9	58	6.8
28	11.7	59	6.6
29	11.5	60	6.5
30	11.4		

Table 19 - Values of K to determine particle diameter in hydrometer analysis. If the specific gravity is not known assume that it is 2.65 (Table 4.2; Hossain et al., 2021).

Temperature	Specific Gravity of Soil Particles								
	2.45	2.5	2.55	2.6	2.65	2.7	2.75	2.8	2.85
16	0.0151	0.01505	0.01481	0.01457	0.01435	0.01414	0.01394	0.01374	0.01356
17	0.01511	0.01486	0.01462	0.01439	0.01417	0.01396	0.01376	0.01356	0.01338
18	0.01492	0.01467	0.01443	0.01421	0.01399	0.01378	0.01359	0.01339	0.01321
19	0.01474	0.01449	0.01425	0.01403	0.01382	0.01361	0.01342	0.01323	0.01305
20	0.01456	0.01431	0.01408	0.01386	0.01365	0.01344	0.01325	0.01307	0.01289
21	0.01438	0.01414	0.01391	0.01369	0.01348	0.01328	0.01309	0.01291	0.01273
22	0.01421	0.01397	0.01374	0.01353	0.01332	0.01312	0.01294	0.01276	0.01258
23	0.01404	0.01381	0.01358	0.01337	0.01317	0.01297	0.01279	0.01261	0.01243
24	0.01388	0.01365	0.01342	0.01321	0.01301	0.01282	0.01264	0.01246	0.01229
25	0.01372	0.01349	0.01327	0.01306	0.01286	0.01267	0.01249	0.01232	0.01215
26	0.01357	0.01334	0.01312	0.01291	0.01272	0.01253	0.01235	0.01218	0.01201
27	0.01342	0.01319	0.01297	0.01277	0.01258	0.01239	0.01221	0.01204	0.01188
28	0.01327	0.01304	0.01283	0.01264	0.01244	0.01255	0.01208	0.01191	0.01175
29	0.01312	0.0129	0.01269	0.01249	0.0123	0.01212	0.01195	0.01178	0.01162
30	0.01298	0.01276	0.01256	0.01236	0.01217	0.01199	0.01182	0.01165	0.01149

Table 20 - Temperature correction factors, CT (Table 4.3; Hossain et al., 2021).

Temperature (C)	factor (CT)
15	1.10
16	-0.90
17	-0.70
18	-0.50
19	-0.30
20	0.00
21	0.20
22	0.40
23	0.70
24	1.00
25	1.30
26	1.65
27	2.00
28	2.50
29	3.05
30	3.80

Table 21 - Correction factors, a, for unit weight of solids (g/cm^3) (Table 4.4; Hossain et al., 2021).

Unit Weight of Soil Solids, g/cm3	Correction factor, a
2.85	0.96
2.8	0.97
2.75	0.98
2.7	0.99
2.65	1
2.6	1.01
2.55	1.02
2.5	1.04

6.5 Appendix E: ADCP Processing

ADCP's are instruments that transmit acoustic pings at a specific frequency and record the return echoes that have scattered off particles at specified depth intervals (i.e. depth bins) throughout the water column. Acoustic pings are emitted from four beams, which are oriented in different directions to measure the north, east, and upward velocity components (Gordon, 1996). ADCPs use principles from the Doppler Effect to measure flow velocity. Because suspended particles are assumed to be moving at the same velocity as the water, the return echo is Doppler-shifted to a lower frequency that is proportional to the relative velocity between the sensor and the particles. The length of time for the echo to return to the sensor, the distance travelled between consecutive pings, and shifted frequency of the return echo are used to measure flow velocity and direction (Gordon, 1996). The returning backscatter is a function of suspended sediment properties (i.e. grain size and concentration), flow velocity, direction, and seabed morphology (Thorne & Hanes, 2002). ADCP's are typically moored to the seafloor looking up or mounted to a vessel looking down.

For this project, a 1200 kHz Teledyne Workhorse Sentinel ADCP was mounted to the hull of a vessel looking down. data were acquired using VmDas and exported as .ENS files. A total of 91 transects were run in Choked Passage (Figure 10). One ping was sent out every 0.84 seconds at 0.25m depth bins and set to water mode 1. Water modes specify the time lag and pulse forms of the acoustic echo, which influences the quality of the flow measurement. Water mode 1 is suitable for a broad range of conditions, including under high flow velocities (Rennie & Millar, 2004).

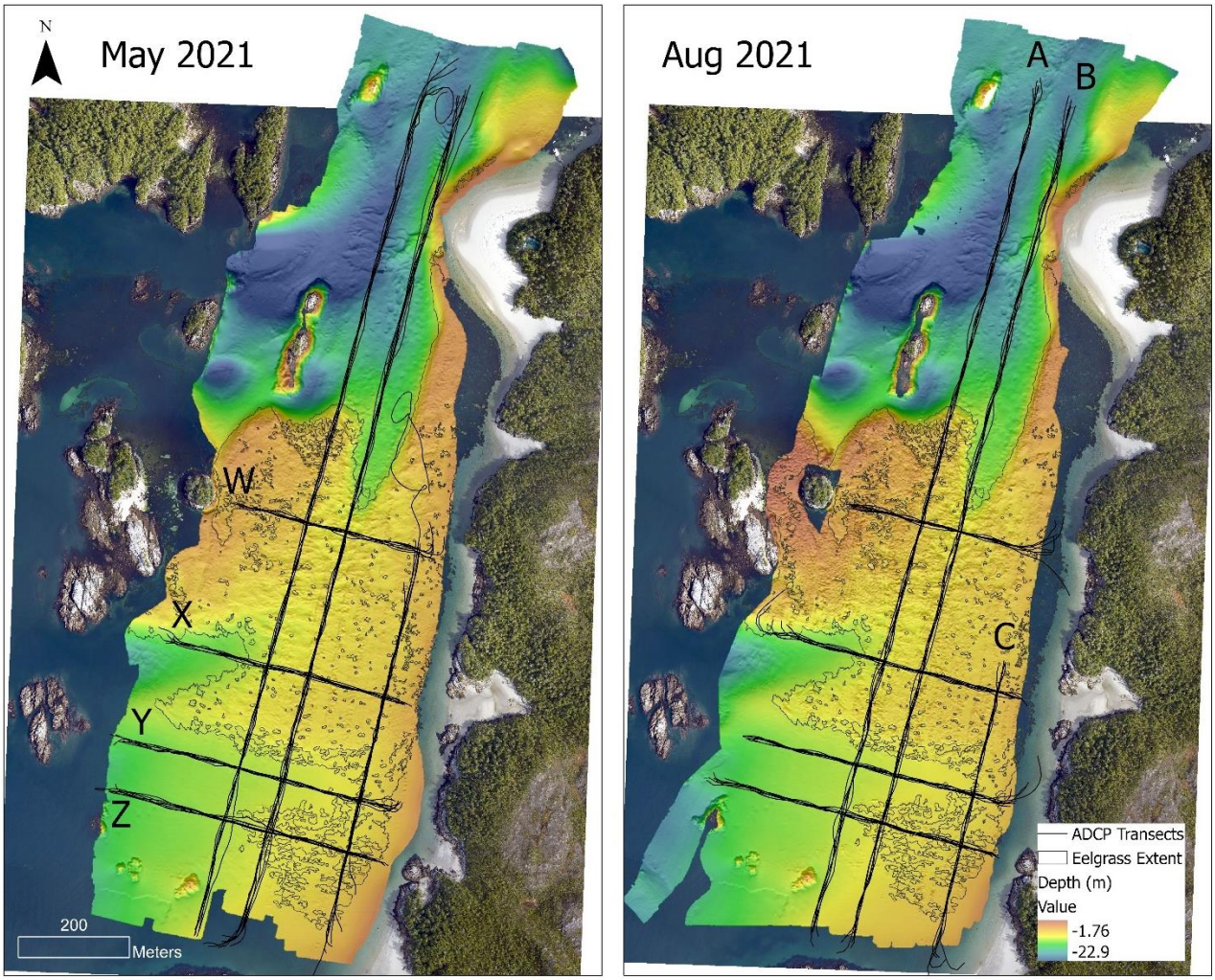

Figure 164 - Longitudinal and cross-passage ADCP transect lines surveyed in May and August of 2021.

The MATLAB function rdradcp was used to convert the ADCP data into .mat files, and all data was processed and analyzed in MATLAB. First, GPS coordinates were converted to local east, north, up (ENU) coordinates (Gilcoto et al, 2009). The atan2 function was used to calculate velocity direction in ENU. The flow velocity and direction measurements were corrected for boat motion (Rennie & Millar, 2004). This method determines the Doppler shift in frequency of the ADCP bottom-track echo, where the shift in frequency is proportional to the boat velocity and removes the boat velocity from velocity data (Rennie, Millar, and Church, 2002). The differences between the internal ADCP and GPS clock, and the bottom-track and GPS track velocities were used to identify and correct the ADCP internal time delay (2.15

seconds). A magnetic declination value of 17.21 was used to correct the flow direction for magnetic variation.

Next, all vales with correlations below 200 counts were removed from the dataset. The bed profile was determined from the bottom track depth values for all four beams for each transect. Raw ADCP data will includes values below the actual seabed because the echoes can be scattered multiple times during their path, which increases the amount of time for the echo to return to the receiver, thus overestimating the distance from the sensor to the bed. All values below the bed profile were removed. Missing bed profile values were interpolated (Wild, 2020). In addition, the first and last 6% of the bins in the dataset were removed, as these bins typically contain sidelobe interference at 20° beam positioning (Yorke & Oberg, 2002).

The ADCP was moored to the seafloor oriented up for four different deployments for a duration of four to 28 hours during each survey period (i.e. 8 deployments total, four in May, and four in August). The instrument sent out five pings per ensemble at a 0.37 ping rate and recorded measurements into 0.25 m bins. Raw data was exported as .000 files. The MATLAB function rdradcp was used to convert the ADCP data into .mat files, and all data was processed and analyzed in MATLAB. First, the velocity magnitude was calculated by adding the squared velocity measurement in each direction. GPS coordinates were converted to local east, north, up (ENU) coordinates (Gilcoto et al, 2009). The rad2deg and atan2 function was used to calculate velocity direction in ENU. Next, the profiles were cleaned to remove the values above the water surface.

6.6 Appendix F: Total Suspended Material Measurements.

Water samples and turbidity measurements were collected during hull mounted ADCP transects. Both longitudinal transects were surveyed during low and high tide on August 11, 2021. A 5L Niskin bottle was attached to an AML CTD-Tu and deployed simultaneously to measure the turbidity profiles and collect a water sample for that specific depth bin and ensemble. The AML density probe was located 1.32 m below the middle of the Niskin bottle. The AML was lowered to a maximum depth of 1 m above the bed to not disturb the sediment and contaminate the water sample. The exact ADCP ensemble that the Niskin bottle was triggered was recorded for each sample collection. Therefore, the depth of the water sample can

be determined by adding 1.45 m to the maximum depth measured by the AML. The 5L samples were transferred into clear Nalgene sample bottles

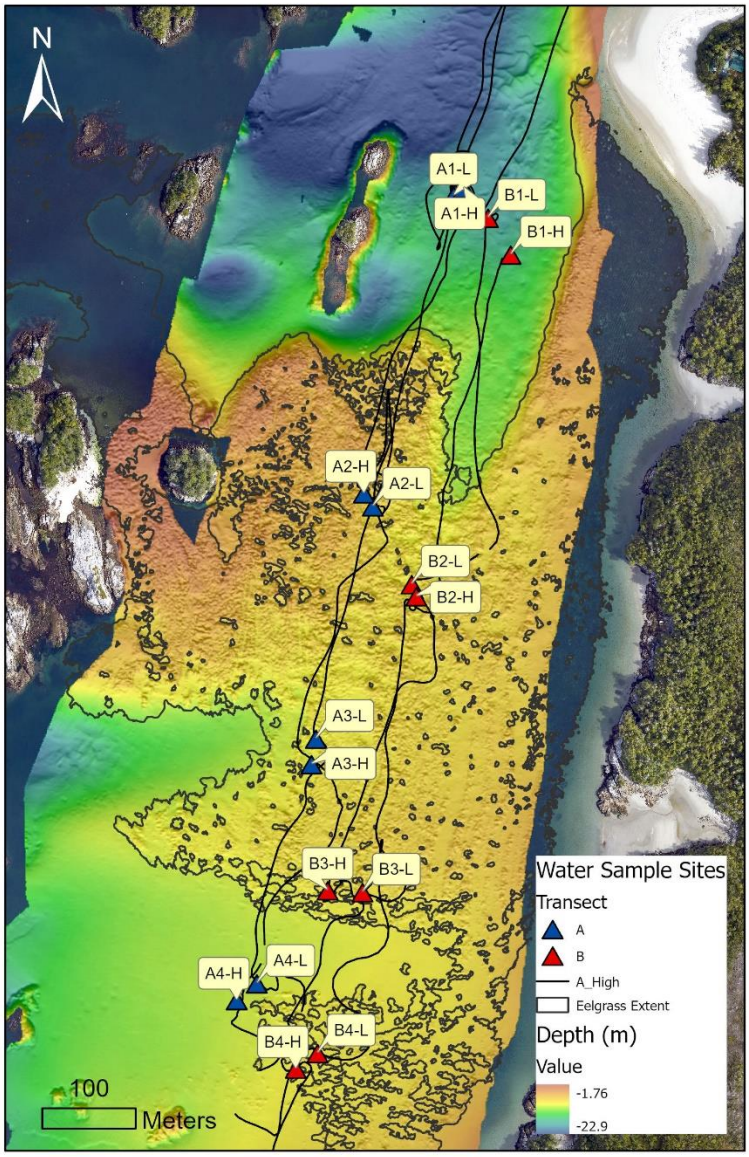

Figure 175 - Hull-mounted ADCP transects and water sampling stations collected on August 11, 2021.

Table 22 - Water sample filtration data and total suspended material (TMS) collected on Aug 11, 2021 in Choked Passage, B.C. Canada.

Sample ID	Site ID	Tidal Stage	Depth (m)	Type	Avg Pre-filter weight (mg)	Total Filtered Volume (mL)	DI Rinse Volume (mL)	Post-Filtered weight 1 (mg)	Post-Filtered weight 2 (mg)	Post-Filtered weight 3 (mg)	Avg Post-Filtered weight (mg)	Net change (mg)	TMS (mg/mL)	TMS (mg/L)
A1-L	A1	Low	6	Whatman	132.6	3000	100	137.4	137.8	137.4	137.5	4.9	0.001644	1.64
A2-L	A2	Low	2.5	Millipore	98.5	3000	100	101.4	101.6	101.8	101.6	3.1	0.001033	1.03
A3-L	A3	Low	3	Whatman	131.3	3000	100	136.1	136.1	136.2	136.1	4.8	0.001611	1.61
A4-L	A4	Low	4	Millipore	95.3	3000	100	98.4	98.6	98.7	98.6	3.3	0.001089	1.09
B1-L	B1	Low	6	Millipore	96.0	3000	100	102.5	102.5	102.4	102.5	6.5	0.002156	2.16
B2-L	B2	Low	3	Whatman	134.7	3000	100	138.7	139.1	139.2	139.0	4.3	0.001433	1.43
B3-L	B3	Low	3	Millipore	95.6	3000	100	98.3	98.6	98.8	98.6	3.0	0.000989	0.99
B4-L	B4	Low	4	Whatman	130.8	3000	100	134.3	134.3	134.5	134.4	3.6	0.001189	1.19
A1-H	A1	High	7	Millipore	95.8	3000	100	99.7	99.5	99.6	99.6	3.8	0.001267	1.27
A2-H	A2	High	4	Whatman	131.3	3000	100	136.0	136.0	135.9	136.0	4.6	0.001544	1.54
A3-H	A3	High	5	Millipore	95.4	3000	100	99.3	99.2	99.3	99.3	3.9	0.001289	1.29
A4-H	A4	High	6	Whatman	131.6	3000	100	136.5	136.4	136.7	136.5	5.0	0.001656	1.66
B1-H	B1	High	10	Whatman	131.7	3000	100	136.0	136.2	136.0	136.1	4.4	0.001456	1.46
B2-H	B2	High	5	Millipore	96.0	3000	100	99.9	100.0	100.0	100.0	4.0	0.001322	1.32
B3-H	B3	High	5	Whatman	130.1	3000	100	136.3	136.2	136.3	136.3	6.2	0.002056	2.06
B4-H	B4	High	5	Millipore	95.5	3000	100	99.6	99.7	99.9	99.7	4.2	0.001411	1.41

6.8 Appendix Bibliography

ASTM, A. (2017). D7928: Standard test method for particle-size distribution (gradation) of fine-grained soil using the sedimentation (hydrometer) analysis. *ASTM International: West Conshohocken (PA)*.

Gilcoto, M., Jones, E., & Fariña-Busto, L. (2009). Robust estimations of current velocities with four-beam broadband ADCPs. *Journal of Atmospheric and Oceanic Technology*, *26*(12), 2642-2654.

Gordon, R. L. (1996). Acoustic Doppler current profiler-Principles of operation: A practical primer. *RD Instruments*.

Hossain, M. S., Islam, M. A., Badhon, F. F., & Imtiaz, T. (2021). Hydrometer Analysis. *Properties and Behavior of Soil-Online Lab Manual*.

Kalra, Y. P., & Maynard, D. G. (1991). *Methods manual for forest soil and plant analysis* (Vol. 319)

Mueller, D. S., Wagner, C. R., Rehmel, M. S., Oberg, K. A., & Rainville, F. (2009). *Measuring discharge with acoustic Doppler current profilers from a moving boat* (p. 72). Reston, Virginia (EUA): US Department of the Interior, US Geological Survey.

Rennie, C. D., & Millar, R. G. (2004). Measurement of the spatial distribution of fluvial bedload transport velocity in both sand and gravel. *Earth Surface Processes and Landforms*, 29(10), 1173–1193. https://doi.org/10.1002/esp.1074

Thorne, P. D., & Hanes, D. M. (2002). A review of acoustic measurement of small-scale sediment processes. *Continental Shelf Research*, 22(4), 603–632. https://doi.org/10.1016/S0278-4343(01)00101-7

Wild, A. L. (2020). *Morphodynamics of a bedrock confined estuary and delta: The Skeena River Estuary* (Masters thesis, University of Victoria).

Yorke, T. H., & Oberg, K. A. (2002). Measuring river velocity and discharge with acoustic Doppler profilers. *Flow Measurement and Instrumentation*, 13(5–6), 191–195. https://doi.org/10.1016/S0955-5986(02)00051-1

Zhang, W., Qi, J., Wan, P., Wang, H., Xie, D., Wang, X., & Yan, G. (2016). An Easy-to-Use Airborne LiDAR Data Filtering Method Based on Cloth Simulation. *Remote Sensing*, 8(6), 501. https://doi.org/10.3390/rs8060501